



A Thermal Management Systems Model for the NASA GTX RBCC Concept

Richard M. Traci, John L. Farr, Jr., and Tony Laganelli
Science Applications International Corporation, Torrance, California

The NASA STI Program Office . . . in Profile

Since its founding, NASA has been dedicated to the advancement of aeronautics and space science. The NASA Scientific and Technical Information (STI) Program Office plays a key part in helping NASA maintain this important role.

The NASA STI Program Office is operated by Langley Research Center, the Lead Center for NASA's scientific and technical information. The NASA STI Program Office provides access to the NASA STI Database, the largest collection of aeronautical and space science STI in the world. The Program Office is also NASA's institutional mechanism for disseminating the results of its research and development activities. These results are published by NASA in the NASA STI Report Series, which includes the following report types:

- **TECHNICAL PUBLICATION.** Reports of completed research or a major significant phase of research that present the results of NASA programs and include extensive data or theoretical analysis. Includes compilations of significant scientific and technical data and information deemed to be of continuing reference value. NASA's counterpart of peer-reviewed formal professional papers but has less stringent limitations on manuscript length and extent of graphic presentations.
- **TECHNICAL MEMORANDUM.** Scientific and technical findings that are preliminary or of specialized interest, e.g., quick release reports, working papers, and bibliographies that contain minimal annotation. Does not contain extensive analysis.
- **CONTRACTOR REPORT.** Scientific and technical findings by NASA-sponsored contractors and grantees.

- **CONFERENCE PUBLICATION.** Collected papers from scientific and technical conferences, symposia, seminars, or other meetings sponsored or cosponsored by NASA.
- **SPECIAL PUBLICATION.** Scientific, technical, or historical information from NASA programs, projects, and missions, often concerned with subjects having substantial public interest.
- **TECHNICAL TRANSLATION.** English-language translations of foreign scientific and technical material pertinent to NASA's mission.

Specialized services that complement the STI Program Office's diverse offerings include creating custom thesauri, building customized data bases, organizing and publishing research results . . . even providing videos.

For more information about the NASA STI Program Office, see the following:

- Access the NASA STI Program Home Page at <http://www.sti.nasa.gov>
- E-mail your question via the Internet to help@sti.nasa.gov
- Fax your question to the NASA Access Help Desk at 301-621-0134
- Telephone the NASA Access Help Desk at 301-621-0390
- Write to:
NASA Access Help Desk
NASA Center for Aerospace Information
7121 Standard Drive
Hanover, MD 21076



A Thermal Management Systems Model for the NASA GTX RBCC Concept

Richard M. Traci, John L. Farr, Jr., and Tony Laganelli
Science Applications International Corporation, Torrance, California

Prepared under Contract NAS3-99147

National Aeronautics and
Space Administration

Glenn Research Center

Trade names or manufacturers' names are used in this report for identification only. This usage does not constitute an official endorsement, either expressed or implied, by the National Aeronautics and Space Administration.

The Aerospace Propulsion and Power Program at NASA Glenn Research Center sponsored this work.

Available from

NASA Center for Aerospace Information
7121 Standard Drive
Hanover, MD 21076

National Technical Information Service
5285 Port Royal Road
Springfield, VA 22100

Available electronically at <http://gltrs.grc.nasa.gov/GLTRS>

Foreword

This model development study was performed for the NASA Glenn Research Center (GRC) under NASA Contract No. NAS3-99147 over the period-of-performance April 1, 1999 through April 30, 2001. The program was performed by the Thermal Analysis and Information Systems Division of Science Applications International Corporation (SAIC) based in Torrance, California. The work built on previous and coincident Air Force contracts to which the program is indebted. Mr. James Walker of NASA GRC was the technical monitor and co-investigator for the program. His interest, persistence, many technical contributions are recognized by the authors—VITMAC would not be nearly as good without him. Thanks also to Valerie Van Griethuysen of the Air Force Research Laboratory, Wright Field, Ohio for her support over the years.

The SAIC participants in the program were: Tony Laganelli, Program Manager, Richard M. Traci, Principal Investigator, John L. Farr, Jr., Engineering Programmer, and Wayne Ikeuchi, GUI Programmer.

Table of Contents

	<u>Page</u>
List of Figures.....	vii
1. Introduction and Background	1
2. VITMAC Thermal Management Model Summary	3
3. VITMAC-CEA Rocket Engine Thrust Chamber Model	5
3.1 Summary of VITMAC-CEA Rocket Engine Flowpath Model	5
3.2 Comparison to Rocket Calorimeter Chamber Experiment.....	9
3.3 Comparison to Rocket Calorimeter Chamber Experiment for LOX/Kerosene.....	13
4. VITMAC RJPA Scramjet Engine Flowpath and Heat Transfer Model	17
4.1 Model Linkage And Heat Transfer Formulation	17
4.2 VITMAC Comparison With NASP DCC Experimental Data	35
4.3 VITMAC Comparison with NASP DCAF Experimental Data.....	39
4.4 VITMAC Comparison with NASP GASL-CALSPAN-Entry 4 Test Data	43
5. Cold-side Heat Transfer Model	47
5.1 Cooling Panel “Cold-Side” Heat Transfer Correlation Summary.....	47
5.2 Two Dimensional Cooling Channel Analysis: Rectangular Channel.....	52
5.3 Cooling Channel Analysis: Circular Channel with Conductive Liner	64
6. Other VITMAC Model Development Studies.....	71
6.1 Gas Generator Source Model.....	71
6.2 Turbo-pump Considerations	75
6.3 Solution Convergence Studies.....	78
7. New Technology.....	81
8. Discussion and Recommendations	83
9. References	85

List of Figures

	<u>Page</u>
Figure 2.1 Overview of VITMAC Thermal Modules and GUI.....	4
Figure 3.1 Generic Rocket Cooling Network	5
Figure 3.2 Definition of Rocket FlowPath Modules and “Cooling Panel” Subsections	6
Figure 3.3 VITMAC CEA Dialog Box.....	8
Figure 3.4 Schematic of Plug-Nozzle Rocket Engine Experiment.....	9
Figure 3.5 VITMAC Rocket Engine Cooling Network.....	10
Figure 3.6 VITMAC Rocket Engine Cooling Network Flowpath Results.....	11
Figure 3.7 VITMAC-CEA Heat Transfer Prediction Comparison to Subscale, Plug Nozzle. Rocket Calorimeter Chamber Results	12
Figure 3.8 VITMAC-CEA “Hot-Wall” Temperature Prediction Comparison to Subscale, Plug Nozzle. Rocket Calorimeter Chamber Results	12
Figure 3.9 VITMAC-CEA “Hot-Wall” Heat Transfer Prediction Comparison to LOX/RP1 Rocket Calorimeter Chamber Results	13
Figure 3.10 VITMAC-CEA “Hot-Wall” Heat Transfer Prediction Comparison to Hydrogen Fueled Rocket Experiment	14
Figure 3.11 VITMAC-CEA “Hot-Wall” Heat Transfer Prediction Comparison to Hydrogen Fueled Rocket Experiment	15
Figure 4.1 Generic Scramjet Cooling Network	18
Figure 4.2 Definition of Scramjet FlowPath Modules and “Cooling Panel” Subsections	19
Figure 4.3 VITMAC RJP Dialog Box	21
Figure 4.4 Fuel/Oxidizer Specification Dialog Box	23
Figure 4.5 Free Stream Condition Dialog Box	25
Figure 4.6 Diffuser Parameters Dialog Box	26
Figure 4.7 RJP Shock Dialog Box	27
Figure 4.8 Combustor Parameters Dialog Box.....	28
Figure 4.9 Nozzle Parameters Dialog Box	29
Figure 4.10 Inlet Heat Transfer Parameters Dialog Box	30
Figure 4.11 Combustor Heat Transfer Parameters Dialog Box.....	31
Figure 4.12 Nozzle Heat Transfer Parameters Dialog Box	32
Figure 4.13 Cowl Heat Transfer Parameters Dialog Box.....	33
Figure 4.14 Generic VITMAC Scramjet Engine Cooling Network	34
Figure 4.15 Schematic of APL Scramjet DCC Experiment	35
Figure 4.16 VITMAC Schematic for Scramjet DCC Experiment.....	36
Figure 4.17 VITMAC Heat Transfer Results for APL DCC Experiment Mach No. ~ 8, Equivalence Ratio ~ .5, $\eta_{\text{comb}} = 95\%$	38
Figure 4.18 VITMAC Heat Transfer Results for APL DCC Experiment Mach No. ~ 6, Equivalence Ratio up to .37, $\eta_{\text{comb}} = 95\%$	38
Figure 4.19 Schematic of DCAF Scramjet Experiment (Direct Connect Arc-jet Facility)	39

List of Figures (Cont'd)

	<u>Page</u>
Figure 4.20 VITMAC Heat Transfer Results for DCAF Experiment (2010). Mach No. ~ 10, Equivalence Ratio ~ 1.15, $\eta_{\text{comb}} = 62\%$	41
Figure 4.21 VITMAC Heat Transfer Results for DCAF Experiment (1034) Mach No. ~ 12, Equivalence Ratio ~ 2.25, $\eta_{\text{comb}} = 40\%$	42
Figure 4.22 VITMAC Comparison to Peak Heat Transfer Results for DCAF. Experiments (10XX-20XX) Mach No. 10 to 12, Equivalence Ratio .5 to 2.25	42
Figure 4.23 Schematic of GASL-CALSPAN-Entry 4 Scramjet Experiment (96” CALSPAN Shock Tunnel Facility).....	43
Figure 4.24 VITMAC Schematic for GASL-CALSPAN-Entry 4 Scramjet Experiment.....	44
Figure 4.25 VITMAC Heat Transfer Results for GASL-CALSPAN-Entry 4.. Mach No. ~ 9.3, Equivalence Ratio ~ 0.9, $\eta_{\text{comb}} = 62\%$	45
Figure 5.1 New Cooling Panel Heat Transfer Options.....	49
Figure 5.2 Cooling Panel Flow Channel Option	50
Figure 5.3a Rectangular Cross-section Channel Option.....	51
Figure 5.3b Circular Cross-section Channel Option.....	51
Figure 5.4 VITMAC Cooling Panel Simulation.....	52
Figure 5.5 Parameters for 2D Channel Geometry Effects Analysis	53
Figure 5.6 Channel Effectiveness Parameter (Square Channel, H/D= 1).....	54
Figure 5.7 ”Fin” Geometry Effect on Channel Effectiveness Parameter	55
Figure 5.8 Cooling Fin Efficiency Correlation for Square Channel, H/D = 1	56
Figure 5.9 Rectangular Channel Effectiveness Correlation (0.01 < H/D < 10., 0.002 < W/D < 5., 0.15 < t/D < 2.)	57
Figure 5.10 Rectangular Channel Effectiveness Correlation for High Biot Number	58
Figure 5.11 Rectangular Channel Effectiveness Correlation.....	59
Figure 5.12 Channel Effectiveness Correlation Scatter Plot	60
Figure 5.13 Channel Effectiveness for H/D = 1	60
Figure 5.14 Channel Effectiveness for H/D = 3	61
Figure 5.15 SINDA 2D Channel Temperature Profiles for H/D ~ 3 and H/D = 1	62
Figure 5.16 “Cold-side” Channel Temperature Comparison of 2D SINDA to 1D VITMAC Calculations	63
Figure 5.17 Parameters for Circular Channel Geometry Analysis	64
Figure 5.18 Circular Channel Effectiveness Correlation for High Biot Number	65
Figure 5.19 Circular Channel Effectiveness Correlation.....	66
Figure 5.20 Circular Channel Effectiveness Correlation Scatter Plot	66
Figure 5.21 SINDA 2D Channel Temperature Profiles for. Circular Channel, Isotropic Conductivity ($k_h : k_v = 35. : 35. \text{ W/m-K}$)	68

List of Figures (Cont'd)

	<u>Page</u>
Figure 5.22 “Cold-side” Channel Surface Temperature Comparison of 2D SINDA to 1D VITMAC Calculations Circular Channel, Isotropic Conductivity ($k_h : k_v = 35. : 35. \text{ W/m-K}$)	68
Figure 5.23 SINDA 2D Channel Temperature Contours for. Circular Channel, Anisotropic Conductivity ($k_h : k_v = 70. : 39.3 \text{ W/m-K}$).....	69
Figure 5.24 “Cold-side” Channel Surface Temperature Comparison of 2D SINDA to 1D VITMAC Calculations Circular Channel, Anisotropic Conductivity ($k_h : k_v = 70. : 39.3 \text{ W/m-K}$).....	70
Figure 6.1 Gas Generator Source Option	71
Figure 6.2 Gas Generator Input Window.....	72
Figure 6.3 CEA Input and Output Definition	73
Figure 6.4 Gas Generator Test Case	74
Figure 6.5 Example Gas Generator/Turbo-pump Loop.....	75
Figure 6.6 Generic Turbine Network.....	76
Figure 6.7 Under-Relaxation Parameter	79
Figure 6.8 Engine Heat Transfer “Ramp-up” Parameter	80

1. Introduction and Background

Air-breathing propulsion technology has long been identified for its potential to reduce launch costs. Specifically, high-efficiency air-breathing cycles combined with a rocket subsystem can greatly reduce the amount of on-board propellant required to reach orbital velocities as compared to an all rocket powered vehicle, and thus offer the potential to reduce the size and weight of the vehicle. These systems, commonly called Rocket-Based Combined Cycles (RBCC), operate in multiple modes including, rocket-ejector, ramjet, scramjet and rocket-only mode to propel a vehicle to orbit. An excellent review on RBCC is provided by Daines and Segal¹ for earth-to-orbit applications. This promising technology has been recognized by NASA Glenn Research Center as a logical step in reducing the costs of delivering payload to orbit. NASA Glenn Research Center (GRC) has identified an integrated propulsion/vehicle concept “GTX” as a first step to demonstrate RBCC propulsion.

One of the critical technical issues is the integration of the propulsion system with the airframe, in particular, the development of efficient thermal management systems. Single-stage-to-orbit (SSTO), reusable air-breathing launch vehicles (ABLV) will require energy management of passive and actively cooled structures that include leading edges, flow impingement areas, and engine flowpath walls. To efficiently cool these structures, thermal analysis design tools and models as described in this paper will be needed for conceptual system design studies.

The Vehicle Integrated Thermal Management Analysis Code (VITMAC) simulates coupled system thermal-hydraulics including interacting fluid circuits, multiple flow/heat exchanger components and structural surfaces subject to various heat loads. The model was originally developed under IR & D funding for application to the National AeroSpace Plane (NASP) program and has subsequently received U.S. Air Force support for thermal management modeling of modern weapon systems. Under additional USAF and NASA GRC support, VITMAC has recently been upgraded to include GUI enhancements, system evaluation tools, additional component models such as cooling panels, and linkages to a rocket engine model and a ram/scramjet engine model. These capabilities, implemented for automated evaluation of engine heat transfer coupled to cooling panel components, are the focus of the present report.

The objective of the program was to enhance the capabilities of the SAIC Vehicle Integrated Thermal Management Analysis Code (VITMAC) to analyze the thermal and power requirements of the RBCC propulsion systems. This included modification and/or additional modules to the code to better represent the RBCC system. The effort also included an engineering level method to predict the surface heat transfer characteristics along the propulsion system flowpath. This effort utilized CFD analysis being conducted by NASA Glenn RC and has built upon the current VITMAC capability for coupling to thermodynamic

¹ Daines, R. and Segal, C., “Combined Rocket and Airbreathing Propulsion Systems for Space-Launch Applications,” *J. of Prop. and Power*, v. 14, No. 5, Sep/Oct 1998.

cycle codes CEA and RJPA—the former to be considered for the RBCC rocket mode and the latter for ramjet/scramjet operation. The scramjet mode is the focus of the investigation to address the severe cooling requirements expected. Additional modifications to VITMAC include an improved method for cooling panel heat conduction, hot and cold side heat transfer models, turbomachinery models, and a structural material/fluid database. A gas generator model has also been developed with appropriate components for inclusion into VITMAC to permit the analysis of gas generator and pre-burner type propellant feed systems.

2. VITMAC Thermal Management Model Summary

VITMAC is a fast-running, PC-based design tool which models thermal management systems (TMS) integrated with propulsion and airframe components subject to various transient heat loads from vehicle subsystems such as: aircraft/missile electronics and environmental control systems (ECS) as well as external aeroheating and internal engine heat loads. VITMAC^{2, 3, 4, 5, 6} is an engineering level thermal-fluid systems model which simulates coupled system thermal-hydraulics including interacting fluid circuits, multiple flow/heat exchanger components, and structural surfaces subject to various heat loads. Iterative, implicit numerical solutions of the mass, momentum and energy equations are used to calculate the steady-state or transient distributions of coolant temperature, pressure and flow rate along with associated structural component temperatures. Easily selectable gas or liquid working fluids and structural/thermal-protection materials are provided within a graphical user interface, which permits the quick construction and analysis of thermal management schemes. For high speed aircraft and missile systems, the considerable thermal capacitance of the fuel system provides the heatsink for use in cooling other subsystem components. This magnifies the need for analyzing the fluid and thermal state of the coupled thermal management and propulsion systems under stressing mission conditions. For example, one important question that can only be addressed in a coupled fashion is the match or mismatch between the engine fuel/oxidizer demand and the coolant flow rate requirements under all operating conditions. Coupling the TMS model with an appropriate engine model, as described here, provides a unique tool for addressing this question in the early preliminary, or even conceptual, design stage.

The capabilities of VITMAC, including the principal modules or TMS components, which are provided for easy “mouse-click” selection, are illustrated in Figure 2.1, below. VITMAC consists of three integrated pieces of software: a Graphical User Interface (GUI), the thermal management simulation code, and a plotting package. The GUI provides an easy to use environment for modeling thermal management systems, inputting geometrical parameters, setting boundary conditions, such as temperature and pressure, and providing an interface between the user and both the VITMAC simulation code, and the plotting package for results display and analysis. The simulation code contains a generalized thermal-fluid network analyzer module (consisting of pumps, flow channels, valves and fittings), a structural protection material thermal response module, a heat loads module, a turbomachinery performance module (pumps, compressors and turbines), a fuel tank module (including a gas generator source and detailed cryogenic fluid tank option), a heat exchanger module, and an

² Wassel, A. T., F. Issacci, and V. Van Griethuysen, “An Integrated Modeling Approach for Hypersonic Aircraft Thermal Management,” AIAA Paper No. AIAA 95-6022, 6th Inter. Aero. Plane and Hyper. Tech. Conf., April 1995.

³ Farr, J. L. Jr., et al., “VITMAC 4.0 User’s Guide,” December 1996.

⁴ Traci, R.M. J.L. Farr Jr., ”Development of an Endothermic Fuel Capability for the Vehicle Integrated Thermal Management Analysis Code (VITMAC),” AFRL-PR-WP-TR-1998-2037, Oct., 1997.

⁵ Farr, J. L. Jr., et al., “VITMAC 5.0 User’s Guide,” June 1999.

⁶ Farr, J. L. Jr., et al., “VITMAC 6.0 User’s Guide,” September 2000.

engine module. The code uses information obtained through the GUI from the user to set-up and perform the simulation; it then produces a detailed output file which can be viewed from the GUI and a plot file for the plotting package. The plotting package uses the plot file to produce graphical displays of the fluid temperature, pressure, and mass flow rate, as well as temperature profiles of any structural components.



VITMAC is an engineering tool developed for the analysis of thermal management concepts

Solves control volume mass, momentum and energy equations for components in a fluid circuit

Provides steady-state and transient fluid response coupled to 1D structures

Models sources, sinks, channels, pumps, compressors, turbines, heat-exchangers, etc.

Includes a range of hydrocarbon and cryogenic fuels, cooling fluids, and thermal protection/structural materials

Provides heat transfer coupling to CEA, rocket engine, and RJP, scramjet engine models

Interacting cooling circuits can be constructed, solved and analyzed using a point-and-click graphical user interface

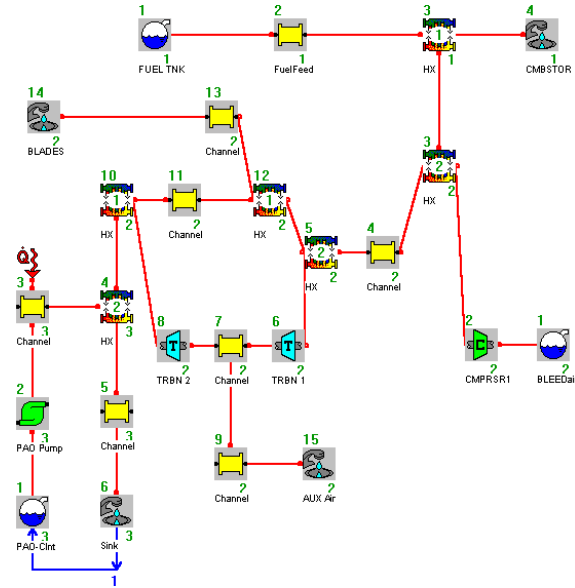


Figure 2.1 Overview of VITMAC Thermal Modules and GUI

In the VITMAC modeling approach, a thermal management system's active cooling network is defined by a set of interconnected components (flow channels, pumps/fans, cooling panels, heat exchangers, plumbing fixtures, turbines, etc.). These components make up interacting coolant loops designed to accept heat from subsystem devices, which require cooling and ultimately reject that heat from the vehicle in the most efficient manner possible. As part of the ongoing Air Force project mentioned above, an optimization module was also developed to facilitate and aid the user in developing improved TMS designs. The approach for an enhanced VITMAC capability for the RBCC/airframe integration is described in the following sections.

3. VITMAC-CEA Rocket Engine Thrust Chamber Model

VITMAC has been linked to the CEA Rocket Engine Model to simplify the evaluation of engine flowpath heat transfer with automatic coupling to VITMAC structural/cooling panel modules. The model is summarized here along with detailed comparisons to heat transfer data from rocket engine thrust chamber experiments to provide a measure of validation of the combined model implementation and the important heat transfer predictive capability.

3.1 Summary of VITMAC-CEA Rocket Engine Flowpath Model

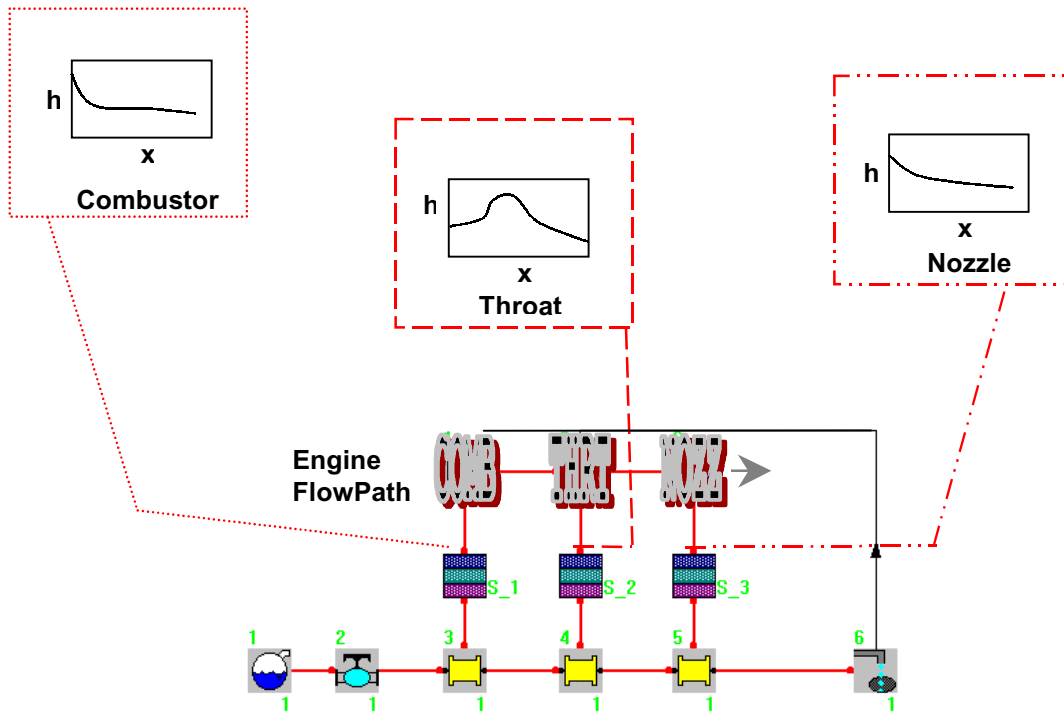


Figure 3.1 Generic Rocket Cooling Network

The approach utilizes an accepted rocket engine flowpath model: namely the CEA model of Gordon & McBride (1976, 1994)^{7,8}, coupled with accepted engineering heat transfer correlations, namely one accepted in the rocket engine community due to Bartz (1957)⁹. As suggested for use with a generic VITMAC cooling network, Figure 3.1. above, the implementation is designed as follows:

⁷ Gordon, S. and B.J. McBride, (1976), "Computer Programs for the Calculation of Complex Chemical Equilibrium Compositions," NASA TR-1751

⁸ Gordon, S. and B.J. McBride, (1994), "Computer Programs for the Calculation of Complex Chemical Equilibrium Compositions and Applications, I. Analysis," NASA RP-1311 Vol. I, II.

⁹ Bartz, D. R., (1957) "A Simple Equation for the Rapid Estimation of Rocket Nozzle Convective Heat Transfer Coefficients," Technical Note, pg. 49, Jet Propulsion, Jan., 1957.

- Calculate the rocket engine flowpath conditions and the heat transfer to engine thrust chamber cooling panel sections.
- engine divided into three modules: combustor, throat and nozzle
- calculate h_{aver} and $(T_{aw})_{aver}$ and automatically connect to structural surface “cooling panel” for up to 5 structures per engine module

The structure heating rate at any time or iteration will be given by:

$$\dot{Q} = h_{aver} A_{pan} (T_{aw} - T_{wall}) \quad (1)$$

where h_{aver} is the heat transfer coefficient averaged over the section, A_{pan} is the surface area of the section (top surface area of structural component), T_{aw} is the adiabatic wall temperature averaged over the section and T_{wall} is the structure heated surface wall temperature calculated by VITMAC.

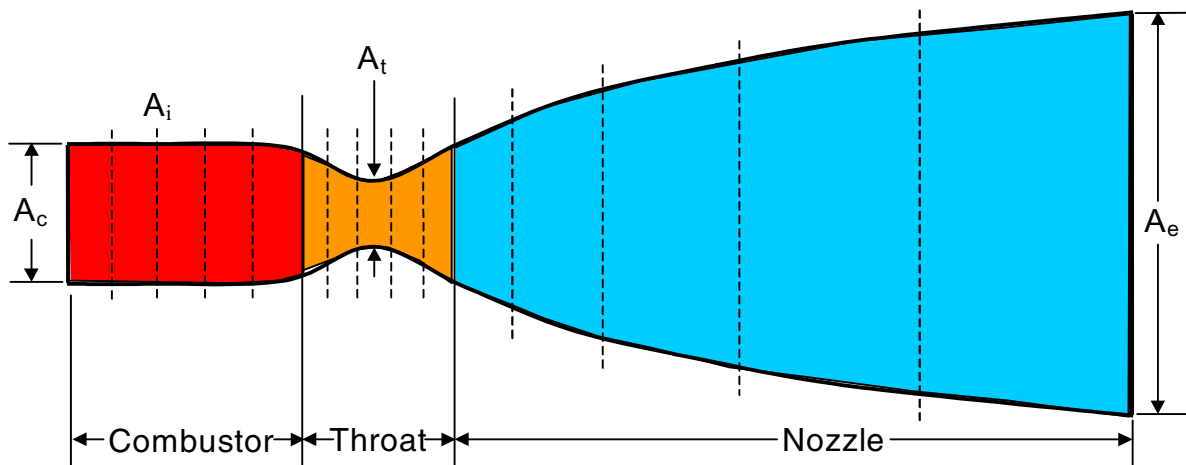


Figure 3.2 Definition of Rocket FlowPath Modules and “Cooling Panel” Subsections

Figure 3.2 shows the engine flowpath with the three principal modules and the separation of each module into up to 5 sections for definition of average heat transfer to the corresponding “cooling panel” (i.e. structural surface and underlying flow channel). The A’s refer to engine cross-sectional area normalized to the throat area, i.e. $A_t = 1$.

The following equations define the implementation of the heat transfer correlations. In each case, all flow quantities (enthalpy, i , pressure, p , temperature, T , velocity, U , and Mach No., M , as well as fluid properties; Prandtl No., Pr , specific heat, C_p , viscosity, μ , gas gamma, γ , etc.) are calculated by calls to the CEA “subroutine”. Numerous such calls are made to determine flow and heat transfer quantities at a multiplicity of subsections, determining average heat transfer quantities over each section of each module. The Bartz correlation, equation 4. below, determines the average heat transfer over the section required by the usual convective heat transfer expression given in equation 1. This equation is then implemented in VITMAC as the heat transfer relation, defining the heating rate to the top surface of a

prearranged structural surface. It should be mentioned that this implementation is fully coupled to the VITMAC structural panel solution. The heating rate given by equation 1. changes as the hot surface temperature of the panel changes during either the steady state solution iteration or the transient time-wise integration.

Adiabatic Wall Enthalpy:

$$i_{aw} = i + (Pr_{ref})^{1/3} (i_o - i) \quad (2)$$

Eckert Reference Enthalpy:

$$i_{ref} = 0.5(i + i_{cold}) + 0.22(Pr_{ref})^{1/3} (i_o - i) \quad (3)$$

Heat Transfer Coefficient:

$$h_{aver} = \tilde{h} \times \sigma \quad (4)$$

Where subsidiary quantities from the Bartz Correlation are:

$$\tilde{h} = \frac{.026}{D_t^{0.2}} \frac{\mu_o^{0.2} C_{p_o}}{Pr_o^{0.6}} \left(\frac{p_o}{c^*} \right)^{0.8} \left(\frac{D_t}{R} \right)^{0.1} \left(\frac{1}{A} \right)^{0.9}$$

$$\sigma = \frac{1}{\left(0.5 \frac{T_{wall}}{T_o} M_\gamma + 0.5 \right)^{0.68} M_\gamma^{0.12}}$$

and:

$$M_\gamma = 1. + \frac{\gamma - 1}{2} M^2$$

In the above, subscript, o, refers to chamber total conditions, c^* , is the chamber characteristic velocity (a measure of theoretical rocket performance), A, is the local cross sectional area, D_t , is the throat diameter, and R, is the axial radius of curvature at the throat.

The Bartz formulation starts with the usual turbulent pipe flow correlation and uses engineering approximations for the flow thermodynamic and transport properties. This more direct approach to defining the heat transfer coefficient can also be used by evaluating all fluid properties at the Eckert Reference enthalpy (equation 3, i_{ref}), and defining a local hydraulic diameter, D_h , for the flow. This relation is referred to here as the “Pipe Flow-Eckert” relation and is given by:

$$h_{\text{aver}} = \frac{C k_{\text{ref}}}{D_h} \left(\frac{\rho_{\text{ref}} U D_h}{\mu_{\text{ref}}} \right)^{0.8} (Pr_{\text{ref}})^{0.34} \quad (5)$$

The approach, just described, is implemented by the VITMAC user by defining engine descriptive parameters, fuel and oxidizer, chamber pressure, combustor throat and nozzle area ratios etc. These are input through the GUI using the dialog box contained in Figure 3.3. The quantities displayed are typical rocket engine parameters, familiar to persons in that field or related fields. For now, the user may use the “Pipe Flow-Eckert” correlation, or the Bartz correlation, each unmodified or with global or local scaling factors. Also, “user defined” heat transfer coefficients may be specified for each section.

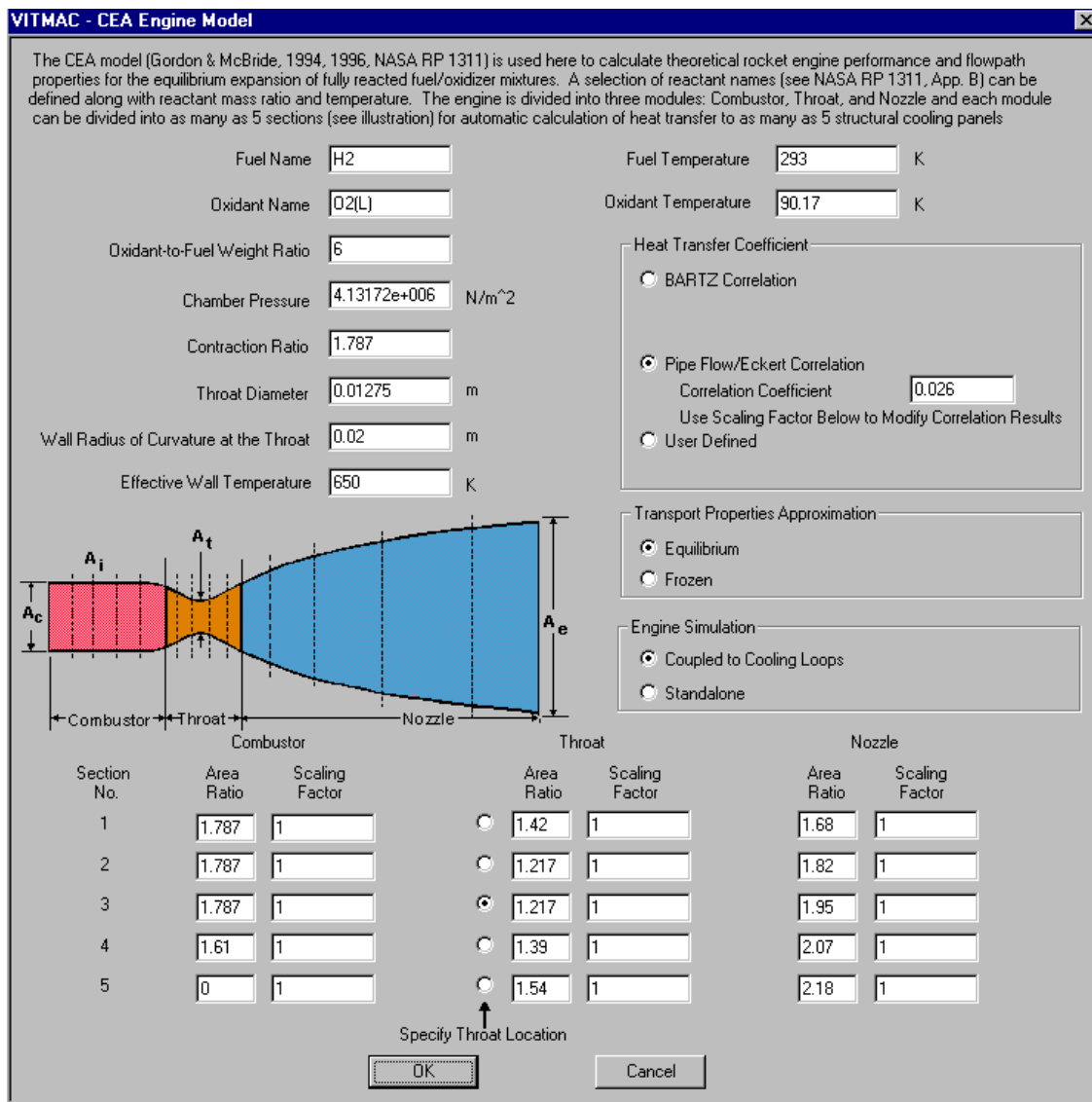


Figure 3.3 VITMAC CEA Dialog Box

3.2 Comparison to Rocket Calorimeter Chamber Experiment

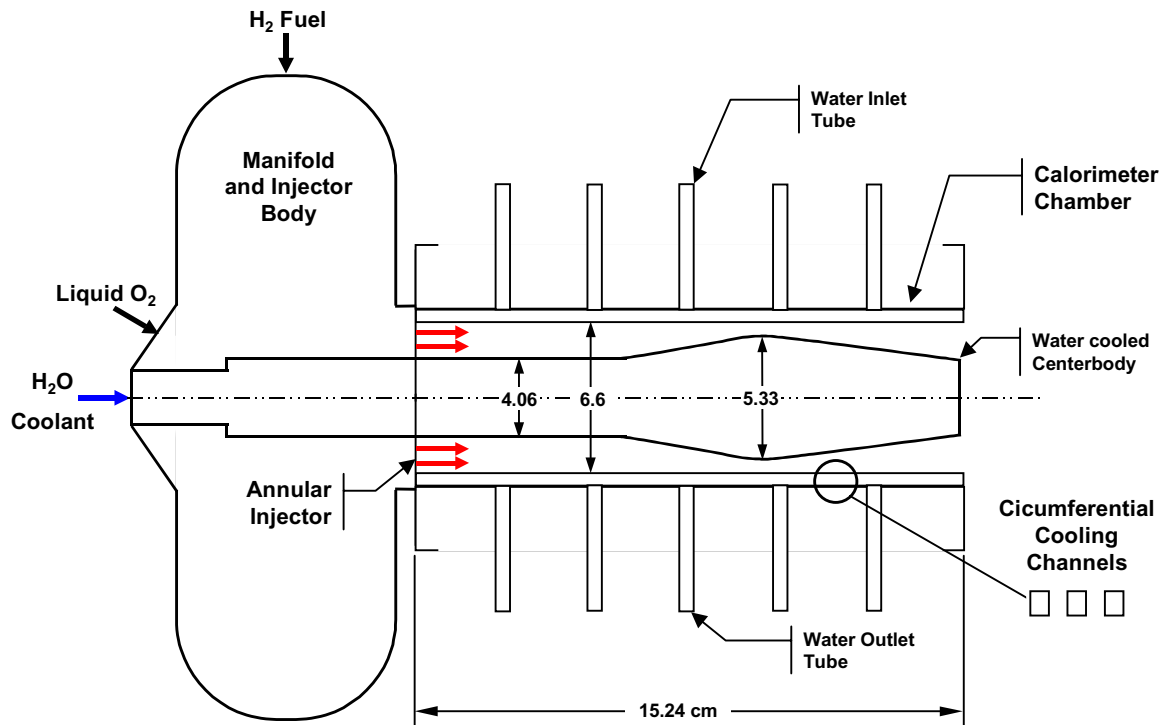


Figure 3.4 Schematic of Plug-Nozzle Rocket Engine Experiment

The rocket engine experiments of Quentmeyer and Roncace (1993)¹⁰, provide an excellent dataset for verifying the VITMAC rocket engine flowpath and heat transfer methodology just described. The tests used a unique plug-nozzle calorimeter chamber illustrated schematically in Figure 3.4. As shown in the figure, the subscale engine used an annular injector and combustion chamber fueled with gaseous hydrogen and liquid oxygen. The hot-gas flow path is formed by a water-cooled plug-nozzle as the inner surface and a highly instrumented constant diameter calorimeter as the outer wall. The copper calorimeter consisted of numerous 0.2 in circumferential cooling channels, which were individually manifolded and instrumented for inlet and outlet temperature measurements. Also numerous thermocouples were imbedded in the calorimeter structure to infer hot gas wall temperature. Experiments were performed at a chamber pressure of 600 psi (4.14 MPa) and an oxidizer/fuel mixture ratio of 6.0. Hot wall heat flux, at various axial stations, was deduced from the coolant water temperatures and flow rates and the authors calculated a heat transfer coefficient from estimated gas adiabatic wall temperature and measured surface temperature. For this single (but repeated) operating condition, the experiments provide a complete data set of heat transfer coefficient and wall temperatures from the injector through the 15° annular nozzle. Comparisons of predictions follow a brief discussion of the VITMAC thermal model for this interesting system.

¹⁰ Quentmeyer, R.J. and E. A. Roncace, "Hot-Gas-Side Heat Transfer Characteristics of Subscale, Plug-Nozzle Rocket Calorimeter Chamber, NASA Technical Paper 3380, July, 1993.

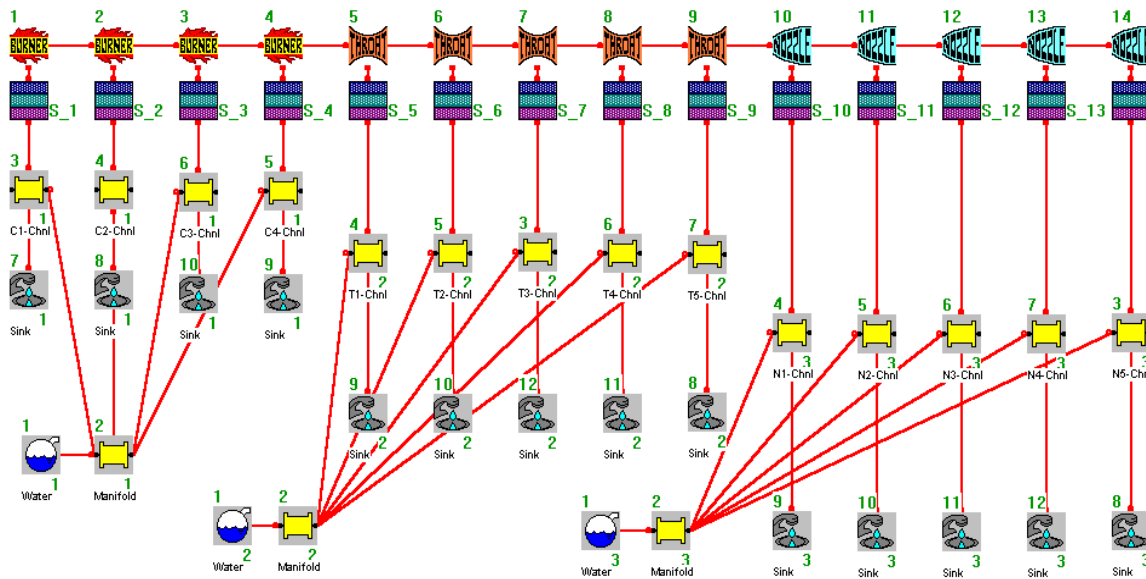


Figure 3.5 VITMAC Rocket Engine Cooling Network

Figure 3.5 shows the VITMAC cooling network utilizing the CEA model capability to simulate the experimental system. In this case, the engine flowpath is divided into 4 sections for the combustion chamber, 5 sections for the throat region and 5 sections for the nozzle. Each engine section imposes the predicted hot-side heat transfer on a cooling panel, with internal water cooling, designed to model each part of the calorimeter. As depicted in the VITMAC schematic, each circumferential section is cooled by a separate water “leg” supplied by and with flow rate controlled by a pressurized source. Figure 3.3 presented earlier defines the VITMAC CEA input parameters and Figure 3.6 below, presents the predicted engine flowpath properties and heat transfer. The input parameters mimic the specified test conditions and test geometry described above. VITMAC results of Figure 3.6 depict the Mach number, adiabatic wall temperature, cold wall heat transfer coefficient and the wall heat flux along the flowpath. As expected, the heat transfer is a maximum in the throat and decreases upstream toward the injector and downstream through the nozzle.

Model results for hot-side heat transfer coefficient and wall temperature are compared to the respective datasets in Figures 3.7 and 3.8. VITMAC heat transfer results (Figure 3.7) are presented for both heat transfer models, the Pipe flow-Eckert and the Bartz correlation. The range shown for the datasets represent multiple test runs with two different injector faceplate designs and are representative of the run-to-run variation in a test of this type. The heat transfer results illustrate that the Pipe-flow-Eckert correlation compares somewhat better to the data than the Bartz correlation especially in the expanding flow region of the nozzle. Both correlations are within the data range in the throat region. Both heat transfer models, however, significantly overpredict the heat transfer in the combustion chamber, perhaps due to nonequilibrium reactive flow effects or separated flow downstream of the injector. Both phenomenon cannot be predicted by an engineering model such as the present one.

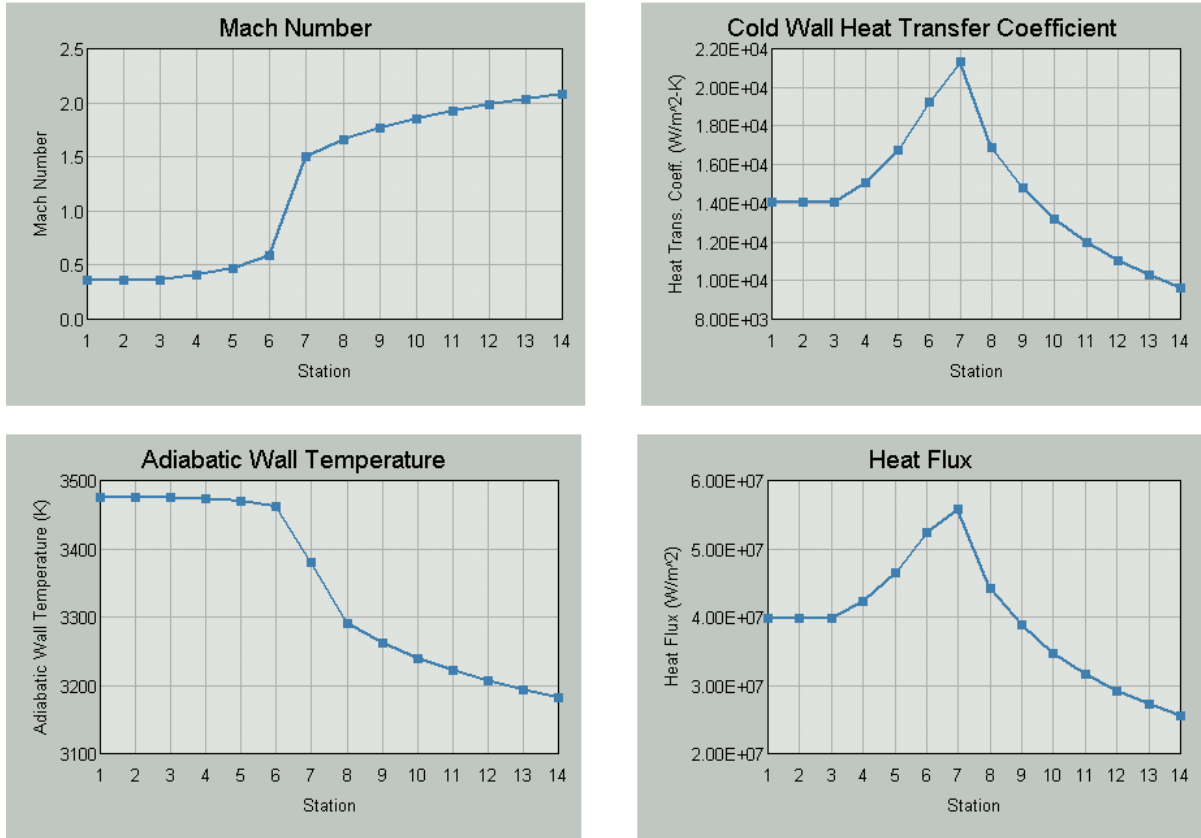


Figure 3.6 VITMAC Rocket Engine Cooling Network Flowpath Results

It also should be pointed out that the present results are calculated with equilibrium gas equation-of-state effects (an option in CEA) for the Pipe-flow-Eckert model and for frozen gas model with the Bartz model. It is found that the opposite gas models in each case significantly overpredict the data. For theoretical reasons, it is believed that equilibrium gas flow properties are more appropriate but the Bartz correlation utilizes approximations for transport properties which would indicate that frozen gas properties are more appropriate for its use.

Finally, model predictions for hot wall temperatures, hot-side and cold-side, are presented in Figure 3.8 along with flow adiabatic wall temperature and the coolant temperature, for comparison. The comparison with the experimental data, also shown, follows the heat transfer coefficient discussion and exhibits a reasonably good prediction, especially within, and downstream of, the throat. It is notable that the prediction for hot wall temperature is well within 100° C of the data even within the combustor region.

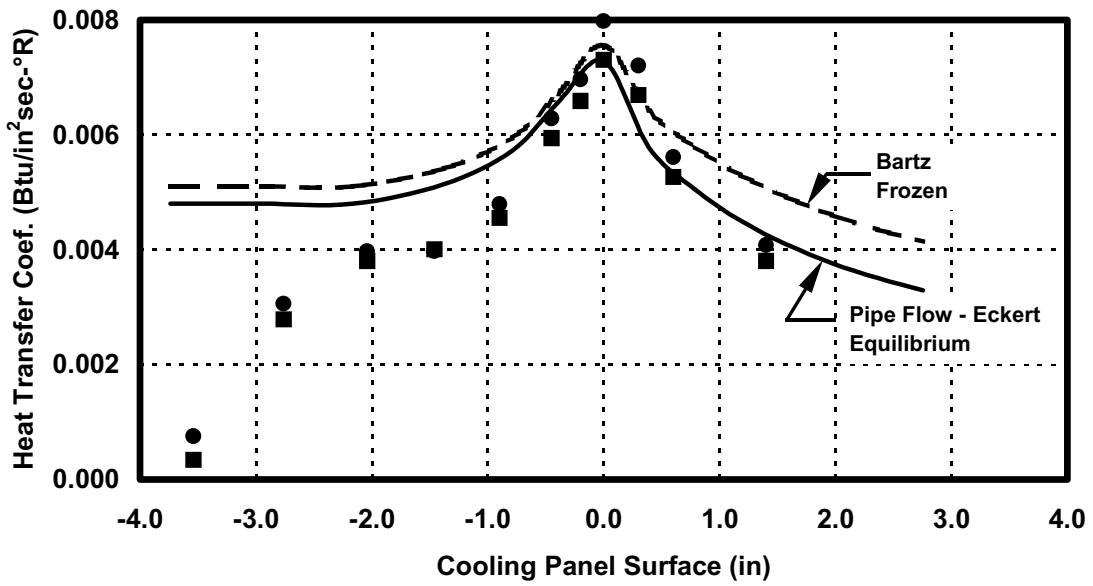


Figure 3.7 VITMAC-CEA Heat Transfer Prediction Comparison to Subscale, Plug Nozzle Rocket Calorimeter Chamber Results

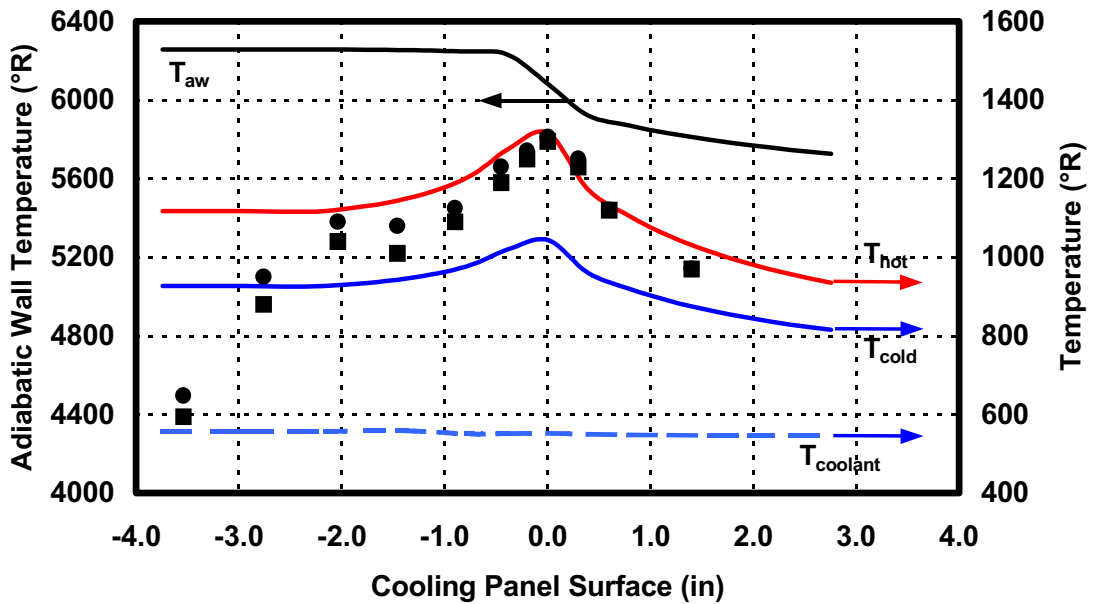


Figure 3.8 VITMAC-CEA “Hot-Wall” Temperature Prediction Comparison to Subscale, Plug Nozzle Rocket Calorimeter Chamber Results

3.3 Comparison to Rocket Calorimeter Chamber Experiment for LOX/Kerosene

Experimental data is also available for a subscale rocket engine experiment that utilizes a hydrocarbon fuel to further validate the VITMAC CEA rocket engine model. The experiment of Masters, Armstrong and Price (1988)¹¹ was primarily designed to examine high pressure kerosene combustion with a “zoned-combustion” injector designed to reduce chamber wall heat transfer. VITMAC-CEA cannot currently model zoned combustion, but a significant part of the experiments were conducted to a conventional uniform injector face which provides the opportunity to compare model results for a hydrocarbon fuel system.

The experiment utilized the same subscale rocket engine test facility as described above with a similar calorimeter chamber design for measuring hot side heat transfer. In contradistinction to the previous plug-flow nozzle, however, the present experiments used a conventional combustion chamber and bell nozzle. Hot-side heat transfer was inferred from the water cooled calorimeter in much the same way as employed by Quentmeyer and Roncace above. VITMAC predictions for the heat transfer coefficient at the all-important throat region are compared to the experimental data in Figure 3.9 below. Two sets of data are presented. The original data and heat transfer data modified to account for the presence of a “soot layer” on the inside surface of the engine. The data modification (see Masters et al., 1988) is made by the authors based on “previous experience” with hydrocarbon fueled rocket chamber. The Pipe-flow-Eckert model compares very well to the unmodified data over a range of operational mixture ratios—less well with the soot-modified heat transfer data. The Bartz model compares almost as well to the unmodified heat transfer coefficient data, except at the higher, near stoichiometric mixture ratios. Data is not reported in this case for the hot-side wall temperature so a more complete comparison is not possible.

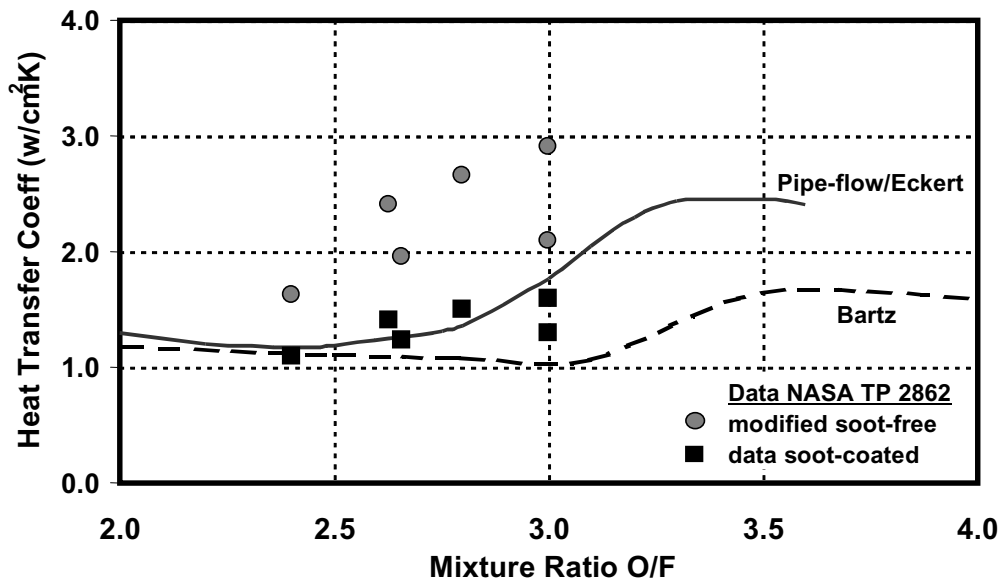


Figure 3.9 VITMAC-CEA “Hot-Wall” Heat Transfer Prediction Comparison to LOX/RP1 Rocket Calorimeter Chamber Results

¹¹ Masters, P. A., E. S. Armstrong, H. G. Price, “High-Pressure Calorimeter Chamber Tests for Liquid Oxygen/Kerosene (LOX/RP1) Rocket Combustion,” NASA Technical Paper 2862, 1988.

3.4 Comparison to Hydrogen-Oxygen Rocket with Liquid Hydrogen Cooling

Experimental data is also available for a subscale rocket engine experiment that uses axial coolant passages and cryogenic hydrogen as the coolant to further validate the VITMAC CEA rocket engine model. The experiment of Schacht and Quentmeyer (1973)¹² was designed to investigate coolant-side heat transfer rates for, at the time, a novel use of cryogenic fuel as a coolant. In addition to testing the new engine heat transfer capability, this experiment provides a measure of VITMAC's ability to treat coolant at cryogenic conditions.

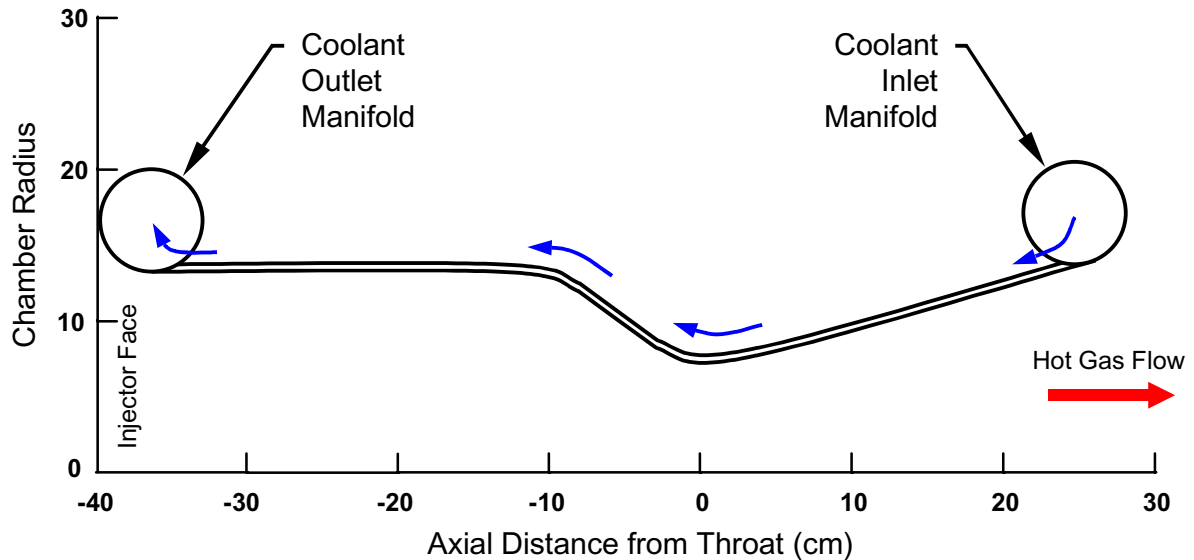


Figure 3.10 VITMAC-CEA “Hot-Wall” Heat Transfer Prediction Comparison to Hydrogen Fueled Rocket Experiment

The experiment utilized a subscale rocket engine test facility with an axial flow coolant scheme shown schematically in Figure 3.10. Stainless steel “oblong-shaped” coolant channels (150 in number) of approximately 0.5 cm made up the inner surface of the thrust chamber and transferred liquid hydrogen from an inlet manifold at the bell housing exit to an outlet manifold at the injector face. Measurements were taken, at a number of engine operating conditions, of wall temperature at a few axial stations and coolant temperature at a range of axial locations. A VITMAC simulation was constructed to mimic the chamber geometry and coolant flow rates and results are compared to the experimental data for an engine operating condition fueled by gaseous hydrogen/liquid oxygen at a mixture ratio of 5.579 which resulted in a chamber pressure of 2.108 MPa. A separate liquid hydrogen coolant loop simulated the experimentally measured flow rate of 5.38 kg/sec. The VITMAC results presented here used the “Pipe-flow-Eckert” hot-side heat transfer model modified by the variation in correlation constant (C) reported by the authors which was based on previous experience with the engine testbed.

¹² Schacht, R. L., R. J. Quentmeyer (1973), “Coolant-side Heat Transfer Rates for a Hydrogen-Oxygen Rocket and a New Technique for Data Correlation,” NASA Technical Note TN D-7207, March, 1973.

Model results are compared to measured temperatures in Figure 3.11 below—the data range indicated on the figure is reported by the authors based on repeated tests at similar operating conditions. As indicated, the VITMAC predictions compare well to the data at the three instrument stations near the throat and within the nozzle. The model under predicts the combustion chamber wall temperatures by about 150 to 300 °K. The measured coolant temperatures from nozzle inlet through the injector outlet are predicted reasonably well indicating that the overall energy balance—hot-side to cold-side—is successfully modeled.

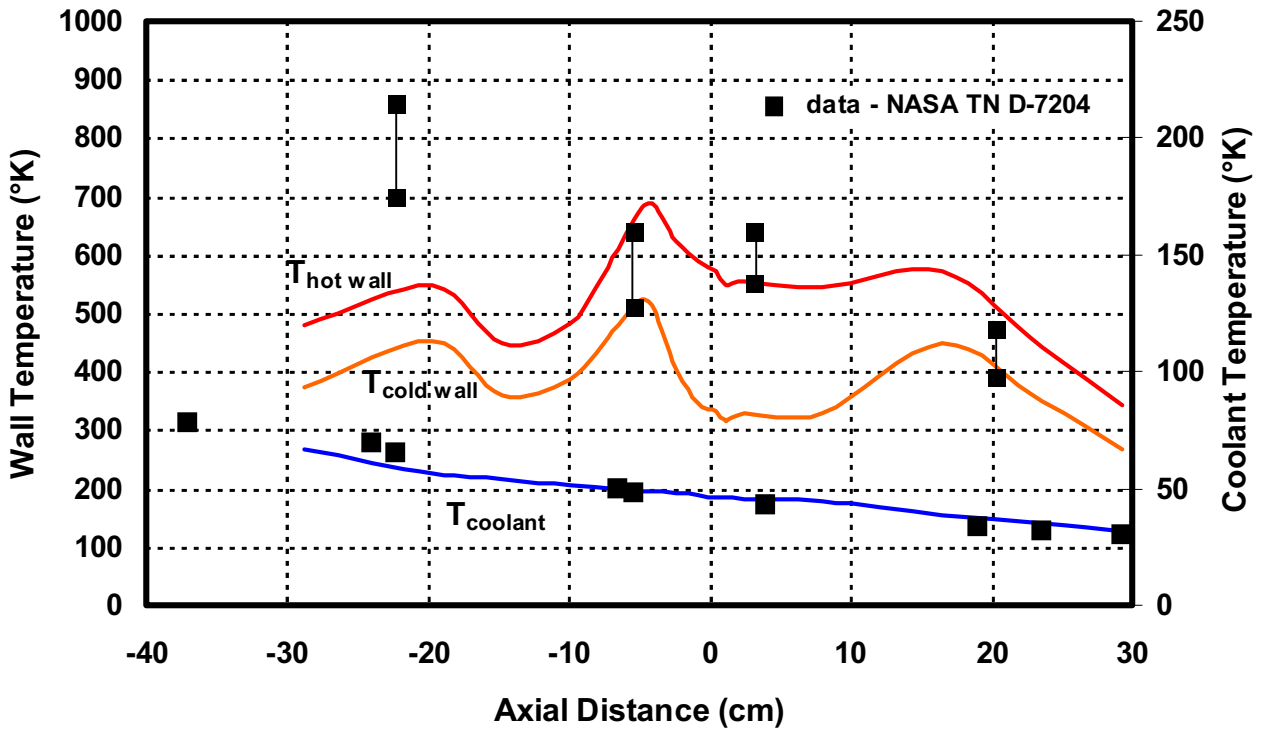


Figure 3.11 VITMAC-CEA “Hot-Wall” Heat Transfer Prediction Comparison to Hydrogen Fueled Rocket Experiment

4. VITMAC RJPA Scramjet Engine Flowpath and Heat Transfer Model

Following the approach, just described for CEA, the RJPA scramjet model of Billig et al.¹³ was linked to VITMAC in a similar manner, with emphasis on the automatic definition of heat transfer to cooling panel surfaces. A user interface was implemented for RJPA which accounts for the extensive input parameter list needed for RJPA operation. Briefly, the RJPA provides the flow conditions at the inlet, diffuser, combustor, and nozzle exit given the operating conditions of the scramjet engine. The VITMAC implementation uses these properties with the engineering level heat transfer models described above to define the “hot-structure” convective heat transfer to representative inlet, combustor, nozzle and cowl surfaces. RJPA does not provide a complete set of gas thermophysical properties so the heat transfer relations are somewhat modified from those given above. In particular, the Bartz combustion gas approximations for gas viscosity and Prandtl No. are used to evaluate properties at the Eckert reference condition, rather than the first principals gas mixture properties evaluated by CEA. Using this approach, verification tests have been performed comparing VITMAC-RJPA heat transfer predictions with NASP program scramjet experimental data. The NASP scramjet engine Direct-Connect-Combustor (DCC), experiments performed by the Applied Physics Lab, as well as the more recent NASP Direct Connect Arcjet Facility (DCAF) experiments have been examined. Comparisons of flowpath heat transfer predictions with these databases are presented here.

4.1 Model Linkage And Heat Transfer Formulation

In addition to rocket engines, there is interest in coupling a ramjet/scramjet model to VITMAC for automatic evaluation of hot-side heat transfer with coupling to VITMAC structural/cooling panel modules. The approach implemented in VITMAC uses the RJPA model of Billig coupled with accepted engineering heat transfer correlations. As suggested for use with a generic VITMAC cooling network, Figure 4.1 below, the implementation follows the approach used for the CEA model:

- Automatically calculate heat transfer to engine cooling panel sections.
- engine divided into modules: inlet, combustor, nozzle and cowl
- calculate h_{aver} and $(T_{aw})_{aver}$ and automatically connect to structural surface “cooling panel” for up to 5 structures per engine module (15 for the Cowl).

¹³ Pandolfini, P.P., and Friedman, M.A., (1992), "Instructions for Using the Ramjet Performance Analysis (RJPA) IBM-PC Version 1.24," JHU/APL AL-92-P175, June 1992

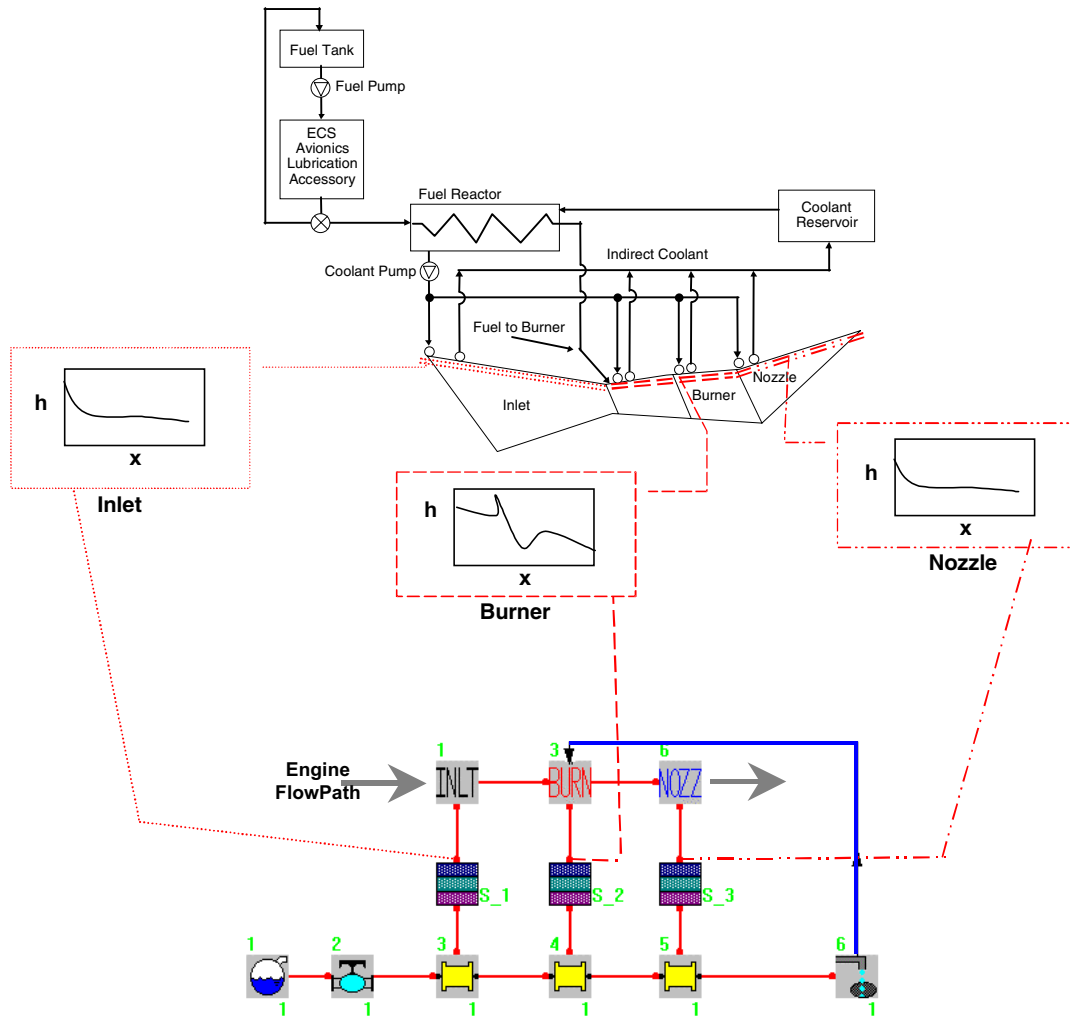


Figure 4.1 Generic Scramjet Cooling Network

The structure heating rate at any time or iteration is given by the usual convective heat transfer relation:

$$\dot{Q} = h_{\text{aver}} A_{\text{pan}} (T_{\text{aw}} - T_{\text{wall}}) \quad (6)$$

where h_{aver} is the heat transfer coefficient averaged over the section, A_{pan} is the surface area of the section (top surface area of structural component), T_{aw} is the adiabatic wall temperature averaged over the section and T_{wall} is the structure top surface wall temperature calculated by VITMAC.

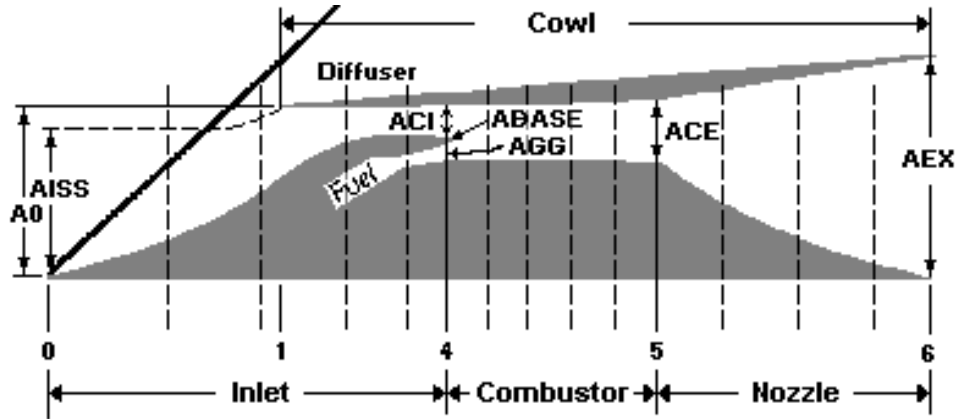


Figure 4.2 Definition of Scramjet FlowPath Modules and “Cooling Panel” Subsections

Figure 4.2 shows the engine flowpath with the principal modules and the separation of each module into up to 5 sections for definition of average heat transfer to the corresponding “cooling panel” (i.e. structural surface and underlying flow channel). The A’s refer to engine cross-sectional areas which follow the RJPA definition and are used in the RJPA calculation.

Defining Equations: The RJPA model calculates the freestream flow conditions and the engine operating conditions necessary to determine the “hot gas” flowpath quantities at various stations through the engine. So for each section RJPA provides the flow properties (but not including transport properties) at the end of the section, call this the section exit station, i.e. inlet or diffuser exit, combustor exit and nozzle exit.

For each station RJPA provides the pressure, p , the temperature, T , enthalpy, i , etc.(normal notation for velocity, U , temperature, T , Mach No., M , Specific Heat C_p etc.); and also the same quantities at the total conditions, call them p_o , i_o , T_o etc. Then the Eckert reference enthalpy is calculated from:

$$i_{\text{ref}} = 0.5(i + i_{\text{wall}}) + 0.22(\text{Pr}_{\text{ref}})^{1/3} (i_o - i) \quad (7)$$

where a “reference” Prandtl No., Pr_{ref} ; is calculated using the Bartz relation which follows:

$$\text{Pr}_{\text{ref}} = \frac{4\gamma_{\text{ref}}}{9\gamma_{\text{ref}} - 5} \quad (8)$$

Other gas properties at the reference conditions are calculated from internal calls within RJPA to its equation of state routine (NOTS), and reference transport properties are calculated from:

$$\mu_{\text{ref}} = 5.6 \cdot 10^{-8} (\mathcal{M})^{1/2} (T_{\text{ref}})^{0.6} \quad (\text{lbm}/(\text{ft}\cdot\text{s})) \quad (9)$$

$$k_{\text{ref}} = \frac{Cp\mu_{\text{ref}}}{Pr_{\text{ref}}} \quad (10)$$

The adiabatic wall enthalpy is calculated using the turbulent boundary layer relation:

$$i_{\text{aw}} = i + (Pr_{\text{ref}})^{1/3} (i_o - i) \quad (11)$$

The required adiabatic wall temperature is also determined from calls to the NOTS equation of state routine in RJPA (i.e. $T_{\text{aw}} = T(p, I_{\text{aw}})$). Finally, the heat transfer coefficient for each station (diffuser exit, combustor exit, nozzle exit) is:

$$h = C \frac{k_{\text{ref}}}{D_h} \left(\frac{\rho_{\text{ref}} U D_h}{\mu_{\text{ref}}} \right)^{0.8} (Pr_{\text{ref}})^{0.34} \quad (12)$$

Define $h = \tilde{h} / D_h^{0.2}$, so:

$$\tilde{h} = C k_{\text{ref}} \left(\frac{\rho_{\text{ref}} U}{\mu_{\text{ref}}} \right)^{0.8} (Pr_{\text{ref}})^{0.34} \quad (13)$$

$C = 0.026$ is the Correlation Constant input value and D_h is a hydraulic diameter scale factor for each section.

Both \tilde{h} and T_{aw} are weighted over each engine section to account for expected flowpath variations as follows:

INLET: Assume $T_{\text{aw}} = \text{constant}$, given by inlet ramp conditions and $D_h = .011 X$ where X is the running length along the inlet ramp for each inlet section. For the “no shock” option, linearly vary \tilde{h} , T_{aw} from freestream conditions to the diffuser exit conditions.

COMBUSTOR: Linearly vary \tilde{h} , T_{aw} from diffuser exit to combustor exit

NOZZLE: Vary \tilde{h} , T_{aw} based on section average nozzle flow conditions.

COWL: Associate \tilde{h} , T_{aw} to corresponding inlet, combustor or nozzle section

The linear weighting is based on the “fraction of component” input values which are interpreted as the fractional distance down the flow path. Then the heating rate to each structural component section is given by:

$$\dot{Q} = h_{\text{aver}} A_{\text{pan}} (T_{\text{aw}} - T_{\text{wall}}) \quad (14)$$

where:

$$h_{\text{aver}} = \tilde{h} / D_h^{0.2}$$

So for each component, consisting of up to 5 sections, the above formulation provides an average T_{aw} and h_{aver} for each section to transfer to VITMAC.

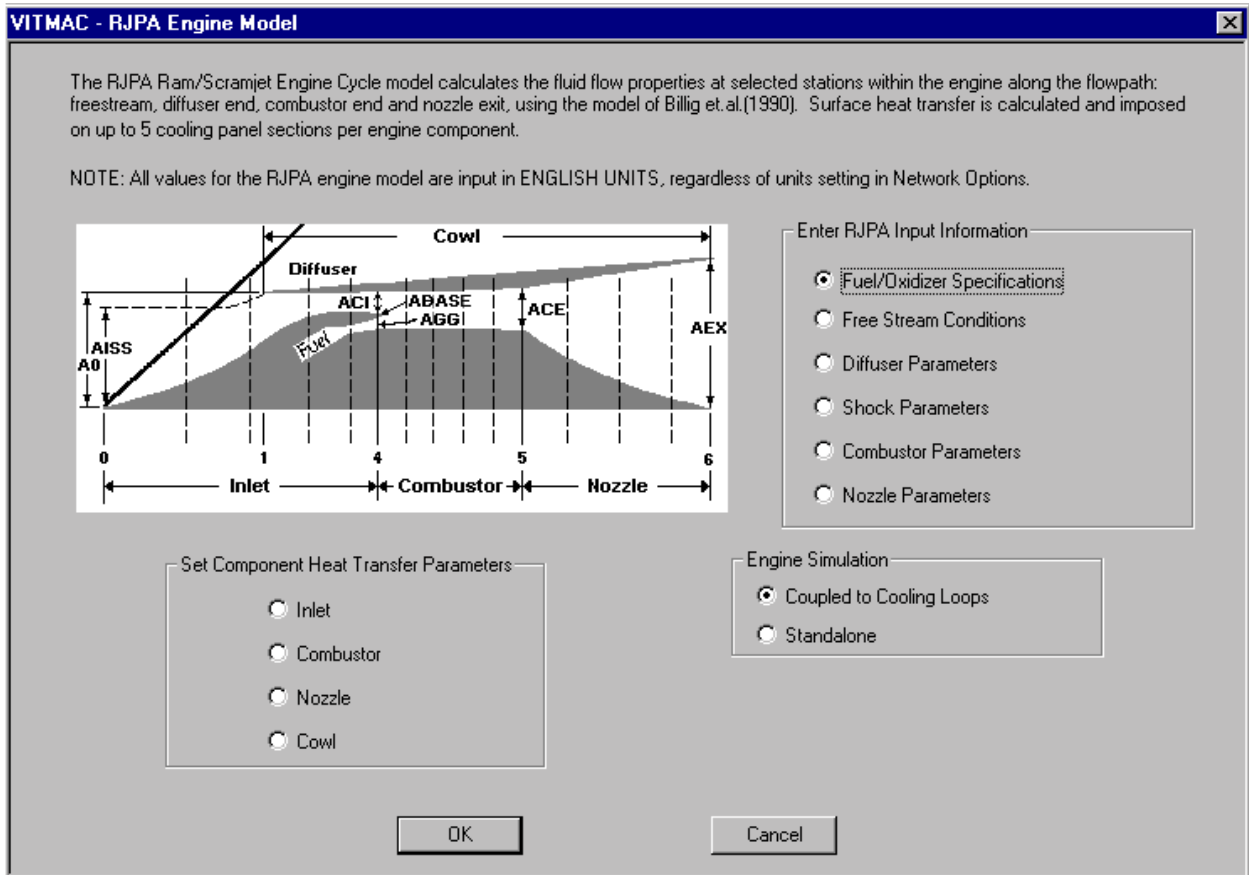


Figure 4.3 VITMAC R/JPA Dialog Box

The approach, just described, is implemented by the VITMAC user by defining engine descriptive parameters, fuel and oxidizer, gas generator conditions, combustor and nozzle areas etc. These are input through the VITMAC GUI using the dialog box contained in Figure 4.3. The radio button options displayed there open dialog boxes which are used to specify the numerous engine parameters required by R/JPA, categorized by function and following the R/JPA input categories, as follows:

- Fuel/ Oxidizer type
- Free Stream Conditions
- Diffuser parameters and R/JPA flowpath Shock Parameters
- Combustor Parameters, and
- Nozzle Parameters

User options for each of these Input specifications are presented below. In addition, heat transfer parameters are set by selecting the radio buttons for each engine component as shown on the main window in Figure 4.3 and as also described below. The user may use the “built-in” correlation, unmodified or with global or local scaling factors, or “user defined” heat transfer coefficients may be defined for each section. In addition, optional “CFD Input values” may be provided for both adiabatic wall temperature and heat transfer coefficient.

Also shown on the RJPA engine dialog box are the Engine Simulation radio buttons for running the engine simulation with coupling to a VITMAC cooling circuit or as “standalone” with no cooling loops needed. It should be mentioned, that all of the RJPA functionality is provided through the RJPA Input Information. All input variables use the original RJPA units (see RJPA User Guide) thereby departing from the VITMAC practice of providing user selection of English or SI units. The User is cautioned that RJPA is a sophisticated research tool and requires a degree of experience to run successfully. It is best run “standalone” with detailed examination of the RJPA output file before coupling to a VITMAC cooling circuit.

Fuel/Oxidizer Specification: The following fuel and oxidizer combinations have been implemented for User selection through a dialog box:

Fuel	Oxidizer
Hydrogen, H ₂	Oxygen, O ₂
Hydrogen, H ₂	Air, O ₂ +N ₂ +Ar
JP Fuels, JP4, JP5, JP7, JP8	Air, O ₂ +N ₂ +Ar
General Hydrocarbons C _x H _y	Air, O ₂ +N ₂ +Ar
User-defined	User-defined

These options are simply selected from the list (general hydrocarbons require an enthalpy of formation for x moles of C and y moles of H) and the fuel/oxidizer mixture ratios are set through RJPA parameters specified in the combustor dialog box presented later. Finally, a “User-Defined” Fuel/Oxidizer mixture may be selected which reads a text file containing the parameters required by RJPA in card image format. The experienced RJPA user may modify this file or create her own to define any fuel/oxidizer combination allowed by RJPA.

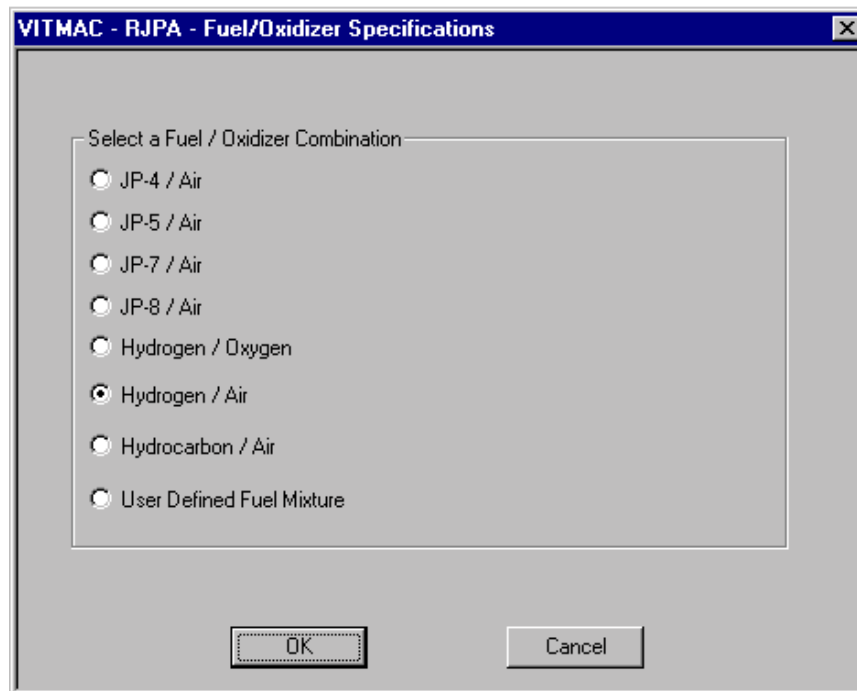


Figure 4.4 Fuel/Oxidizer Specification Dialog Box

The simplified molecular formulas for JP fuels have been determined from an available fuel data set and the composite Enthalpies of Formation needed for RJPA calculations have been included below.

JP4:

C5H12	N-PENTANE	0.0746285
C8H18	N-OCTANE	0.12255
C12H26	N-DODECANE	0.0758131
C7H16	2-METHYLHEXANE	0.268684
C8H18	2-METHYLHEPTANE	0.141396
C9H20	2-METHYLOCTANE	0.0839974
C7H8	TOLUENE	0.0584751
C8H10	META-XYLENE	0.0507215
C6H6	BENZENE	0.068921
C7H14	METHYLCYCLOHEXANE	0.0548137

JP5:

C10H22	N-DECANE	0.15564
C11H24	N-UNDECANE	0.05134
C12H26	N-DODECANE	0.37254
C10H14	T-BUTYLBENZENE	0.13138
C13H28	N-TRIDECANE	0.13348
C11H10	1-METHYLNAPHTHALENE	0.02345
C14H30	N-TETRADECANE	0.09251
C15H32	N-PENTADECANE	0.03966

JP7:

C10H20	N-DECANE	0.00343085
C8H16	ETHYLCYCLOHEXANE	0.00163007
C6H6	BENZENE	0.0517008
C11H10	1-METHYLNAPHTHALENE	0.00159571
C11H24	N-UNDECANE	0.159843
C12H26	N-DODECANE	0.493614
C6H12	METHLCYCLOPENTANE	0.00637273
C13H28	N-TRIDECANE	0.194704
C14H30	N-TETRADECANE	0.0644494
C15H32	N-PENTADECANE	0.0199546

JP8:

C7H14	METHYLCYCLOHEXANE	0.075
C8H10	META-XYLENE	0.07
C8H18	N-OCTANE	0.13
C10H22	N-DECANE	0.156
C10H14	BUTYLBENZENE	0.055
C10H14	ISOBUTYLBENZENE	0.055
C10H14	T-BUTYLBENZENE	0.055
C12H26	N-DODECANE	0.175
C11H10	1-METHYLNAPHTHALENE	0.052
C14H30	N-TETRADECANE	0.112
C16H34	N-HEXADECANE	0.065

Simplified Molecular Formulas and Enthalpies of Formation:

	C	H	Enthalpy (cal/mole)
JP4	10	20.32116	-52121.86535
JP5	10	20.29812	-57301.3737
JP7	10	20.94739	-61109.83507
JP8	10	15.70405	-27805.36363

Methane CH₄ or propane C₃H₈ are intended to be used as the default fuel for C_xH_y + Air input selection in the VITMAC/RJPA linkage.

Free Stream Parameters: Various RJPA options for defining freestream conditions are provided in the dialog box shown in Figure 4.5—various flight parameter combinations as well as test facility parameters are possible. Various other RJPA area parameters such as; reference area, inlet capture area, and dual-mode scramjet gas generator inlet capture area, along with the freestream oxidizer to fuel ratio (use large default value for pure air), are also input through this dialog box.

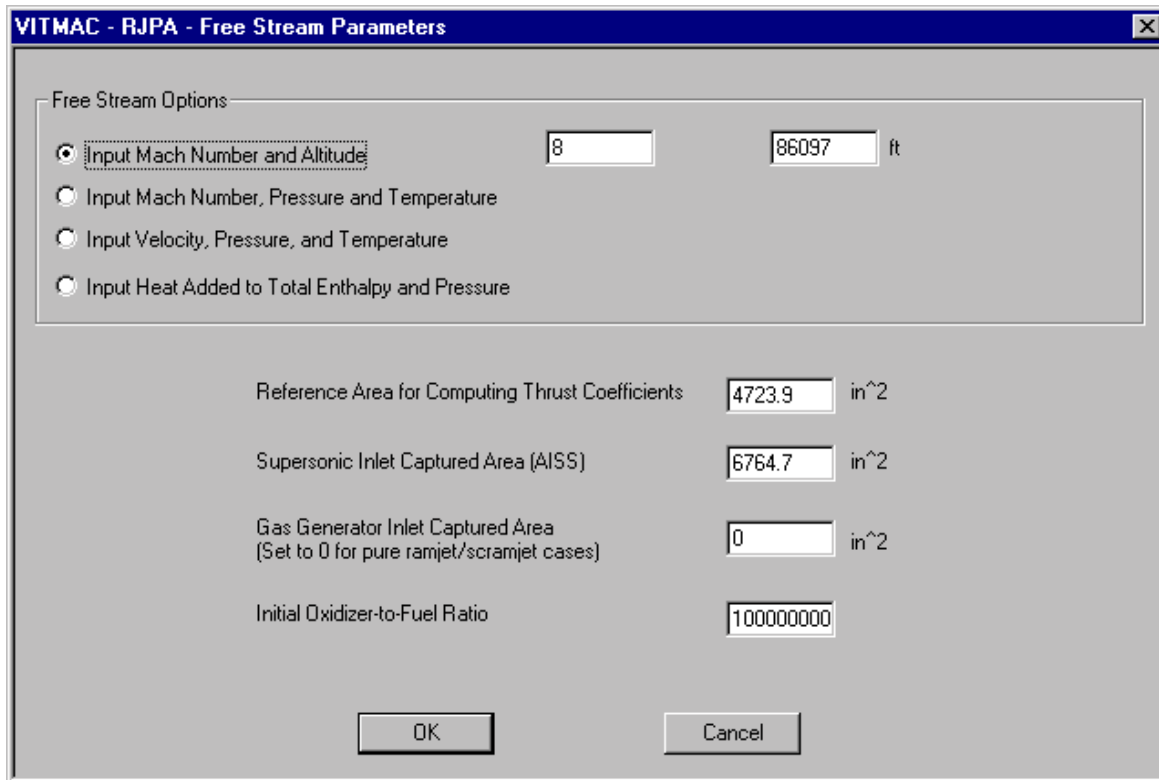


Figure 4.5 Free Stream Condition Dialog Box

Diffuser Parameters: The RJPA diffuser module models the partial compression of the airstream prior to entering the combustor using a number of options selected through the dialog box presented in Figure 4.6. Diffuser exit conditions are defined through a combination of selected diffuser exit area (same as combustor entrance area, ACI), pressure or Mach No. and a diffuser efficiency parameter. Kinetic energy efficiency, process efficiency, total pressure recovery and the “Billig” compression efficiency parameters (see RJPA User Guide) may be selected.

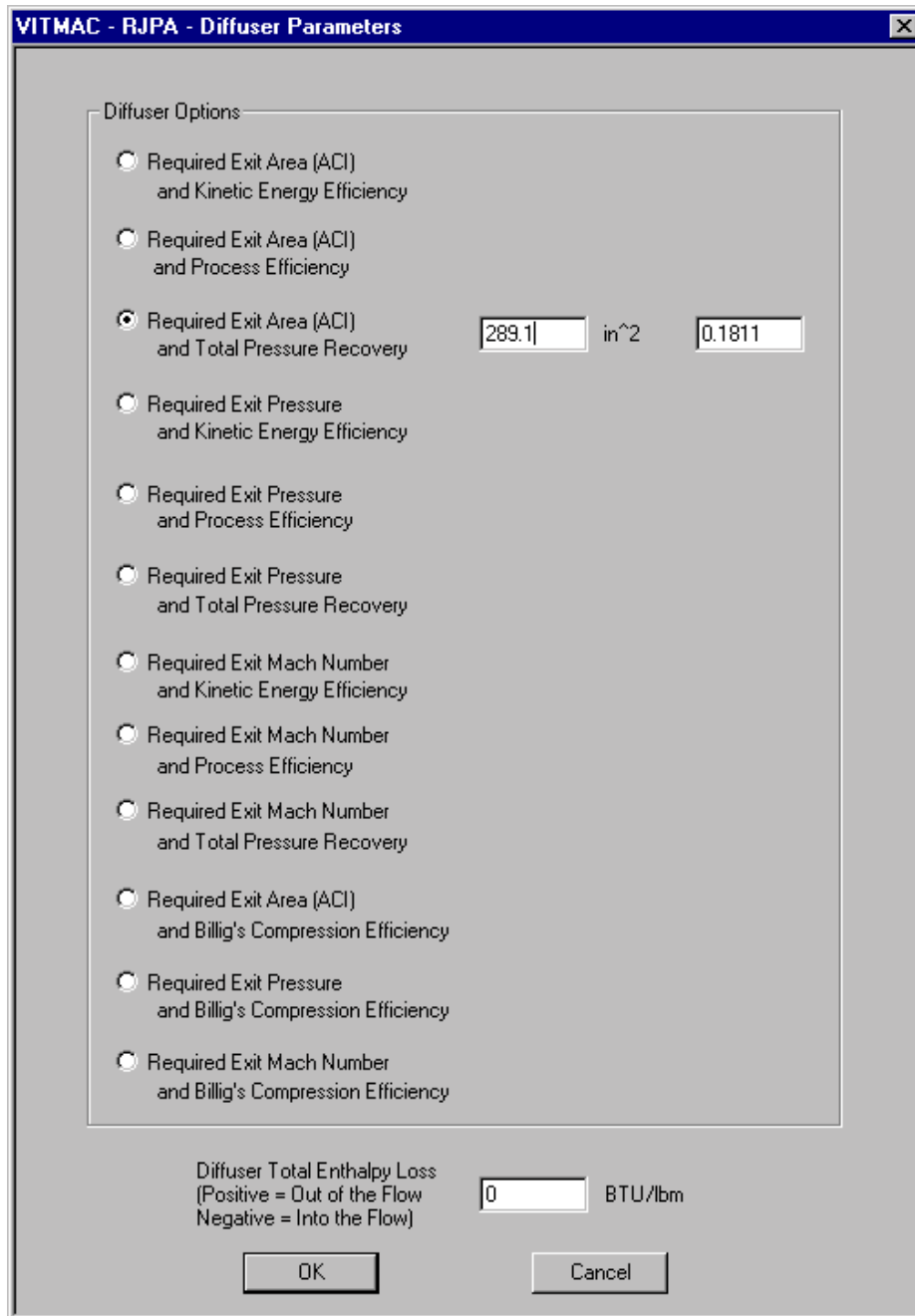


Figure 4.6 Diffuser Parameters Dialog Box

RJPA Shock Parameters: Under some operating conditions an oblique or normal shock may reside in the isolator duct upstream of the combustor and RJPA includes its Shock module to model this phenomena. The model simulates the equilibrium gas “jump” conditions for an oblique or normal shock from diffuser exit conditions to combustor entrance conditions. The dialog box shown in Figure 4.7 provides the User with the RJPA input options for this module.

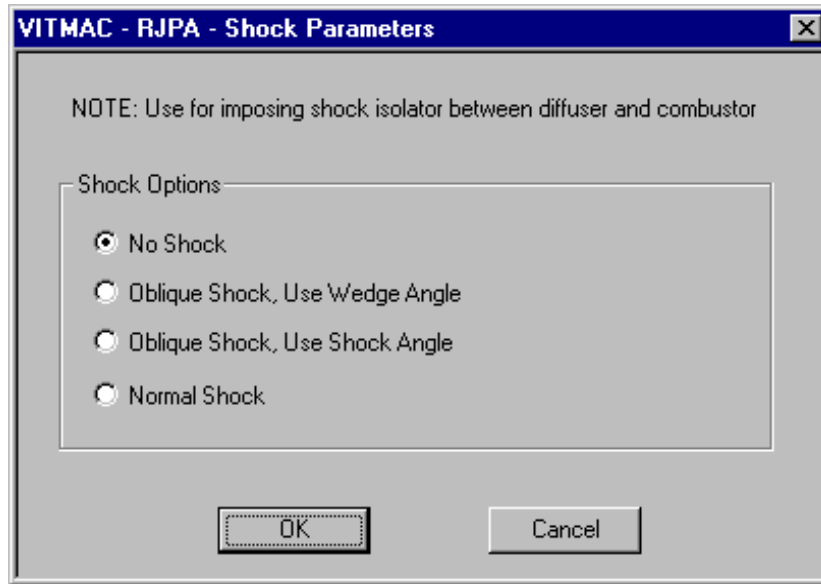


Figure 4.7 RJPA Shock Dialog Box

Combustor Parameters: The Combustor model is the heart of RJPA which simulates the supersonic or subsonic combustion of a scramjet or ramjet engine given the parametric specification contained in the dialog box of Figure 4.8. All of the RJPA combustor options can be selected through radio buttons and selection or data boxes, including specified combustor area or pressure with/without entropy limit constraint, supersonic or subsonic combustion, wall shear and heat loss parameters and “gas generator” outflow specifications. Various required area, pressure and injection angle parameters can also be specified. For use in VITMAC, three “gas generator” options have been added to treat general gas generator, dual mode scramjet, or gaseous fuel injection. These include specifying the usual RJPA gas generator parameters (enthalpy, molecular weight, density, temperature and velocity) or calculating these parameters using CEA (see previous section) or using analytical expressions for ideal gas expansion to a specified Mach number. Default values simulate hydrogen gas injection at an equivalence ratio (relative to stoichiometric fuel/air ratio) of 1.

VITMAC - RJPA - Combustor Parameters

RJPA Combustor Option:

Combustion Type: Supersonic Subsonic

Gas Generator Outflow Quantities: Input RJPA Parameters Calculate from Analytical Expressions Automatically Calculate Using CEA

Base Pressure: psi

Combustor Exit Pressure Guess #1: psi

Combustor Exit Pressure Guess #2: psi

Axial Projection of the Base Area: in²

Combustor Exit Area (ACE): in²

Axial Projection of Diffuser Exit Area (ACI): in²

Gas Generator Exit Area (AGG): in²

Injection Angle of Gas Generator Flow: degrees

Combustor Wall Area: in²

Supersonic Air Inlet Dump Angle (Positive = Inward Toward Centerline): degrees

Stoichiometric Fuel/Air Weight Ratio:

Wall Shear Parameter Option:

Wall Shear Parameter:

Ratio of Diffuser Flow to Total Gas Generator Outflow (Gas Generator Air Plus Fuel):

Ratio of Diffuser Flow to Sum of Diffuser Flow and Gas Generator Air Flow:

Gas Generator Exit Mixture Enthalpy: BTU/lbm

Gas Generator Exit Mixture Molecular Weight: lbm/lbm-mole

Gas Generator Exit Mixture Density: lbm/ft³

Gas Generator Exit Mixture Temperature: R

Gas Generator Exit Mixture Velocity: ft/s

Ratio of Pressures Fore and Aft of the Precombustion Shock:

Heat Loss Through the Combustor Walls (Positive = Out of the Flow, Negative = Into the Flow): BTU/s

OK Cancel

Figure 4.8 Combustor Parameters Dialog Box

Nozzle Parameters: The RJPA Nozzle module expands the combustor outflow to a User specified exit pressure, exit area or to a sonic throat. Expanded flow results are calculated for various Nozzle efficiencies and an arithmetic average of Frozen-to-Equilibrium results is used to calculate engine thrust and specific impulse estimates. The parameters are input through the self-explanatory Nozzle dialog box shown in Figure 4.9.

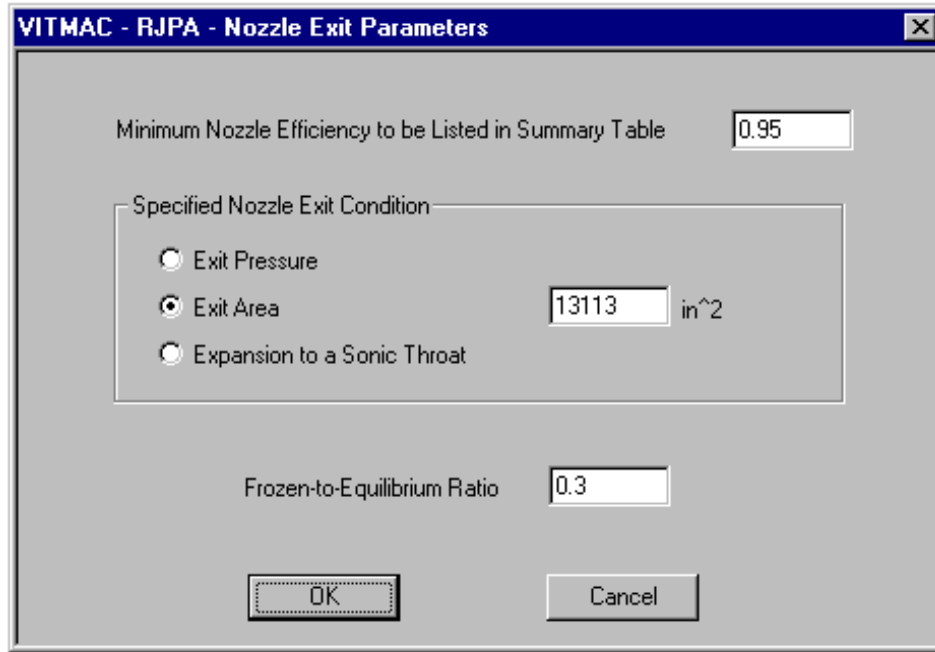


Figure 4.9 Nozzle Parameters Dialog Box

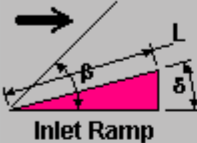
Component Heat Transfer Specification: For heat transfer specification purposes, VITMAC divides the ramjet/scramjet engine into four engine modules, Inlet, Combustor, Nozzle and Cowl, which represent the “hot-structure” encompassing the engine flowpath. Each module can be further divided into up to five VITMAC components (fifteen for the Cowl) which are automatically connected to a VITMAC structure. Each engine module is considered separately and the User may specify the method of heat transfer calculation using the separate input dialog boxes described below.

Inlet Heat Transfer Parameters: The Inlet component represents the hot structure behind the inlet ramp shock through the diffuser. The RJPA shock model is used to provide flow properties behind an oblique shock based on user input of a ramp angle/shock angle, or user selection of no shock or normal shock. A turbulent boundary layer approximation is used to define the effective hydraulic diameter for each inlet component section, as a function of the inlet running length and the fraction of component input values for use in the heat transfer formulation presented above. The heat transfer correlation factor, the effective wall temperature and an additional scaling factor are also user selectable, as shown in Figure 4.10. In addition to the “Built-in” correlation, a “User-defined” option and “CFD Input” option are also provided. The “user-defined” option allows the user to input heat transfer coefficient

values for each section while using the calculated adiabatic wall temperature, while the “CFD Input” option provides for user input of both heat transfer coefficient and adiabatic wall temperature for each section.

VITMAC - Inlet ✕

 The Inlet Component represents the engine "Hot Structure" from the inlet ramp shock through the diffuser. The ramp or shock angle here define the post shock flow quantities for heat transfer estimation purposes and have NO relation to the similar quantities used in the RJPA "Shock" routine.

 **Inlet Ramp**

Shock Options

- No Shock
- Oblique Shock, Use Wedge Angle
- Oblique Shock, Use Shock Angle
- Normal Shock

Inlet "Running" Length, L ft

Heat Transfer Coefficient

- Use Built-in Correlation
 - Correlation Coefficient
- User Defined
- CFD Input Values

Effective Wall Temperature R

Section No.	Fraction of Component	Hydraulic Diameter (ft)	Scaling Factor
1	<input type="text" value="0.5"/>	<input type="text" value="0.1"/>	<input type="text" value="1"/>
2	<input type="text" value="0.5"/>	<input type="text" value="0.1"/>	<input type="text" value="1"/>
3	<input type="text" value="0"/>	<input type="text" value="0.1"/>	<input type="text" value="1"/>
4	<input type="text" value="0"/>	<input type="text" value="0.1"/>	<input type="text" value="1"/>
5	<input type="text" value="0"/>	<input type="text" value="0.1"/>	<input type="text" value="1"/>

Figure 4.10 Inlet Heat Transfer Parameters Dialog Box

Combustor Heat Transfer Parameters: RJPA flow quantities for the Diffuser station and Combustor exit station are used, based on user input selections, to calculate the heat transfer coefficient and adiabatic wall temperature for each of up to five combustor sections. In this case, the “built-in” correlation with user input of correlation constant, effective wall temperature, and section specific hydraulic diameter is used with the above formulation to define the heat transfer coefficient and adiabatic wall temperature at the diffuser exit and combustor exit. For now, a linear variation based on the user input values of “fraction of component”, is used to determine section specific values of both quantities. “User-defined” and “CFD Input” options, described above, are also provided for the combustor components, as shown in Figure 4.11.

In the Combustor component, RJPA flow quantities at the Diffuser exit and Combustor exit are used, along with the hydraulic diameter, to calculate heat transfer parameters (Taw and HTC) for up to 5 sections. Optionally, a user defined HTC may be input below, using Taw calculated from RJPA; or both HTC and Taw may be input from CFD or experimental data.

Heat Transfer Coefficient

Use Built-in Correlation
Correlation Coefficient

User Defined

CFD Input Values

Effective Wall Temperature R

Section No.	Fraction of Component	Hydraulic Diameter (ft)	Scaling Factor
1	<input type="text" value="0.5"/>	<input type="text" value="0.1"/>	<input type="text" value="1"/>
2	<input type="text" value="0.5"/>	<input type="text" value="0.1"/>	<input type="text" value="1"/>
3	<input type="text" value="0"/>	<input type="text" value="0.1"/>	<input type="text" value="1"/>
4	<input type="text" value="0"/>	<input type="text" value="0.1"/>	<input type="text" value="1"/>
5	<input type="text" value="0"/>	<input type="text" value="0.1"/>	<input type="text" value="1"/>

OK Cancel

Figure 4.11 Combustor Heat Transfer Parameters Dialog Box

Nozzle Heat Transfer Parameters: RJPA provides flow quantities at a nozzle exit calculated by expanding the combustor exit flow to a specified area or pressure. To define the flow quantities throughout the nozzle, successive RJPA calculations are performed for section areas based on user input of a total nozzle exit area and section area ratios, as defined in Figure 4.12. The flow quantities, starting at the combustor exit and proceeding downstream section-by-section, are used with the user specified correlation constant, hydraulic diameter and effective wall temperature to define an average heat transfer coefficient and adiabatic wall temperature for each section. An enthalpy loss input parameter for each section is also provided to simulate the effect of heat loss from the nozzle flow on wall heat transfer. As before the “Built-in” correlation approach is used— “User-defined” and “CFD-Input” options are included as well.

The Nozzle component uses RJPA flow quantities at the combustor exit and at various nozzle area ratios (A/A_{exit} as a fraction of the nozzle exit area), to calculate heat transfer parameters (T_{aw} and HTC) for up to 5 Nozzle sections. User defined HTC may be input below (with calculated T_{aw} from RJPA quantities) or both HTC and T_{aw} may be input from CFD or experimental data.

Heat Transfer Coefficient

Use Built-in Correlation
Correlation Coefficient

User Defined

CFD Input Values

Effective Wall Temperature R

Nozzle Exit Area in²

Section No.	A/A _{exit}	Hydraulic Diameter (ft)	Scaling Factor	Enthalpy Loss (BTU/lbm)
1	<input type="text" value="0.5"/>	<input type="text" value="0.1"/>	<input type="text" value="1"/>	<input type="text" value="0"/>
2	<input type="text" value="1"/>	<input type="text" value="0.1"/>	<input type="text" value="1"/>	<input type="text" value="0"/>
3	<input type="text" value="0"/>	<input type="text" value="0.1"/>	<input type="text" value="1"/>	<input type="text" value="0"/>
4	<input type="text" value="0"/>	<input type="text" value="0.1"/>	<input type="text" value="1"/>	<input type="text" value="0"/>
5	<input type="text" value="0"/>	<input type="text" value="0.1"/>	<input type="text" value="1"/>	<input type="text" value="0"/>

OK Cancel

Figure 4.12 Nozzle Heat Transfer Parameters Dialog Box

Cowl Heat Transfer Parameters: The Cowl components are considered somewhat differently than the other engine components since they are considered to be on the other side of the flow path. Presently, in VITMAC Cowl sections take their average flow quantities from the other three engine components and then use the same “Built-in” correlation with specified correlation coefficient, effective wall temperature, hydraulic diameter and scaling factor to determine the adiabatic wall temperature and heat transfer coefficient. For the Cowl sections, the user must define the “connection” using the input matrix shown in Figure 4.13. For example, as shown there, Cowl Section No. 1 uses flow properties from Inlet Section No. 2, Cowl Section No. 2 uses Combustor Section No. 1 etc. As always, “User-defined” and “CFD-Input” options are included as well.

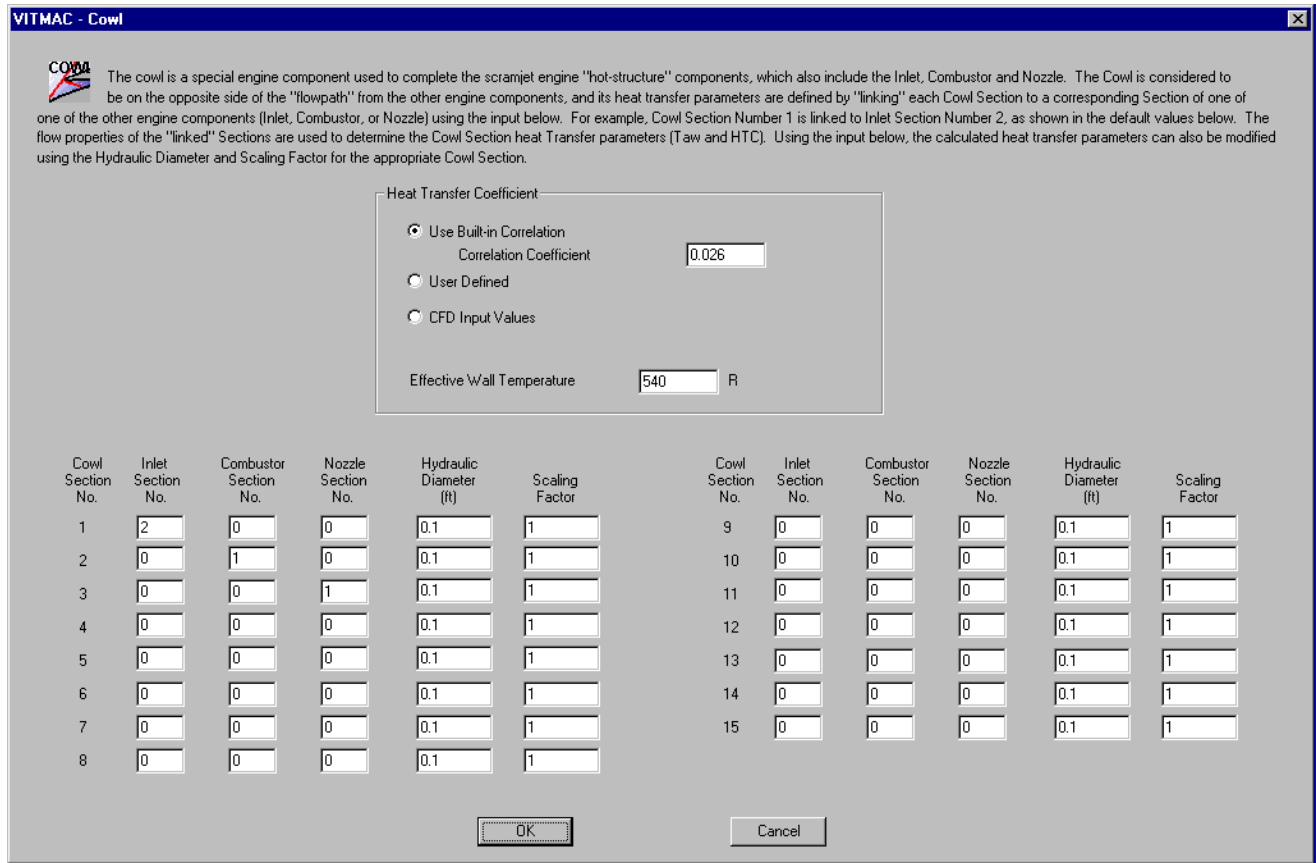


Figure 4.13 Cowl Heat Transfer Parameters Dialog Box

Figure 4.14 shows the default VITMAC scramjet engine depiction utilizing the RJPA model capability. In this case, two cooling panels sections cool each of the inlet, combustor, and nozzle components, while three panels cool the Cowl. Upon entry on to the VITMAC palette, the Cowl sections, as shown, are lined up with the corresponding engine component to which they are “connected.” They of course can be moved around as any other VITMAC component. New icons depicting the engine “hot structure” surfaces are shown, as is the automatic connection of the engine to the corresponding structural surfaces. Except for their automatic generation by the GUI and linkage to engine heat transfer by VITMAC, these structures are the same as other VITMAC structures and they may (must!) be manipulated and defined as before.

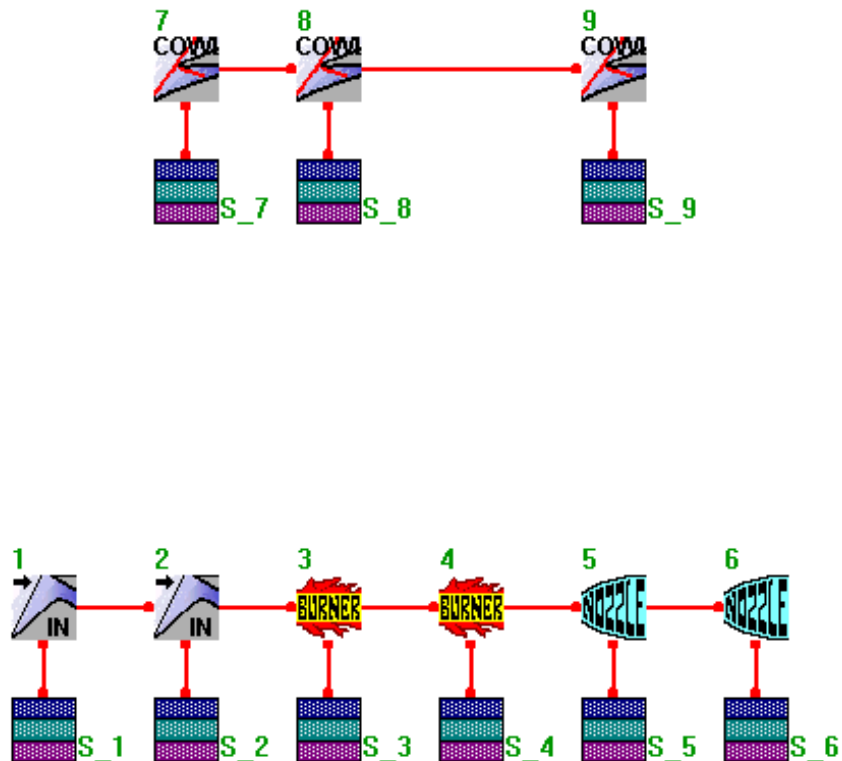


Figure 4.14 Generic VITMAC Scramjet Engine Cooling Network

4.2 VITMAC Comparison With NASP DCC Experimental Data

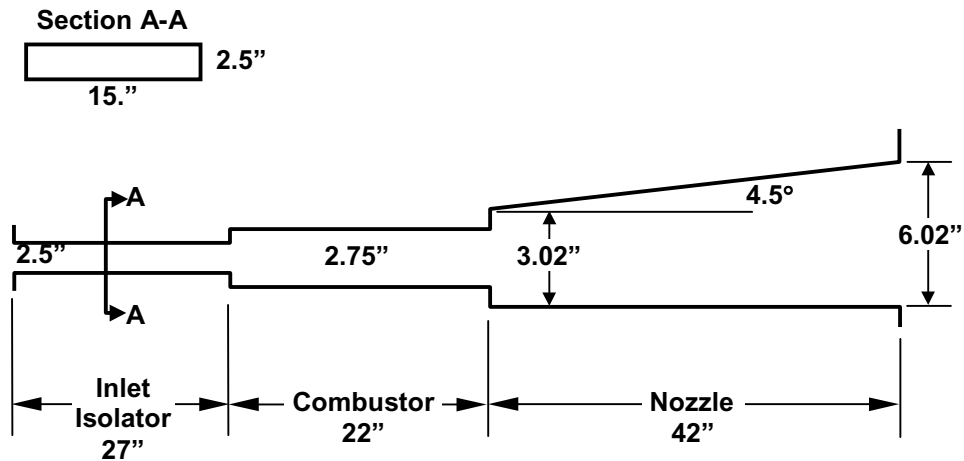


Figure 4.15 Schematic of APL Scramjet DCC Experiment

The DCC experiments¹⁴, performed for the NASP program in the late 80's, involved the scramjet engine configuration, illustrated schematically in Figure 4.15, which was “directly-connected” to a high pressure, combustion-heated air source to provide hypersonic flow conditions at the combustor inlet. Two experimental conditions which provided enthalpy simulation of Mach 6 and Mach 8 flight were considered, since heat transfer data was available for a number of runs at each condition. Calculations were performed with the VITMAC circuit model shown in Figure 4.16, below, consisting of four hot surface material sections in each of the inlet and combustor components and five sections in the nozzle component. As suggested in the figure, each engine section is connected to a water-cooled structural panel simulating the wall of the test section. VITMAC automatically calculates flow and hot-wall temperature dependent heat transfer to each structure as well as the cooling on the outside (bottom) surface. Since wall temperature measurements were not available, no attempt was made to simulate the Zirconia coated nickel walls of the test. Using the available (but not complete) datasets, the simulations were defined using “best efforts” estimates of the test conditions and used coolant flow rates to establish “cold wall” hot-side heat transfer conditions. Heat transfer was measured using water-cooled calorimeters so that cold-wall conditions (~530° R surface temperature) provides the most appropriate simulation—wall temperature was not independently reported.

¹⁴ Sullins, C. A., et al., “Direct-Connect Combustor Experiments,” Fifth National Aerospace Plane Tech. Sym., Oct. 1988, also other presentations from 1988 to 1990.

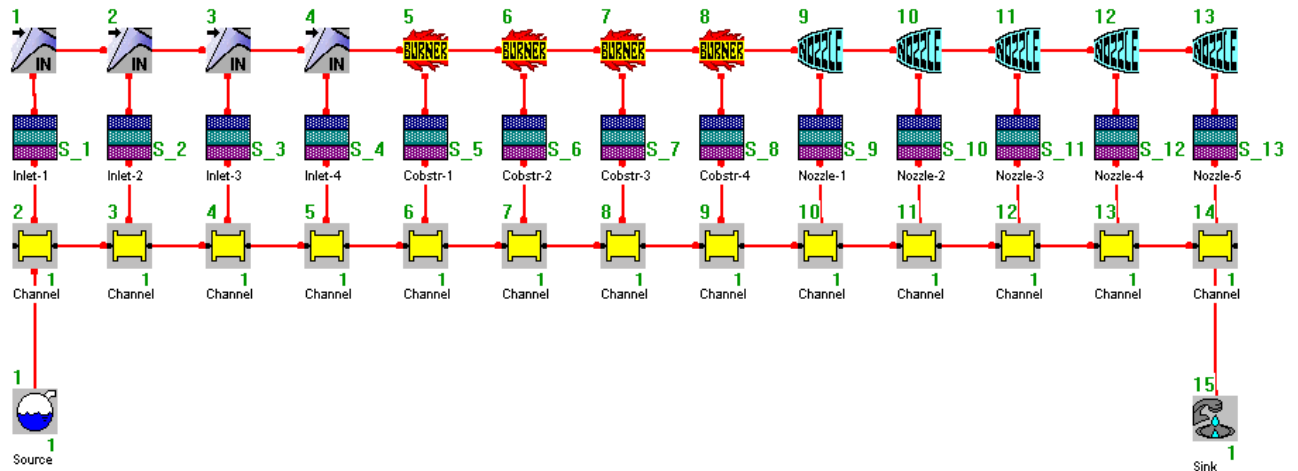


Figure 4.16 VITMAC Schematic for Scramjet DCC Experiment

Two cases have been considered in the DCC validation studies, as described by the following inlet flow and combustor fuel conditions:

Case 1: M ~ 8 simulation, H₂+ Vitiated Air, ER = 0.52 (designated APL II Condition)

- “Inlet” Conditions: M = 3.25. P_{inlet} = 6.5 psi, T_{inlet} = 1950°R
- Determined from facility nozzle calibration data. Also compares with supply “setting” P_{total} = 400 psi and H_{total} ~1250 Btu/lbm and air flow ~16 lbm/sec.

Case 2: M ~ 6 simulation, H₂+ Vitiated Air, ER = 0.37 (designated APL I Condition)

- “Inlet” Conditions: M = 3.25. P_{inlet} = 7 psi, T_{inlet} = 1100°R
- Determined from facility nozzle calibration data. Also compares with supply “setting” P_{total} = 400 psi and H_{total} ~670 Btu/lbm and air flow ~21 lbm/sec

The facility nozzle was calibrated to provide Mach 3.2 flow conditions at the “inlet” test section, which corresponds to the measured static pressures, 6.5 to 7 psi, at this location, for the 400 psi supply total pressure condition. Flight simulation was provided by varying the combustion heating (accomplished by injecting hydrogen and ‘make-up’ oxygen into the pressurized gas source) to the specified total enthalpy given above. Freestream total temperature, or mass flow measurements were not directly measured to verify the design conditions, but were inferred from facility calibration data collected separately. Input to VITMAC-RJPA reproduces the specified flow areas, inlet Mach number and pressure, and inlet temperature was adjusted to match the appropriate total enthalpy and mass flow rate. In each case these were duplicated to within a few percent. The RJPA air/fuel ratio was adjusted to simulate the reported fuel equivalence ratio, and a combustion or “mixing” efficiency of 95% was simulated by using 5% frozen Hydrogen in the fuel mixture.

Heat transfer comparisons for the Mach 8 case are compared in Figure 4.17, and for the Mach 6 case in Figure 4.18 below. In each case, VITMAC predictions are compared to

measured data for hot structure panel cold wall heat flux as a function of distance along the test channel. The results represent a “nearly cold wall”, for two temperatures (1000 °R and 600 °R), believed to best represent the calorimeter measurements. As indicated, heat flux results are not particularly sensitive to this parameter as long as temperatures are within normal metal wall temperature limits. Also, variations in inlet temperature are found to have only a moderate effect on combustor heat flux predictions.

The results of most interest at this time are the values downstream of the combustor beginning at about $x = 25$. The results show that the peak combustor heating is predicted fairly well in each case—well within data scatter at Mach 8 and low by about 20%, 25% and 35% at Mach 6, equivalence ratio = .14, .23, .37 respectively. Heat transfer predictions in the unheated inlet seem to be slightly high in each case, as are the predictions in the expanding nozzle section. For reference, cold flow (ER = 0.) heat transfer measurements are available for the Mach 8 case (not reported for Mach 6 case) and the VITMAC comparisons are also shown in Figure 4.17. As indicated, the “cold-flow” predictions compare well with the test data. They are, however, high in the nozzle, perhaps indicating some three dimensional flow condition that is not captured by the RJPA cycle code for obvious reasons.

A few observations (caveats) concerning these test comparisons are in order. Apparently, both test cases result in significant combustion/inlet interactions above a certain fuel flow rate; the Mach 8 case above ER = 0.5 and the Mach 6 case above ER = .23. In both cases, for higher equivalence ratios, significant pressure increases are measured well upstream of the combustor within the isolator duct. In the Mach 8 comparison presented in Figure 4.17, the predicted combustor pressure is 16 psi, which compares well to the measured values of about 20 to 25 psi. This, combined with the set inlet conditions, indicates that RJPA is predicting the flow conditions reasonably well for this case. The heat transfer predictions are supported. This is also true of the two lower fuel flow cases for Mach 6; i.e. at ER = .14, $P_{\text{comb}} = 14.3$ psi predicted vs 14 – 19 psi measured, and at ER = .23, $P_{\text{comb}} = 19.3$ psi predicted vs about 20 psi measured. The under-prediction of heat transfer by 20 to 25 % in these cases would seem to be a better measure of the accuracy to be expected. Finally, for the Mach 6, ER = .37 case, the pressure data exhibited combustor/inlet interaction, which resulted in a combustor pressure of over 40 psi vs a predicted value of about 27 psi. The less accurate heat transfer prediction for this case could be attributed to this discrepancy.

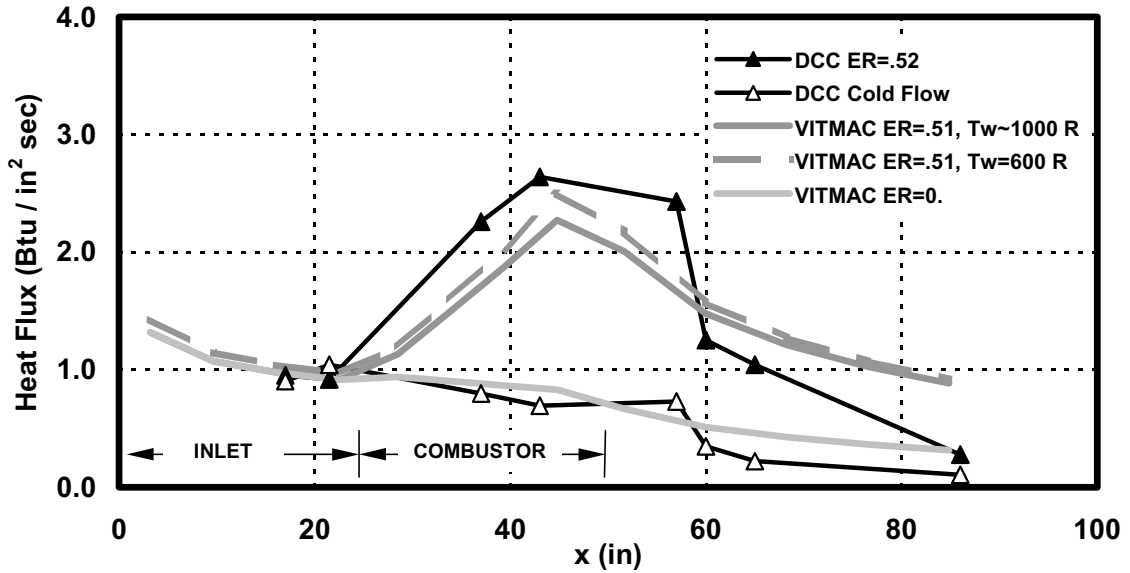


Figure 4.17 VITMAC Heat Transfer Results for APL DCC Experiment
Mach No. ~ 8, Equivalence Ratio ~ .5, $\eta_{\text{comb}} = 95\%$

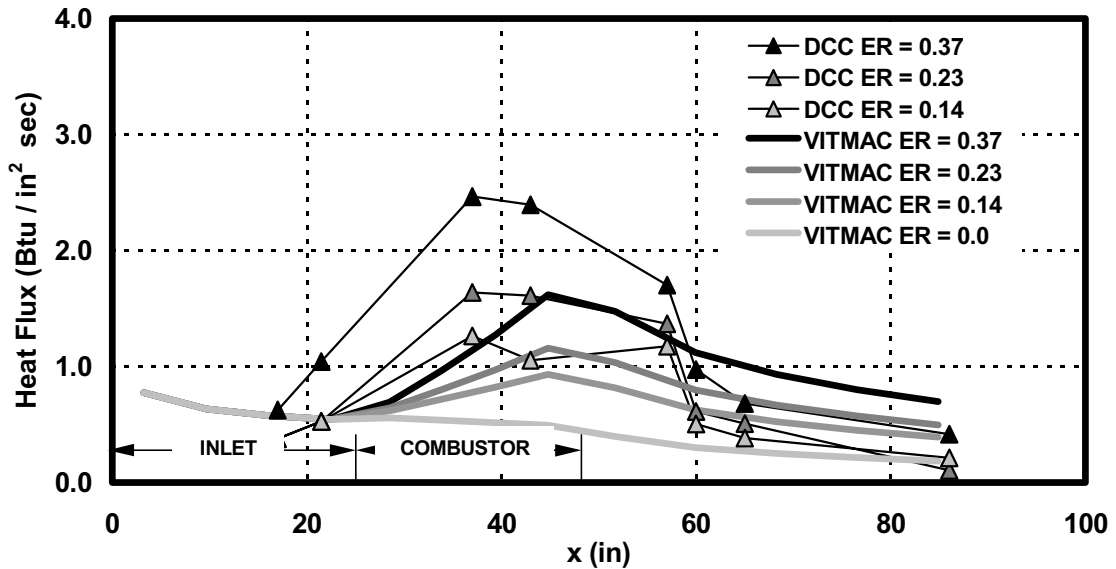


Figure 4.18 VITMAC Heat Transfer Results for APL DCC Experiment
Mach No. ~ 6, Equivalence Ratio up to .37, $\eta_{\text{comb}} = 95\%$

4.3 VITMAC Comparison with NASP DCAF Experimental Data

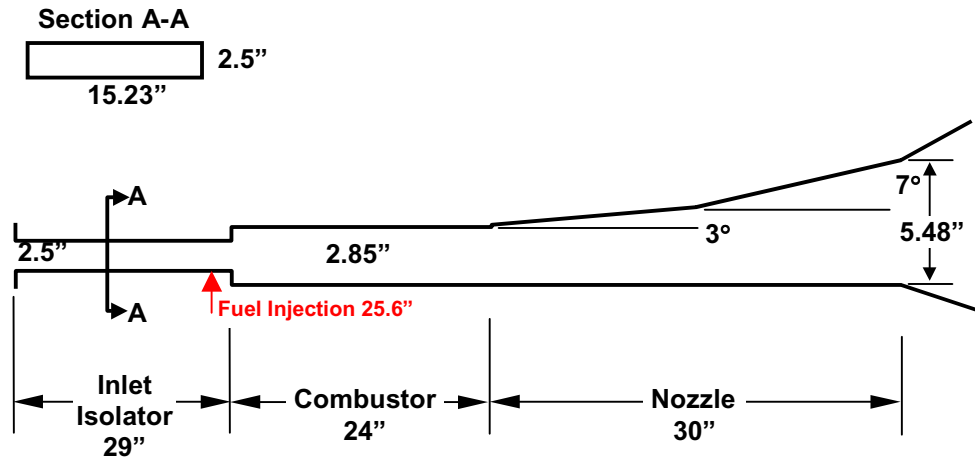


Figure 4.19 Schematic of DCAF Scramjet Experiment (Direct Connect Arc-jet Facility)

In addition to the DCC experiments, a significant NASP-funded experimental program was also performed and is referred to here as the DCAF experiments^{15, 16}. These tests involved the scramjet engine configuration (modified CEDAR hardware), illustrated schematically in Figure 4.19. In this case, the test section was “directly-connected” to a high pressure, arc-jet-heated air source to provide hypersonic flow conditions at the combustor inlet, making it possible to provide enthalpy simulation of higher flight Mach numbers. Two experimental conditions were considered here—which provided enthalpy simulation of Mach 10 and Mach 12 flight. These cases expand the VITMAC comparisons to higher Mach numbers and to higher fuel equivalence ratios (ER) as shown below.

Case 1: M ~ 10 simulation, H₂+Air, ER = 1.15 (Run No. 2010)

- “Inlet” Conditions: M = 3.25. P_{inlet} = 5.1 psi, T_{inlet} = 2750°R
- Determined from facility nozzle calibration data. Also compares with supply “setting” P_{total} ~ 350 psi and H_{total} ~1850 Btu/lbm and air flow ~ 10.3 lbm/sec.

Case 2: M ~ 12 simulation, H₂+Air, ER = 2.25 (Run No. 1034)

- “Inlet” Conditions: M = 3.25. P_{inlet} = 5.3 psi, T_{inlet} = 3200°R
- Determined from facility nozzle calibration data. Also compares with supply “setting” P_{total} ~ 400 psi and H_{total} ~ 2280 Btu/lbm and air flow ~ 10.4 lbm/sec

¹⁵ Sullins, C. A., et al., “Final Report for High Enthalpy Arc Tunnel Combustor Tests GWP 107A, Vol. 1,” APL-NASP-94-004, March 4, 1994.

¹⁶ Pandolfini, P., and M. W. Thompson, “High Enthalpy Direct-Connect Combustor Tests Final Report GWP#50,” APL-NASP-92-005, June 12, 1992.

In these test series, the test section was constructed from ¼” Zirconium-Copper alloy and heat flux measurements were determined by inner and outer wall thermocouple measurements. Thus the wall temperature can be expected to be higher than “cold wall” conditions even though the walls were cooled on the outside by a water spray. The temperatures are reported to reach steady state in about 2 sec (verified by our calculation) so that a relatively steady state heat flux results. The limited temperature data that was reported, imply that the hot wall temperature was kept below 1000°R in all cases. Hence, the simulations were performed with sufficient water cooling to keep the hot-side wall temperature in the same range. Recall, variations of a few hundred degrees produce a relatively small effect on the calculated wall heat transfer rates.

The heat transfer results for the Mach 10 and Mach 12 cases are presented in Figures 4.20 and 4.21 along with predictions for a range of mixing or combustion efficiencies. Data was taken (side 1 and side 2) on either side of the test section and shows a high degree of side-to-side and streamwise variability. The side-to-side variation is especially large for Run 1034 for the high equivalence ratio indicating that the fuel streams (stronger for higher ER) may be perturbing the flow through the relatively narrow combustor channel. In each case, the VITMAC prediction in blue utilizes the “best guess” at the fuel mixing (or combustion) efficiency as reported by the experimental reports. These values, $\eta_{\text{comb}} = 62\%$ for DCAF2010 and $\eta_{\text{comb}} = 40\%$ DCAF1034 are based on finite rate streamline analysis of the experimental pressure and calorimetry data performed in support of the test programs. The other results illustrate the sensitivity of heat transfer predictions to the assumed combustion efficiency.

Within the uncertainty caused by the combustion efficiency parameter, the current predictions are judged to be quite good except for the “cold flow” heat transfer upstream of the combustor. In this regime the current predictions seem to be significantly higher than the data in contradistinction to the cold flow prediction for the DCC cases for which the cold flow compared well. It should be pointed out however, that the VITMAC inlet model is designed for a ramp inlet with a defined boundary layer origin set by the shock inducing ramp edge. In the current cases the inlet flow is established far upstream of the test section within the arcjet nozzle so no such boundary layer origin is evident which results in an uncertain estimate for the inlet boundary layer thickness. The model has been verified by approximate calculations as well as the GASL/CALSPAN Entry 4 data for a complete scramjet inlet/combustor tested in a expanded flow shock tunnel. For the Entry 4 case with 20 degree inlet ramp at nominal Mach 10 flow conditions (Mach 9.3), the model compares well to the quick response resistance type heat flux data.

Finally, the dominating influence of the combustion efficiency on the heat transfer results is illustrated in Figure 4.22 below. The data for peak combustor heat flux (with side-to-side variation) is plotted against equivalence ratio (ER) for all of the DCAF tests revealed to the author to date. Results for the same quantity are also plotted for the two combustion efficiencies, $\eta_{\text{comb}} = 62\%$ and $\eta_{\text{comb}} = 95\%$. The latter case represents nearly the maximum possible heat transfer driving potential at any equivalence ratio and exhibits a substantial variation in combustor heat flux vs fuel flow rate. The data, on the other hand, exhibit only a

slight increase in combustor heat flux. This comparison implies that, for these tests at least, only so much fuel can be burned in these subscale combustors. From a heat transfer modeling perspective, it means that the combustion efficiency parameter must be a strong function of the fuel equivalence ratio. It also means that the current VITMAC-RJPA heat transfer model cannot be truly predictive without additional information about this crucial free parameter.

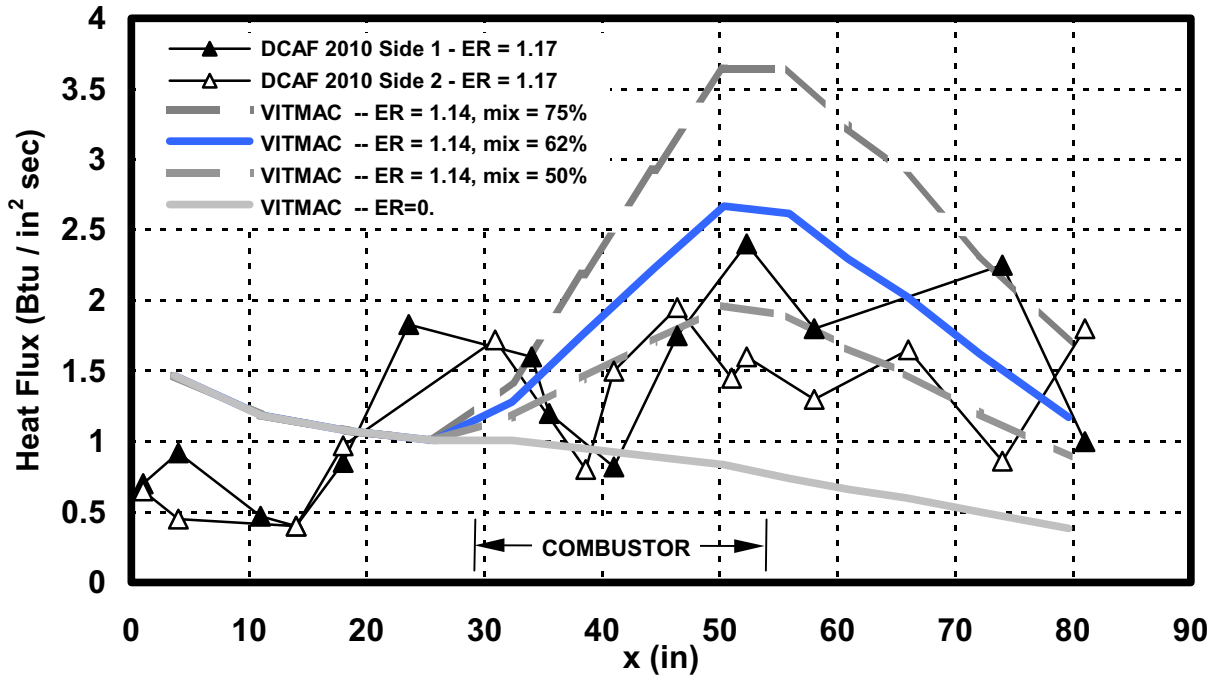


Figure 4.20 VITMAC Heat Transfer Results for DCAF Experiment (2010)
Mach No. ~ 10, Equivalence Ratio ~ 1.15, $\eta_{\text{comb}} = 62\%$

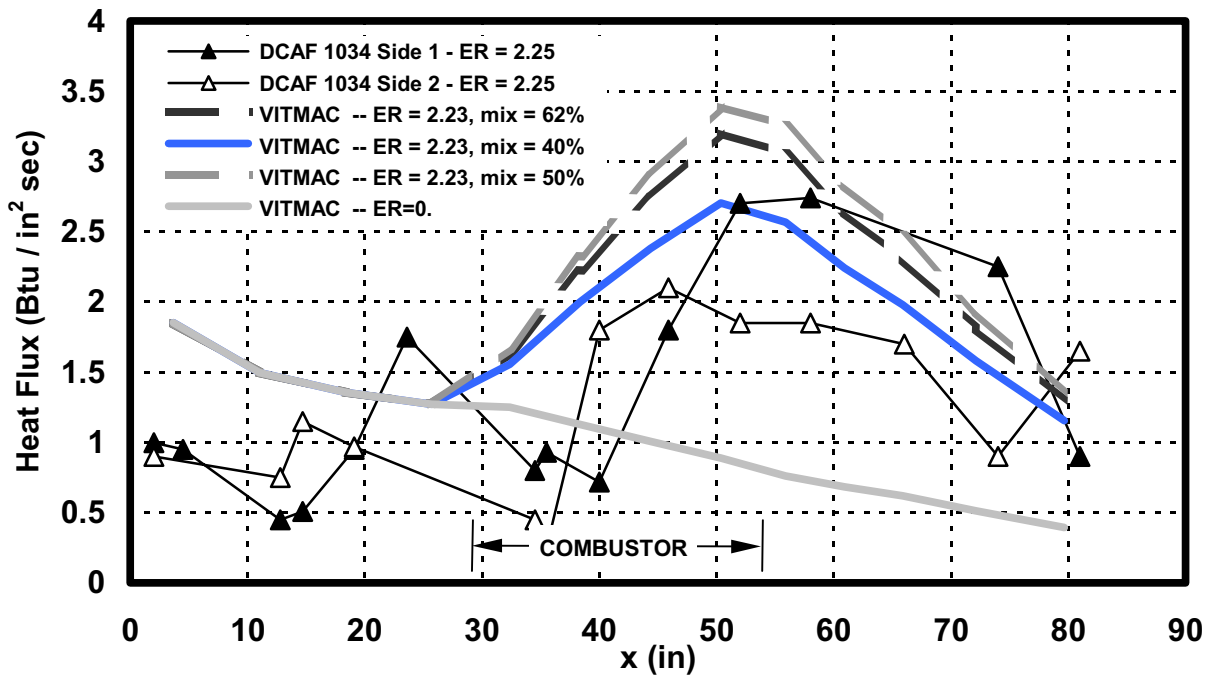


Figure 4.21 VITMAC Heat Transfer Results for DCAF Experiment (1034)
Mach No. ~ 12, Equivalence Ratio ~ 2.25, $\eta_{\text{comb}} = 40\%$

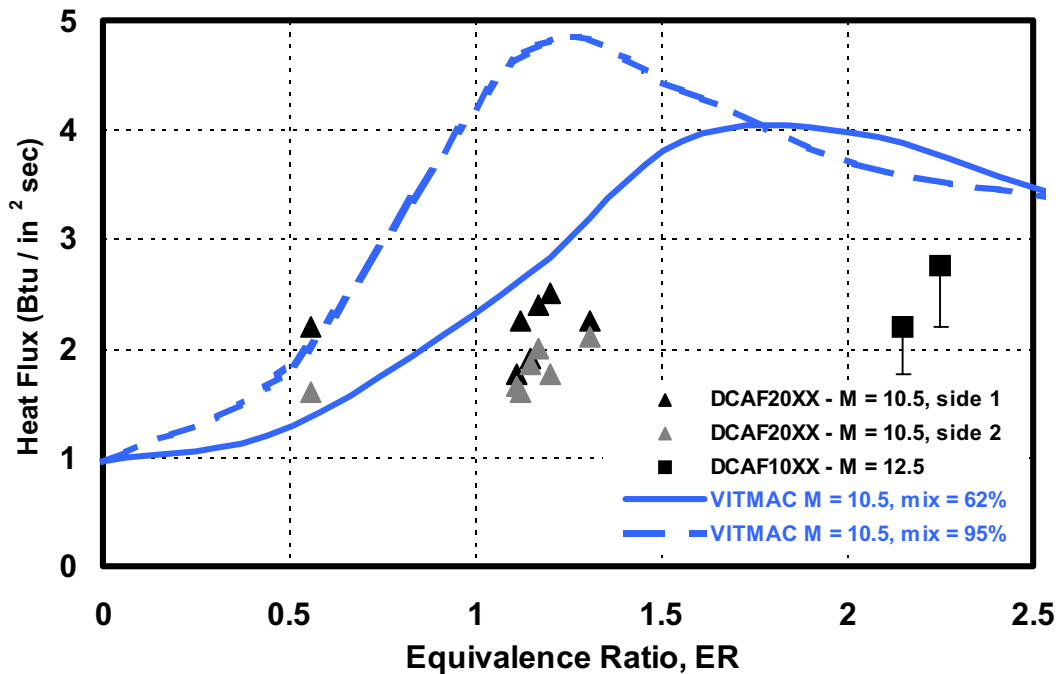


Figure 4.22 VITMAC Comparison to Peak Heat Transfer Results for DCAF Experiments (10XX-20XX) Mach No. 10 to 12, Equivalence Ratio .5 to 2.25

4.4 VITMAC Comparison with NASP GASL-CALSPAN-Entry 4 Test Data

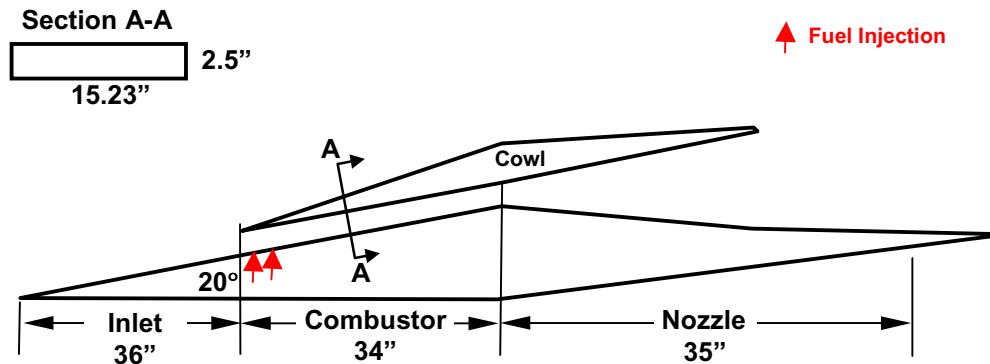


Figure 4.23 Schematic of GASL-CALSPAN-Entry 4 Scramjet Experiment (96" CALSPAN Shock Tunnel Facility)

Another scramjet dataset was collected in the CALSPAN 96" reflected shock tunnel facility and is referred to here as the GASL-CALSPAN Entry 4 test series.¹⁷ This large scale shock tunnel facility establishes a high enthalpy flow by expanding the flow behind a reflected shock to a representative flight Mach number. The flow in the test section is near steady state conditions for only a few milliseconds but provides a relatively high degree of fidelity to flight conditions. A simulated engine was used which is shown schematically in Figure 4.23. In this case a 20° inlet ramp processed the flow leading to a combustor formed by the ramp and a cowl section. Hydrogen fuel was injected through a slot injector as shown and the reacted flow was expanded through a nozzle. At least six repeat tests were performed at a Mach No. ~ 9.3 , and a combustor equivalence ratio, $ER = 1$. Fast response heat flux gauges were used to measure heat transfer at numerous locations on all engine surfaces and are compared to VITMAC simulations in this section.

As above, the VITMAC simulation attempts to duplicate engine inlet conditions as closely as allowed by the reported data. In this case the VITMAC circuit shown below in Figure 4.24 was used, with RJPA input and resulting combustor conditions given by:

- Freestream Conditions: $M_\infty = 9.3$, $P_\infty = 0.3$ psi, $T_\infty = 475^\circ$ R
- Combustor "Inlet" Conditions: $M = 4.1$, $P_{inlet} = 6.25$ psi, $T_{inlet} = 1980^\circ$ R
- Also compares with supply "setting" $P_{pitot} = 138$ psi and $H_{total} = 1967$. Btu/lbm and air flux ~ 75.1 lbm/ft²-sec.

¹⁷ Orth, R.C., D. Torrillo, O.F. Rizkalla, and J. I. Erdos, "Summary Report of Parametric Scramjet Experiments Conducted for Pratt & Whitney in the Calspan Shock Tunnel- 4th Entry," Vol. 1 GASL TM 243, March 1991.

These conditions compare very well to the 125 psi measured pitot pressure and 75 to 80 lbf/ft²-sec air flow rate in the combustor inlet. Wall heat flux measured on both walls of the combustor are very repeatable for all six runs performed at an equivalence ratio of unity.

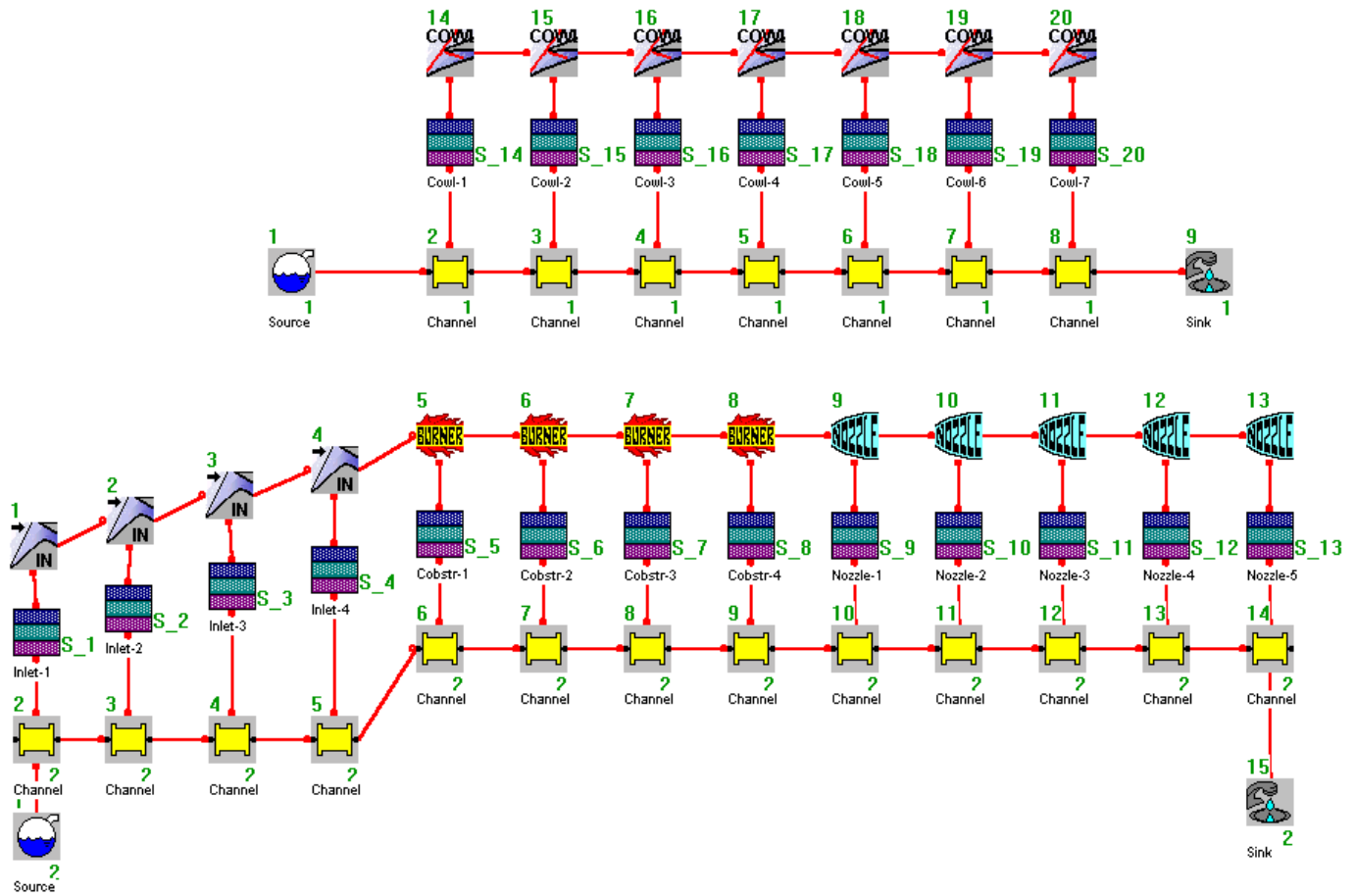


Figure 4.24 VITMAC Schematic for GASL-CALSPAN-Entry 4 Scramjet Experiment

Using the simulation setup described above, the VITMAC heat transfer results are presented in Figure 4.25 below with comparison to the measured “cold wall” heat flux for Run 06 of the test series. This test resulted in an equivalence ratio of $ER = 0.9$. The figure shows the model results for both cold flow and reacting flow compared to the range of heat transfer measurements indicated by the shaded region. The experimental data show no consistent trend of “combustor-side” versus “cowl-side” measurements indicating that the shaded region is a measure of the uncertainty or variation in the data. The results indicate that VITMAC is providing a good prediction of the maximum heat transfer in the combustor, a 30 % overprediction on the inlet ramp and a less rapid decrease in heat transfer in the nozzle than the data. All-in-all a reasonably good, albeit conservative, prediction of the flow path heat transfer.

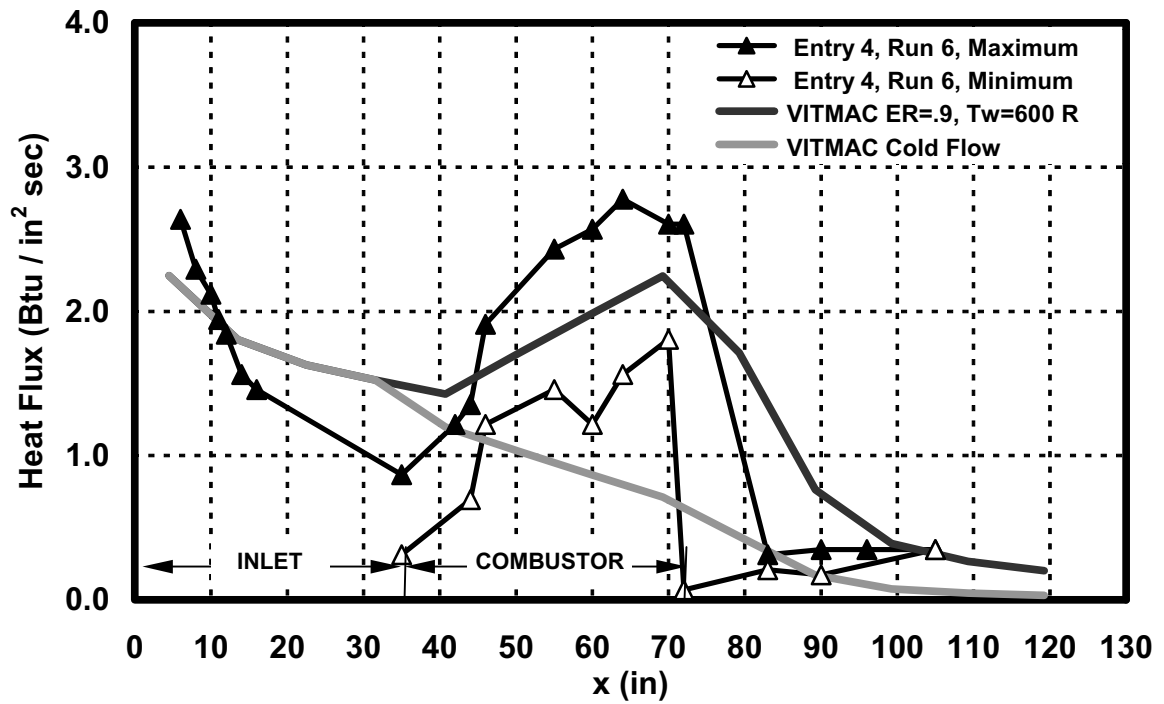


Figure 4.25 VITMAC Heat Transfer Results for GASL-CALSPAN-Entry 4
Mach No. ~ 9.3, Equivalence Ratio ~ 0.9, $\eta_{\text{comb}} = 62\%$

5. Cold-side Heat Transfer Model

5.1 Cooling Panel “Cold-Side” Heat Transfer Correlation Summary

VITMAC models cooling panels as a one-dimensional structure component cooled on its internal surface by a flow channel. The so-called “cold-side” heat transfer has been upgraded to include known modifying effects due to: two-dimensional geometry, ϕ_{2D} , fluid property “film” temperature variation, ϕ_{prop} , channel entrance flow development, ϕ_{in} , and longitudinal curvature flow modification, ϕ_{curv} . The approach uses a general pipe flow Nusselt Number correlation for the effective “cold-side” heat transfer coefficient, h , modified by engineering correlations:

$$Nu = \frac{hD_h}{k_{ref}} = C Re^{.8} Pr^{.4} \times \phi_{2D} \times \phi_{prop} \times \phi_{in} \times \phi_{curv} \quad (15)$$

where D_h is the hydraulic diameter and k_{ref} is the solid thermal conductivity evaluated at the reference temperature, T_{ref} . The reference temperature and the fluid bulk temperature, T_b , for fluid properties are related to the flow channel inflow and outflow temperatures, T_{in} and T_{out} , respectively, and the structure internal wall temperature, T_{wall} , by:

$$T_b = T_{in} + \alpha (T_{out} - T_{in}) \quad (16)$$

$$T_{ref} = T_b + \beta (T_{wall} - T_b) \quad (17)$$

where α and β are user-specified weighting factors. The various heat transfer effects correlations are given by:

$$\phi_{2D} = (P/L) \times \left\{ \text{Tanh} [(0.9hPH/kW)^{1/2}] / (0.9hPH/kW)^{1/2} + 0.5 / [(1+5kW/hPH)^2 (H/D+1)] \right\} \quad (18)$$

$$\phi_{prop} = \left(\frac{T_w}{T_b} \right)^{-(.57-1.59D_h/S)} \quad (19)^{18}$$

$$\phi_{in} = 1 + 5 \left(\frac{D_h}{S} \right) \quad (20)^{19}$$

¹⁸ Taylor, M. F., “Correlation of Local Heat Transfer Coefficients for Single Phase Turbulent Flow of Hydrogen in Tubes with Temperature Ratios to 23,” NASA TN D-4332, 1968.

¹⁹ Taylor, M. F., “A Method of Predicting Heat Transfer Coefficients in the Cooling Passages of NERVA and Phoebus-2 Rocket Nozzles,” NASA TM X-52437, 1968.

$$\phi_{\text{curv}} = \left[\text{Re} \left(\frac{D_h/2}{R_c} \right)^2 \right]^{0.05} \quad (21)^{20}$$

where:

Re	Bulk Flow Reynolds No.	
Pr	Bulk Flow Prandtl No.	
k	solid thermal conductivity	
h	film coefficient	
H	flow channel height	see Figure 5.5
D	flow channel width	see Figure 5.5
P	wetted perimeter	see Figure 5.5
W	Solid web thickness	see Figure 5.5
L	total cell width	see Figure 5.5
S	distance from entrance	
R _c	radius of curvature	

²⁰ Ito, H., Friction Factors in Turbulent Flow in Curved Pipes," J. Basic Engineering., Vol.81, No. 2, June 1959, pp. 123-134

The correlations are based on established engineering research studies with attribution shown along with the equations. They have been developed primarily for rocket system cooling panel applications using cryogenic fluids but can be expected to apply more generally. This correlation has been implemented into VITMAC using the interface design described in the following figures. It has been decided to combine the heat transfer option definition with the fluid friction model for user selection in the Flow Channel window, shown below. The “Cooling panel flow channel” option is included as a new option along with the usual VITMAC pipe flow, channel flow and cooling panel options. In addition, a “User Defined” option has been added that permits the user to input a specific value for friction factor and heat transfer coefficient. Also new to the option is the user-specified weighting factors for the bulk fluid temperature, T_b , and the fluid reference temperature, T_{ref} , as well as the specification of the turbulent heat transfer coefficient, C . These are included to provide additional flexibility to all flow channel heat transfer options.

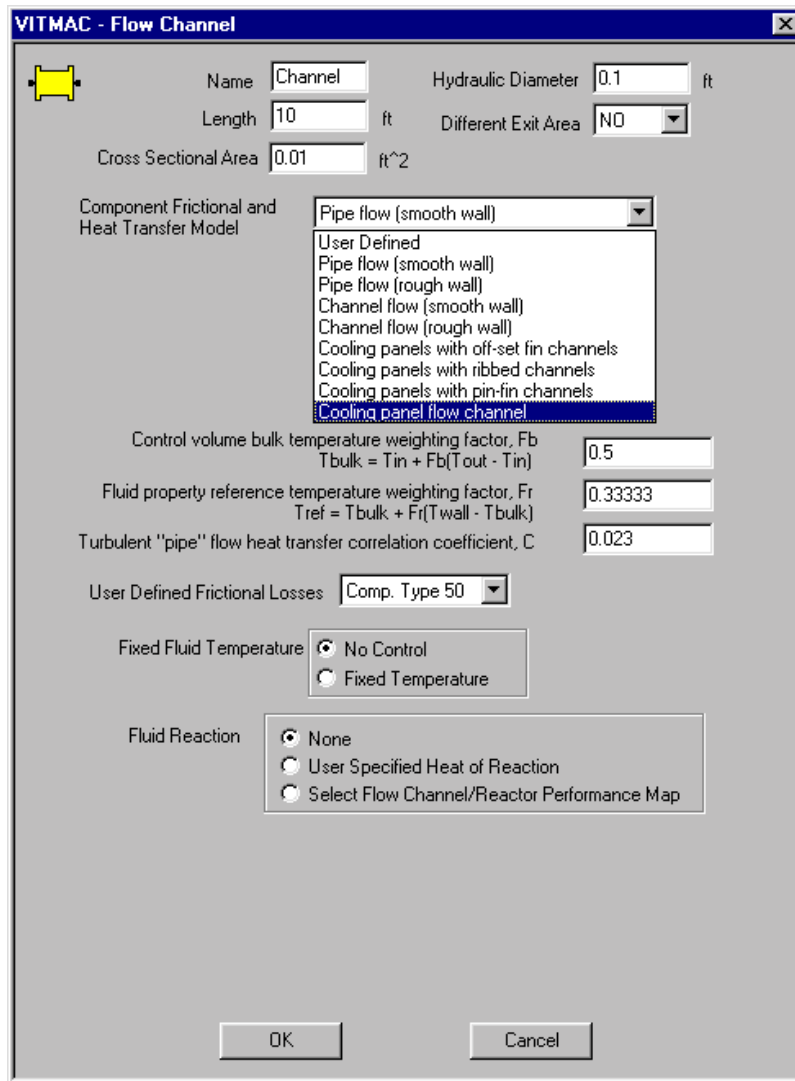


Figure 5.1 New Cooling Panel Heat Transfer Options

Upon selecting the Cooling Panel Flow Channel option, another window (shown below in Figure 5.2) will open to define the flow channel options—each of which can be turned on or off selectively. In addition, the channel effectiveness factor will permit the selection of the rectangular channel correlation described below or the soon-to-be-developed circular channel correlation. Also provided will be the ability to open an information window which will display the correlation equations presented earlier.

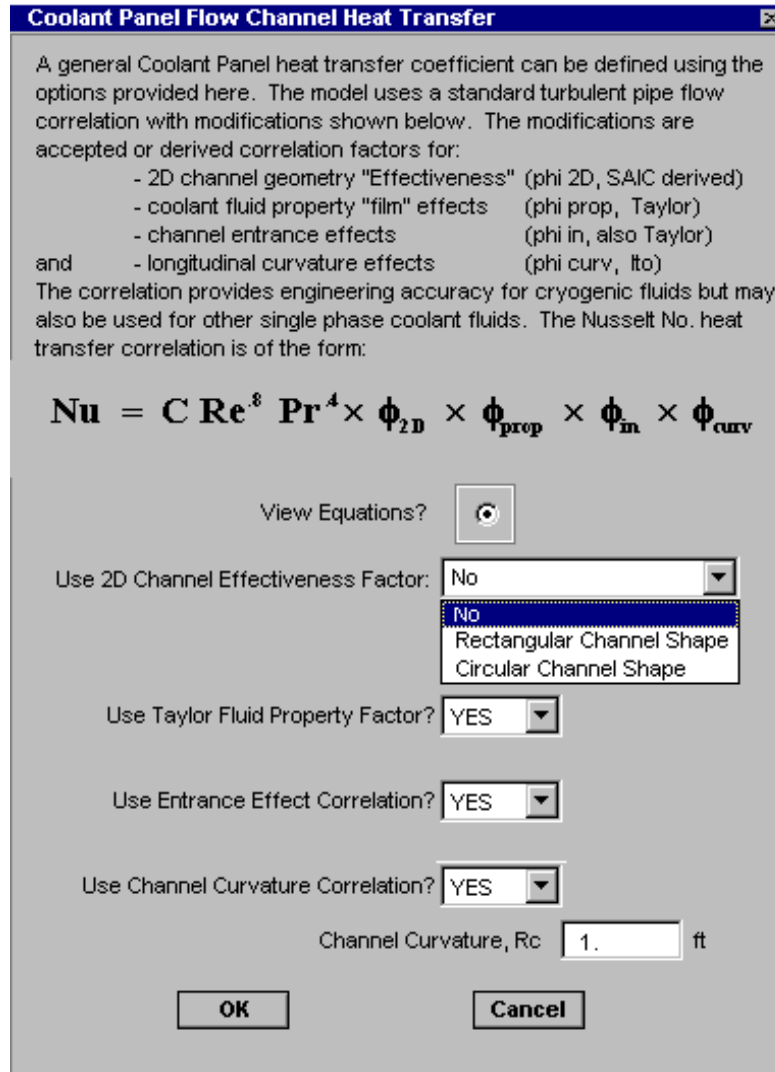


Figure 5.2 Cooling Panel Flow Channel Option

Finally, selecting the rectangular channel shape option will open the window provided below (Figure 5.3a) which defines, and provides for user input, of the channel geometry parameters; height, H, width, D and web thickness, W. A similar window (Figure 5.3b) is available for the circular channel geometry option. The circular channel geometry is defined by the channel diameter, D, the web thickness, W, a metallic liner thickness, t_w , and liner conductivity, k_w .

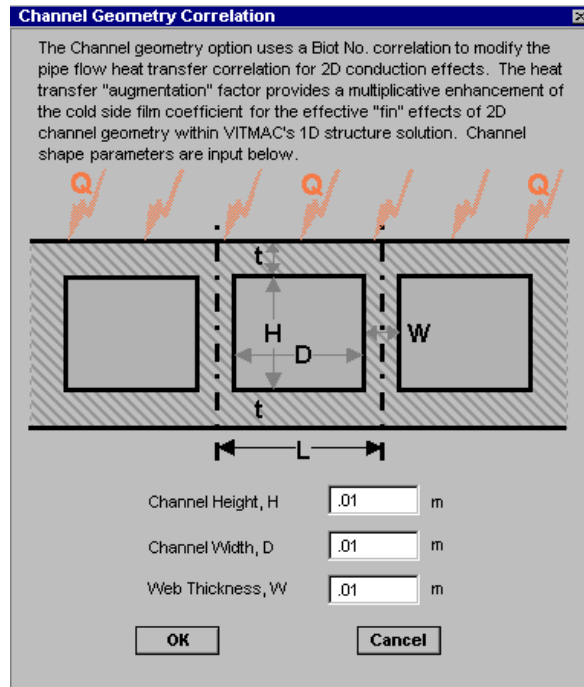


Figure 5.3a Rectangular Cross-section Channel Option

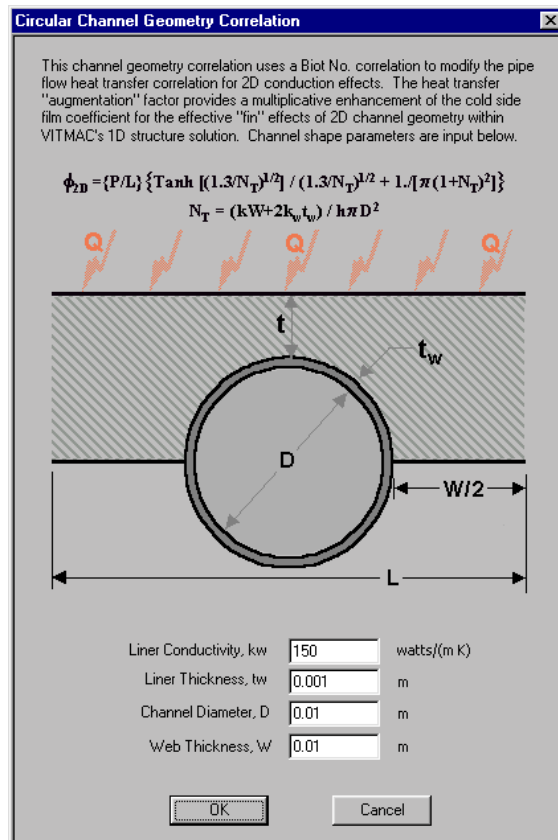


Figure 5.3b Circular Cross-section Channel Option

5.2 Two Dimensional Cooling Channel Analysis: Rectangular Channel

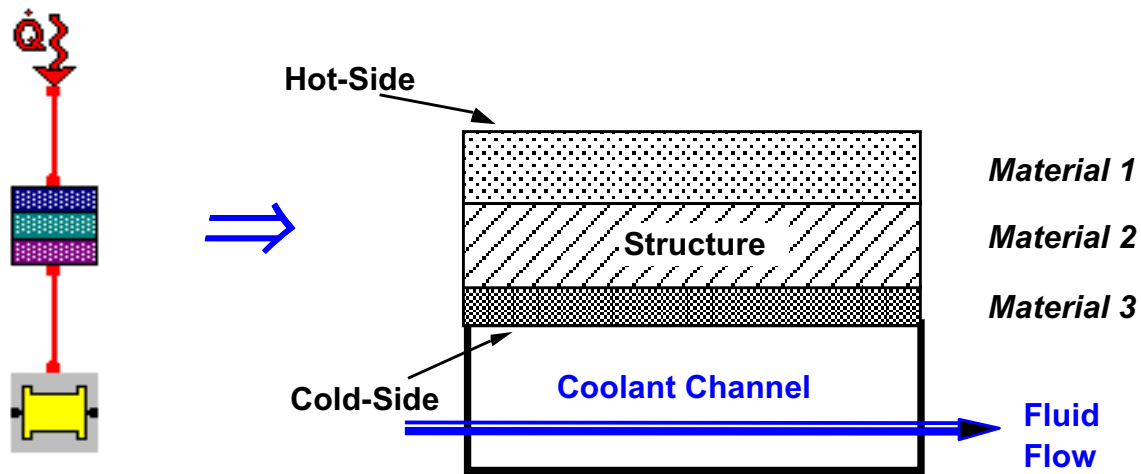


Figure 5.4 VITMAC Cooling Panel Simulation

Cooling panels are simulated in VITMAC as a one-dimensional (1D) structural surface, with an imposed heat load, connected to a fluid channel element as suggested above. A 1D transient solution of the structure response is performed using various built-in “cold-side” heat transfer correlations to connect the bottom side of the structure with the cooling fluid. These correlations have been tested and upgraded for cryogenic fluid operating conditions and for two-dimensional channel “shape effects.” General flow channel effects are accounted for using the correlations described above, which are implemented as a user option. Two-dimensional channel shape effects have been studied by performing two-dimensional (2D) SINDA conduction calculations for representative shapes, fluid properties and fluid operating conditions. Such calculations anchor the scaling analysis to provide a heat transfer augmentation factor due to 2D geometry effects. Results of the analysis are presented here.

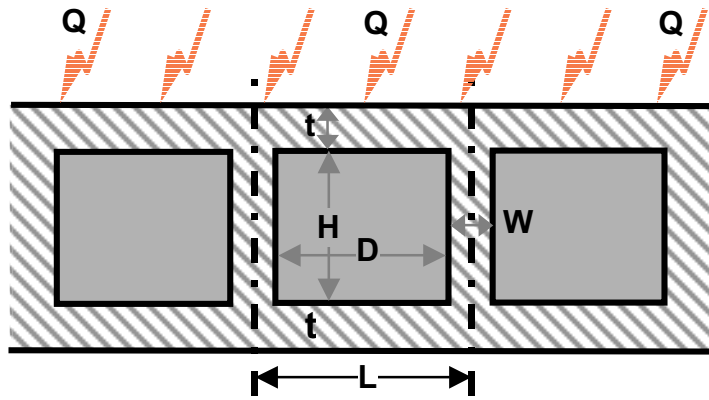
The initial analysis assumes rectangular channels with the geometry, property and heat transfer parameters defined in the Figure 5.5 below. Under steady state conditions, the two-dimensional and VITMAC one-dimensional heat transfer on the cold side can be related through a “Channel Effectiveness parameter”, as follows:

$$Q \times L = h P (\langle T_w \rangle - T_f) = h L \phi_{2D} (T_{w1D} - T_f) \quad (22)$$

Where T_{w1D} is the inner wall temperature for the one-dimensional VITMAC simulation

So that:

$$\phi_{2D} = \frac{P (\langle T_w \rangle - T_f)}{L (T_{w1D} - T_f)} \quad (23)$$



Symbol	Definition
k	solid thermal conductivity
T_f	fluid bulk temperature
h	film coefficient
q	heat flux (per unit area)
t	panel wall thickness
H	flow channel height
D	flow channel width
W	solid web thickness
L	total cell width
D_h	hydraulic diameter
H/W	dimensionless geom. factor
Q	total heat applied to cell
$\langle T_w \rangle$	average wall temp. of wetted perimeter
$k/(hD_h)$	dimensionless heat transfer factor (recipricol of Biot)
$T_{w,max}$	maximum wall temp.
ϕ_{2D}	dimensionless temp, $(\langle T_w \rangle - T_f) / (T_{w,max} - T_f)$

Figure 5.5 Parameters for 2D Channel Geometry Effects Analysis

This channel effectiveness parameter can be viewed as an augmentation of the cold-side heat transfer much like the more normal fin efficiency parameter and, in fact, our approach to correlating it for use in VITMAC follows the usual fin efficiency analysis. But first, it should be noted that the calculation of ϕ_{2D} from 2D calculations requires an additional assumption concerning the desired value for T_{w1D} . For example, the above relation indicates that the present unaugmented VITMAC calculation, i.e., $\phi_{2D} = 1.$, results in a 1D wall temperature that is given by:

$$T_{w1D} - T_f = (P/L) \times (\langle T_w \rangle - T_f) \quad (24)$$

This suggests that the present VITMAC solution is some weighted average of the “true” 2D average wall temperature and the bulk fluid temperature. On the other hand, if $\phi_{2D} = P/L$, which is the maximum possible augmentation factor, then T_{w1D} equals $\langle T_w \rangle$, the average 2D channel wall temperature, an interesting result. For present analysis purposes ϕ_{2D} will be defined from the equation presented above under the assumption that the desired T_{w1D} is the

maximum 2D wall temperature from the SINDA calculation. It is believed that this will result in the best 1D approximation to the real 2D channel solution and, moreover, follows conservative engineering practice.

Results have been developed, using this formulation, for rectangular channels and are presented in the figures below. Figure 5.6 shows $P/L - \phi_{2D}$ plotted against the inverse Biot Number. The Biot number relates the rate of internal conduction to the rate of surface convection and, as mentioned above, can be shown to correlate fin effectiveness. The results for square channel and a range of height to web thickness (H/W) ratios span the range of parameters of interest to RBCC. Also shown on the figure is the range of Biot Number for subcooled hydrogen in the RBCC application. The results illustrate the effect of increased material conductivity on increased channel effectiveness, i.e. as $1/\text{Biot}$ increases, ϕ_{2D} increases to its maximum value of P/L .

Additional results for the effect of channel aspect ratio, H/D , are shown in Figure 5.7 below, which illustrate the relatively weak effect of aspect ratio on the present results. Channel effectiveness is plotted as a function of channel height, H , to web thickness, W , to illustrate the effect over a range of “fin” lengths, i.e. fin length to thickness ratio.

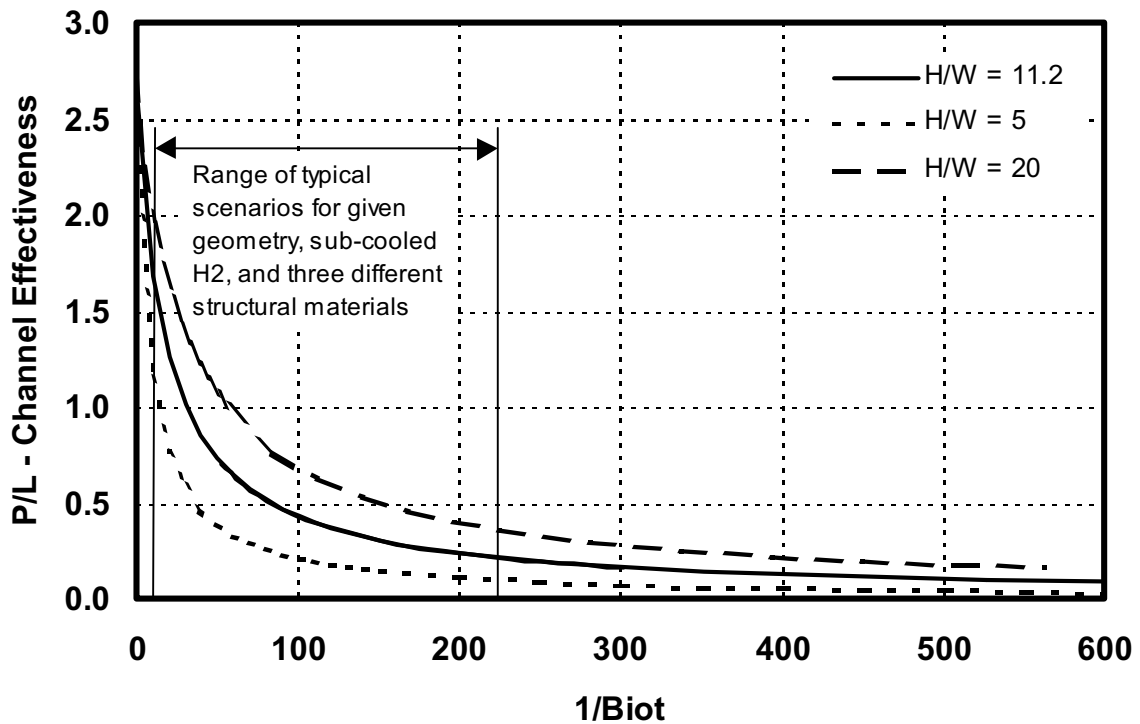


Figure 5.6 Channel Effectiveness Parameter (Square Channel, $H/D= 1$)

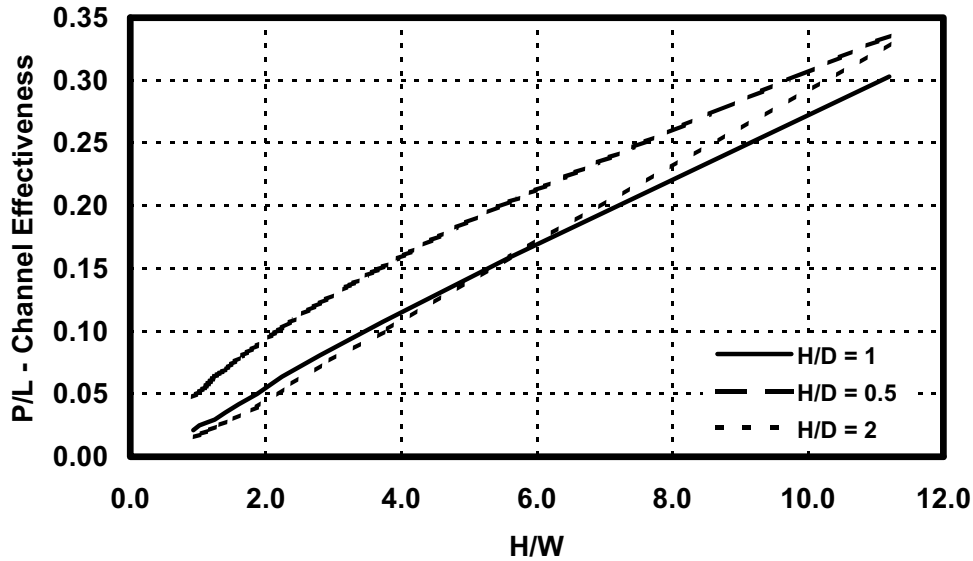


Figure 5.7 "Fin" Geometry Effect on Channel Effectiveness Parameter

The final step in the analysis involves developing a curvefit of the above results for use in VITMAC so that the user can, on option, select the channel augmentation parameter. The relatively well behaved and well understood behavior of the parametric variations make this final step a seemingly straightforward task. In fact, detailed examination of the so-called "fin-efficiency" analysis, for example, Mills (1995)²¹, shows that the fin efficiency for a rectangular fin follows the equation:

$$\eta_{fin} = \text{Tanh} [(hL^2/kW)^{1/2}] / (hL^2/kW)^{1/2} \quad (25)$$

where L is the fin length and all other parameters are the same as our channel effectiveness analysis. Modifying this relation for our channel effectiveness, where the perimeter for convective heat transfer is the internal channel perimeter (see Figure 5.) and H is the fin length implies that the channel effectiveness (normalized by P/L) should follow a modified inverse Biot number, for now call it the Traci No., given by:

$$N_T = kW/hPH \quad (26)$$

And the correlating equation would be:

$$\phi_{2D} / (P/L) = \text{Tanh} [(hPH/kW)^{1/2}] / (hPH/kW)^{1/2} \quad (27)$$

The SINDA 2D channel results for a square channel are plotted in Figure 5.8 as a function of N_T and illustrate that this is indeed a viable correlating parameter and correlating equation.

²¹ Mills, A.T., *Basic Heat and Mass Transfer*, Richard H. Irwin, Inc., 1995

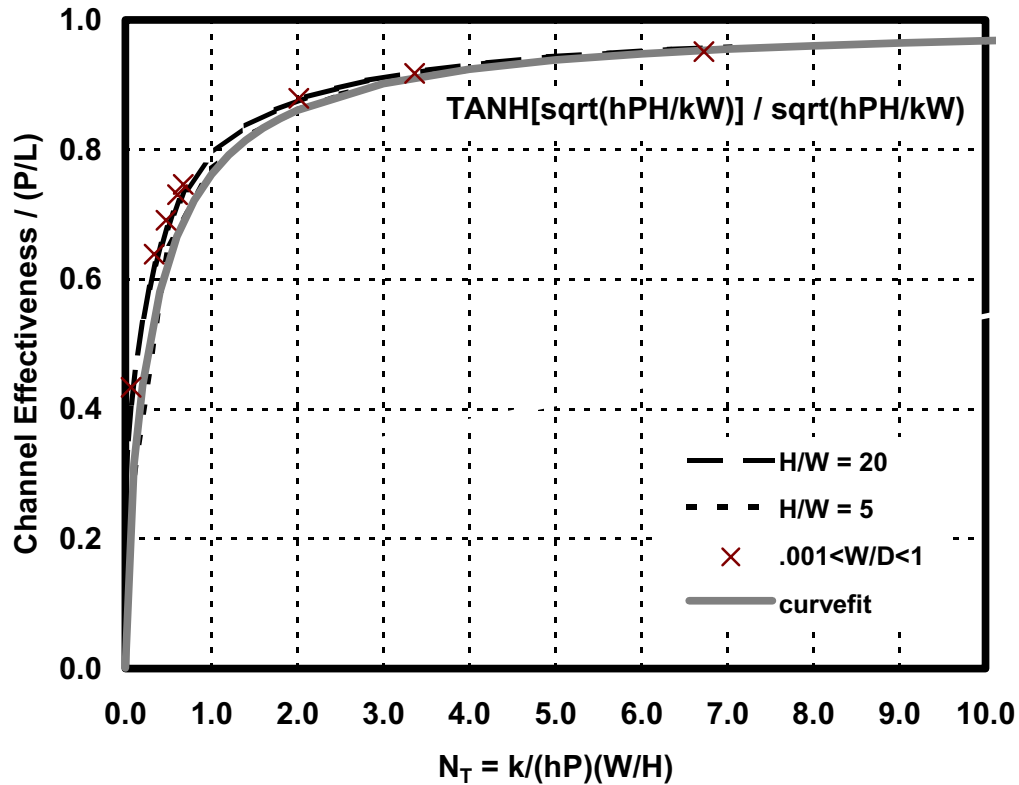


Figure 5.8 Cooling Fin Efficiency Correlation for Square Channel, H/D = 1

The current SINDA calculations for rectangular cooling channels span the following range of parameters:

$$\begin{aligned}
 &0.0 < H/D < 10. \\
 &0.002 < W/D < 5. \\
 &0.15 < t/D < 2. \\
 &.001 < N_{Traci} < 4000
 \end{aligned}$$

and spans the material conductivity and fluid heat transfer ranges of:

$$\begin{aligned}
 &0.1 < k < 1000 \text{ w/(mK)} \\
 &10 < h < 2000 \text{ w/(m}^2\text{K)}
 \end{aligned}$$

All of the SINDA results are plotted below against N_T in Figure 5.9 along with a modification of the fin efficiency equation given by:

$$\phi_{2D} / (P/L) = \text{Tanh} [(\mathbf{0.8hPH/kW})^{1/2}] / (\mathbf{0.8hPH/kW})^{1/2} \quad (28)$$

The equation correlates all of the 2D “data” within a couple of percent.

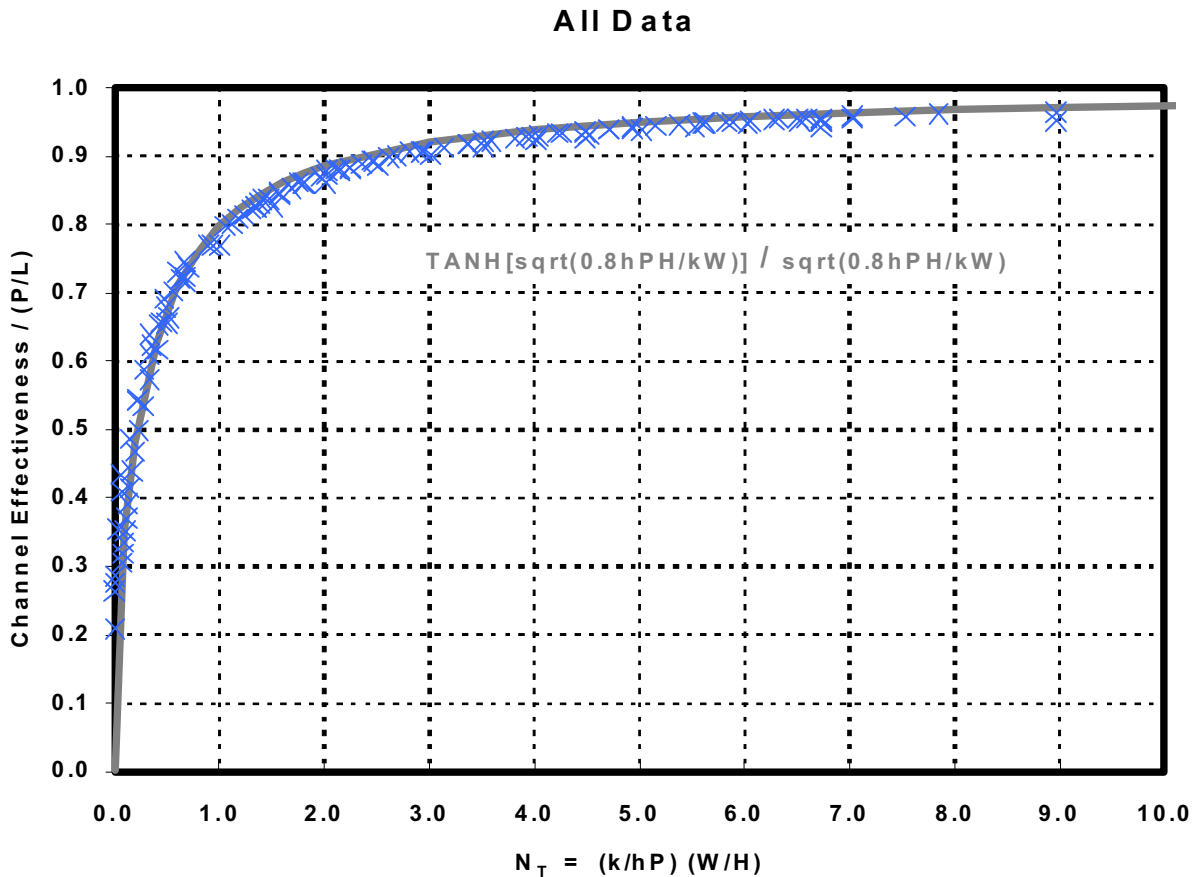


**Figure 5.9 Rectangular Channel Effectiveness Correlation
(0.01 < H/D < 10., 0.002 < W/D < 5., 0.15 < t/D < 2.)**

Upon examining the SINDA 2D results and correlation more completely, it became obvious that an important parameter range for typical cooling panel geometries and material properties of interest would be Biot number = 1 or greater. This implies the parameter range of most interest is N_T less than 1. It is also clear that the above correlation does not result in the correct limiting result for Biot Number = $hD/k \rightarrow \infty$ or for the web thickness, $W \rightarrow 0$. In these limiting cases, the 2D effectiveness parameter should approach P/L or:

$$\phi_{2D} / (P/L) \rightarrow 0.5/(H/D+1)$$

The SINDA results along with a modified correlation for this important parameter range are shown in Figure 5.10. The new correlation modifies the fin effectiveness term to account for the proper limiting case for what is called here the “fin decrement” limit. In other words, for low conduction (small k or W) relative to convection, only the “top” (heated) side of the channel is effective in transferring heat to the cooling fluid. Thus the “fins” or sides of the channels play little role in the heat transfer. In this case, the modified term in the correlation accounts for this effect without altering the “fin effectiveness” limit which is adequately modeled by the previous correlation. As shown in Figure 5.10, the new correlation possesses

an additional geometry variation which seems to capture the variation in 2D SINDA results in this important region.

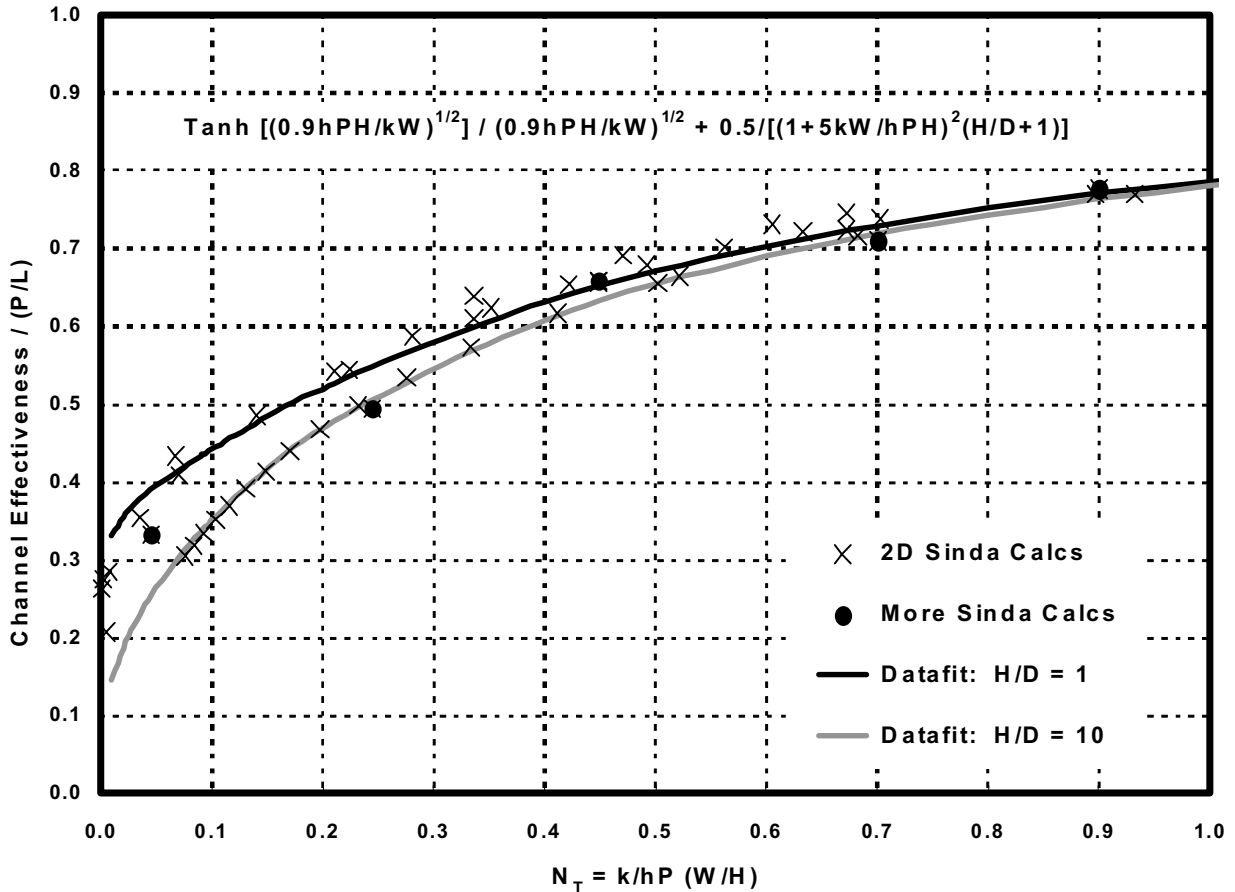


Figure 5.10 Rectangular Channel Effectiveness Correlation for High Biot Number

The new correlation, given by equation 29, is plotted along with all of the SINDA results in Figure 5.11. below. It exhibits the good comparison of the correlation with the SINDA calculations and hints at the improvement in the correlation for the low Traci number limit. Finally, Figure 5.12 presents a scatter plot of the correlation vs the SINDA calculations. With the exception of one “outlier” it illustrates the accuracy of the final correlation with a standard deviation well within 1%.

$$\phi_{2D}/(P/L) = \text{Tanh} [(0.9hPH/kW)^{1/2}] / (0.9hPH/kW)^{1/2} + 0.5/[(1+5kW/hPH)^2(H/D+1)] \quad (29)$$

The correlation can be used to explore the parametric variation of the channel effectiveness parameter for relevant parameter ranges. Figures 5.13 and 5.14 present some of these results for a square channel, H/D = 1, and rectangular channel, H/D = 3, respectively. In this case

the channel effectiveness is defined as ϕ_{2D} as the VITMAC heat transfer correlation factor for 2D channel effects (see above). Both figures show that the channel effectiveness parameter is greater than 1 for a restricted range of web thickness, W/D , depending upon the value of Biot number and channel aspect ratio. They also show that $\phi_{2D} \rightarrow 1$ as $W \rightarrow 0$ and $\phi_{2D} \rightarrow P/L \rightarrow 2(H/D+1)/(W/D)$ for large web thickness. Both tendencies are in concert with analytical and numerical expectations, although it is noted that the comparison of 1D to 2D results will become suspect for large W/D . It is also shown that the channel effectiveness parameter is greater than one for a restricted range of web thickness, again depending upon the Biot number or the ratio of convective to conductive cooling. Finally, the results show that the channel effectiveness parameter can indeed be <1 for large web thickness and for large Biot numbers. This means that the channel heat transfer must be reduced in order for the 1D solution to predict an representative 2D temperature.

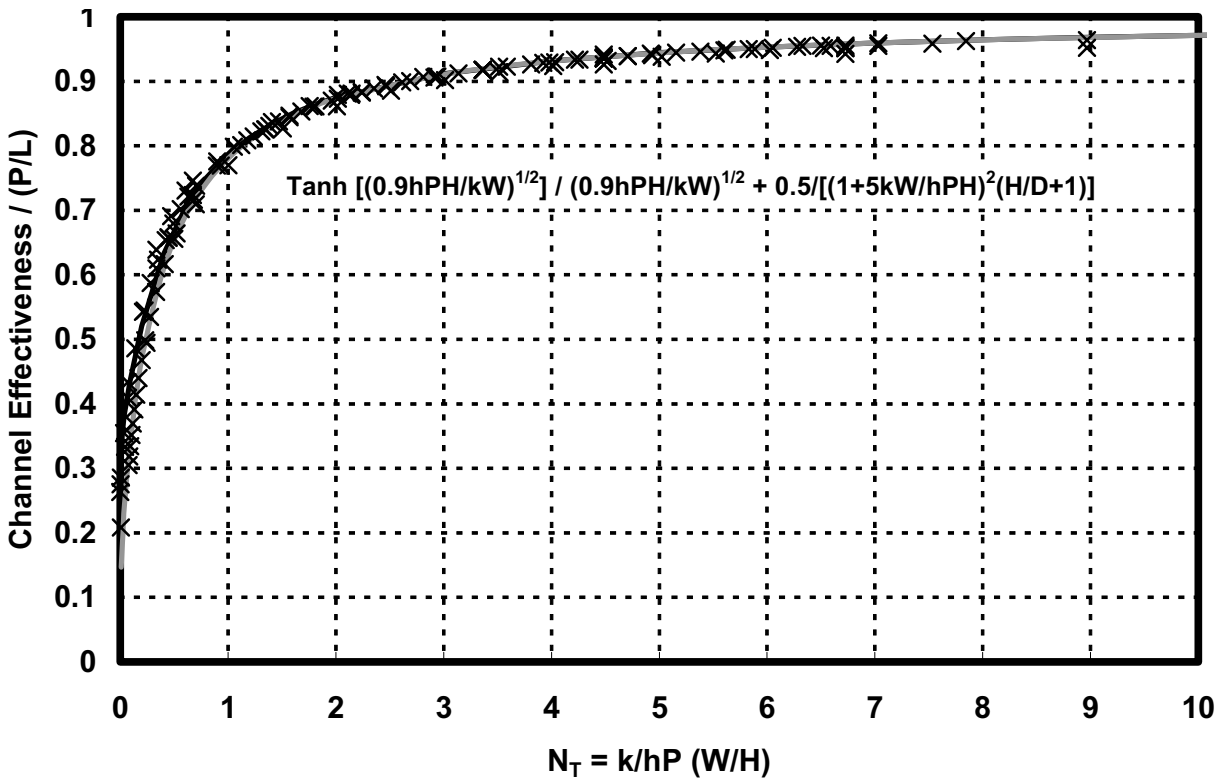


Figure 5.11 Rectangular Channel Effectiveness Correlation

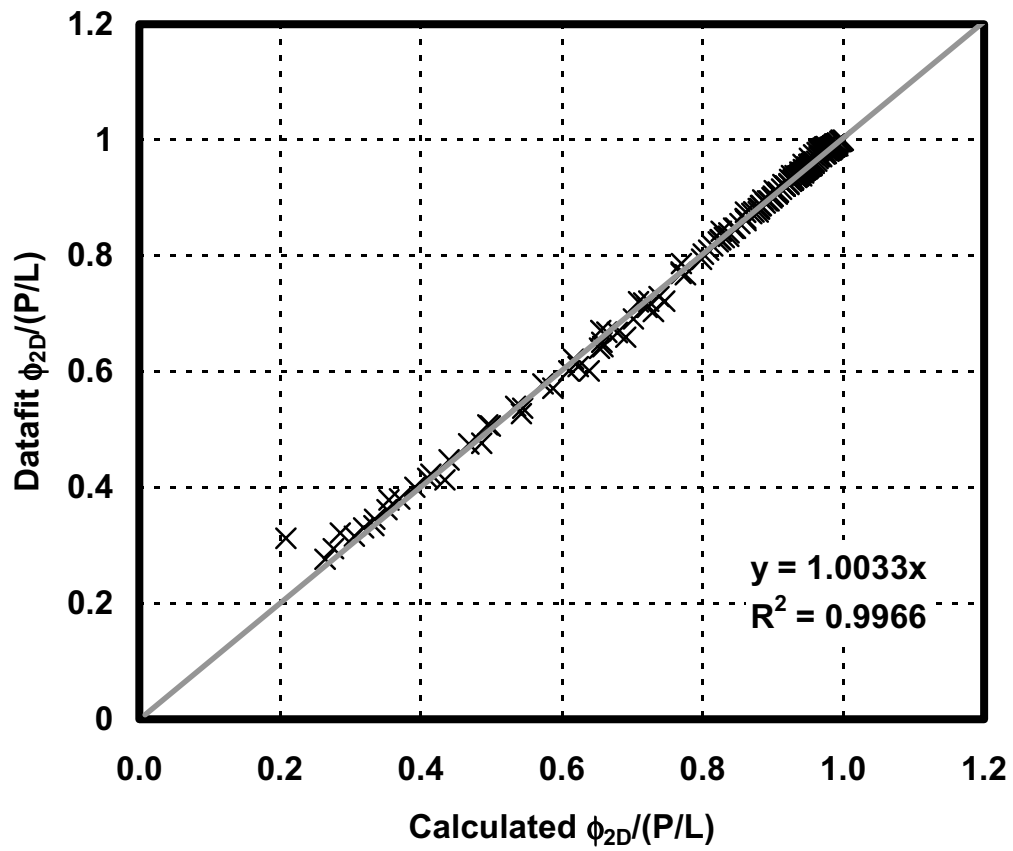


Figure 5.12 Channel Effectiveness Correlation Scatter Plot

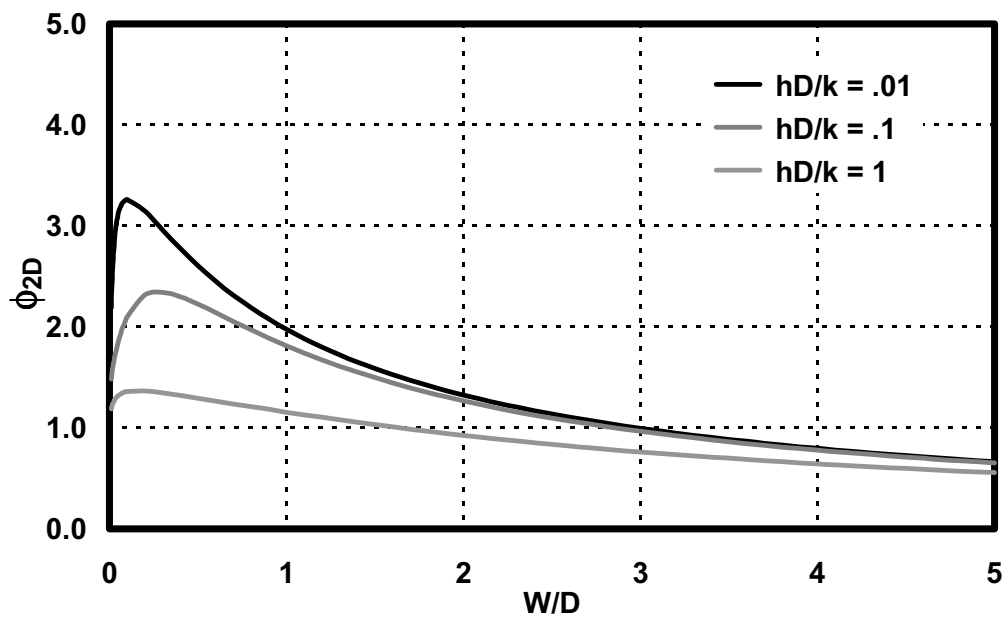


Figure 5.13 Channel Effectiveness for $H/D = 1$

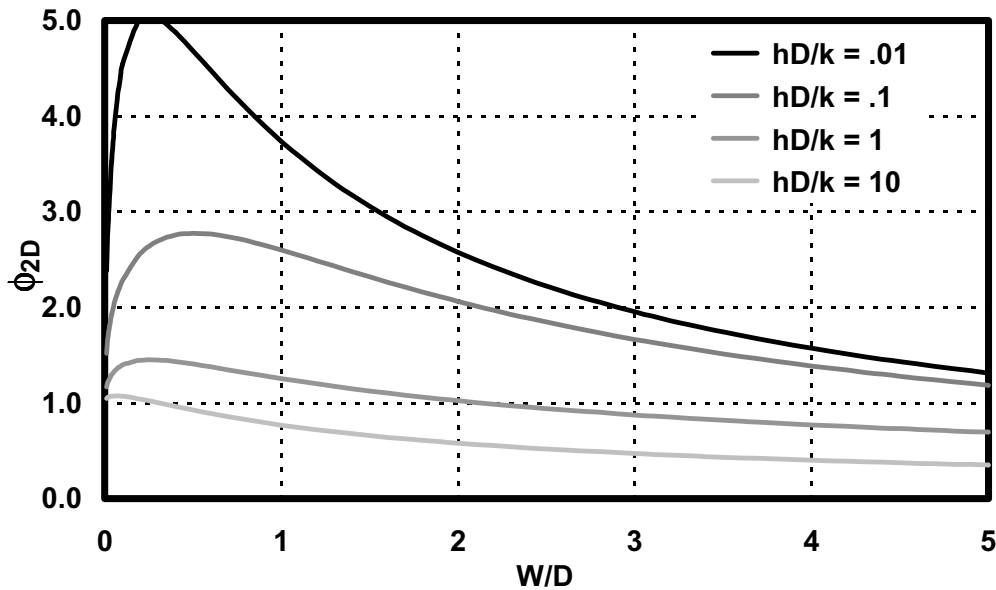


Figure 5.14 Channel Effectiveness for H/D = 3

The final step in the channel effectiveness analysis is to compare a representative two-dimensional analysis with the corresponding one-dimensional VITMAC results. To this end, two SINDA calculations were performed for two representative cooling channel shapes that are being used in a laboratory rocket thrust chamber. The channels, along with the SINDA temperature contour predictions are presented in Figures 5.15 and 5.16 for a channel aspect ratio of 3 and 1. Both calculations are performed using a copper type material (Narloy-Z) with a uniform heat flux on the top surface and convective cooling on the inside channel surface, using representative thrust chamber operational values given by:

Heat flux =	7027 watts/cm ²
Cooling fluid (water) temperature =	29 °C
Channel Heat transfer Coefficient =	25.23 watts/(cm ² °C)
Channel geometry: H, D, W, t	.567, .177, .061, .128 cm

Both results exhibit a relatively one-dimensional temperature distribution from “hot-side” surface to the top-inside surface of the channel with some deviations due to the fin-effect of the sides of the channel. It is also obvious that the increased aspect ratio case (H/D ~ 3) does not have a significantly greater heat transfer augmentation compared to the square channel case. However, the increased thermal gradients due to the web material indicate that both cases should augment the vertical heat transfer relative to the one-dimensional case.

The channel effectiveness correlation presented above implies that for both these cases, the 2D channel augmentation factor would be about $\phi_{2D} \sim 1.25$, indicating, as deduced from the 2D temperature profiles, a modest degree of cold side heat transfer augmentation would be required for the 1D VITMAC calculation to compare to the more accurate 2D result.

Comparative VITMAC simulations were performed for both of these cases, and the “cold-side” temperature predicted by VITMAC is compared to the temperature profiles on the top side of the channel from the SINDA calculations in Figure 16. As indicated there, the VITMAC temperature for the $H/D = 1$ case is within 1°C of the peak temperature predicted by SINDA. Similarly, the VITMAC prediction for $H/D = 3$ is about 7°C lower than the SINDA calculation. Note that the unaugmented VITMAC result ($\phi_{2D} = 1$) predicts a cold-side temperature that is over 40°C higher than the SINDA results as well as the new VITMAC results.

These results indicate that the degree to which the channel effectiveness parameter developed here can improve the interpretation of VITMAC’s one-dimensional results if not the quantitative accuracy for representative cooling panel design parameters.

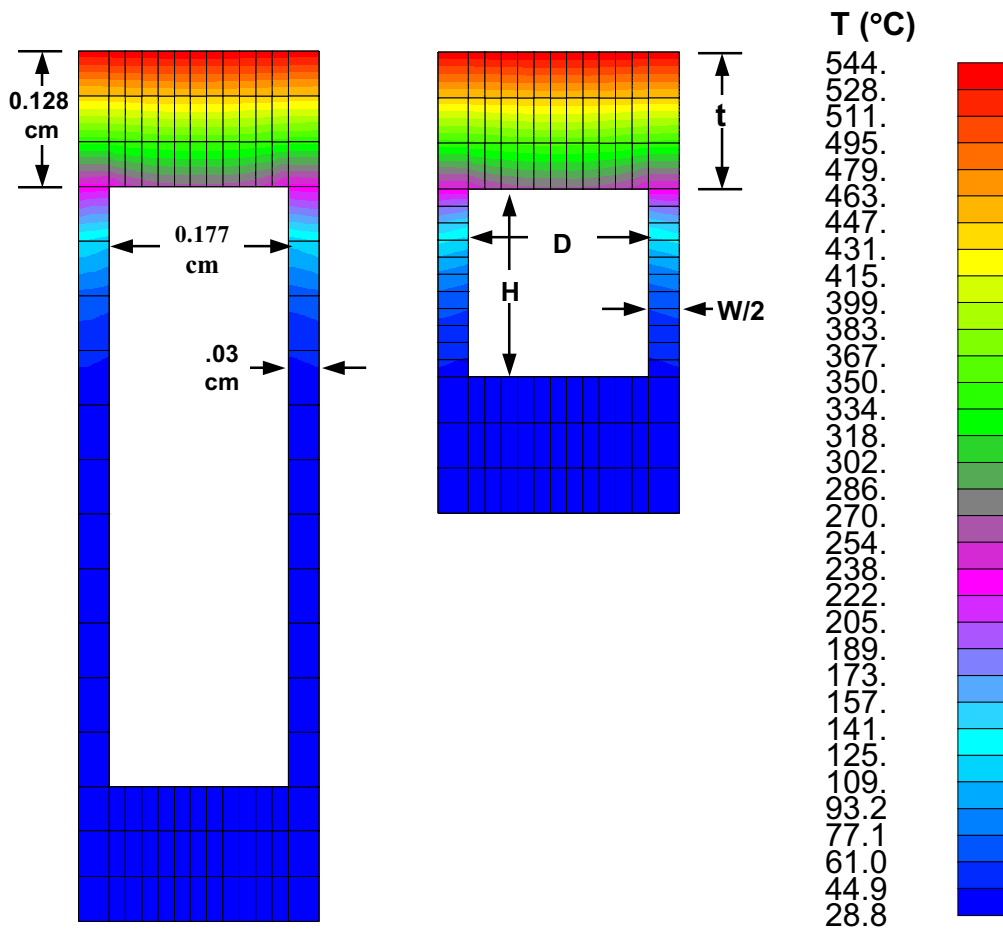


Figure 5.15 SINDA 2D Channel Temperature Profiles for $H/D \sim 3$ and $H/D = 1$

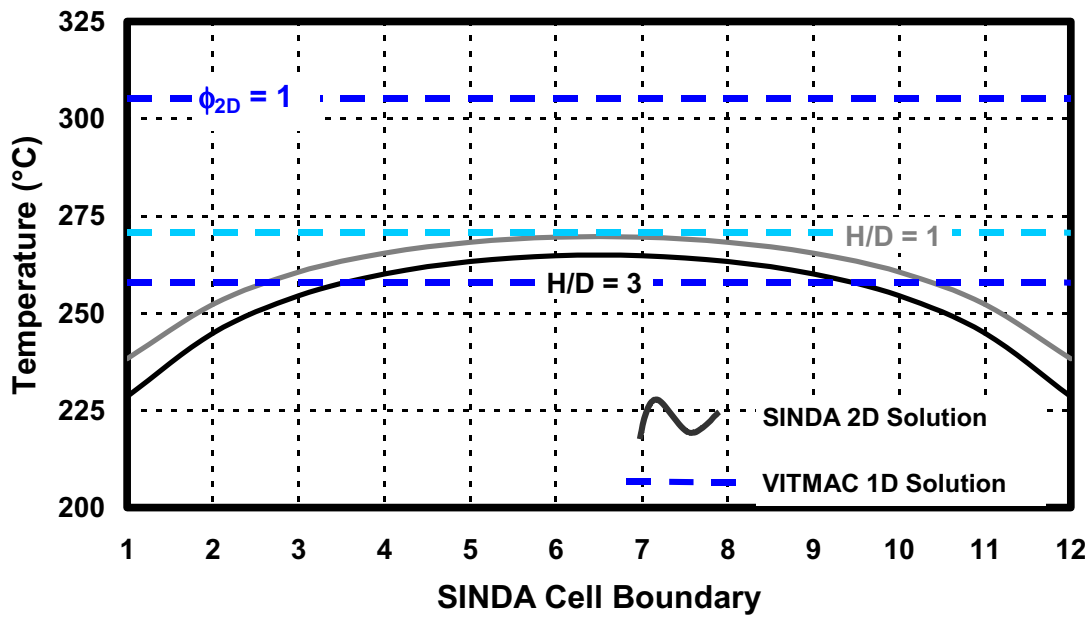


Figure 5.16 “Cold-side” Channel Temperature Comparison of 2D SINDA to 1D VITMAC Calculations

5.3 Cooling Channel Analysis: Circular Channel with Conductive Liner

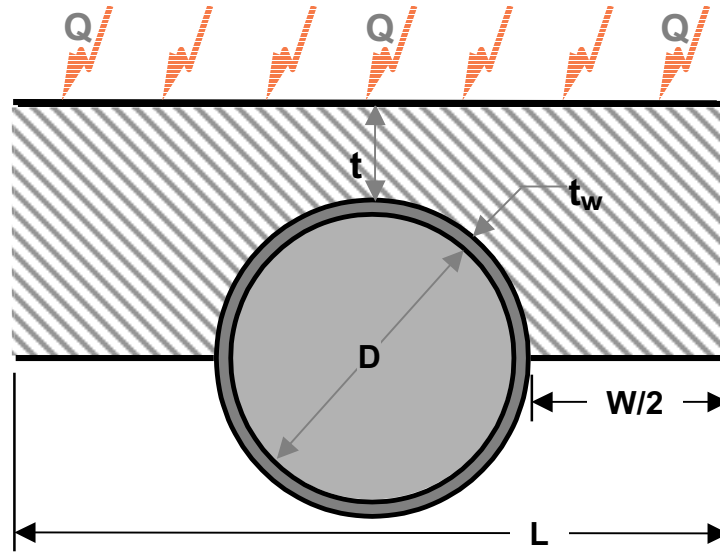


Figure 5.17 Parameters for Circular Channel Geometry Analysis

The potentially important aspect ratio effect shown for the rectangular channel correlation presented above indicates that the 2D channel effectiveness parameter will also be sensitive to the shape of the channel. Since circular coolant channels are also of interest, the channel geometry shown in Figure 5.17 was also considered to expand the utility of the present approach. For the circular geometry it was decided to account for a relatively thin conductive liner (typically metallic, with thickness t_w and conductivity k_w) since this is a likely design for refractory composite coolant panels. The approach (and parameter definitions) used here directly follows the approach described above. Two-dimensional SINDA calculations were performed for the circular channel section over a range of relevant quantities and used to calculate the channel effectiveness parameter. Program resources did not permit the numerous calculations described above but the calculation matrix (15 calculations) was designed to cover a relevant range of Biot Number and geometric quantities.

The first attempt at a correlation of the circular channel results used the rectangular correlation with $H = D$, and is shown in Figure 5.18 along with the ultimate correlation. The results were relatively good except for the usual $W \rightarrow 0$ and $k \rightarrow 0$ limits, as before. In addition, the sometimes dominant effect of the thermally conductive liner had to be accounted for. Taking these factors into account resulted in the correlation given by:

$$\phi_{2D} / (P/L) = \text{Tanh} [(1.3/N_T)^{1/2}] / (1.3/N_T)^{1/2} + 0.5/(\pi(1+5N_T)^2) \quad (30)$$

where the inverse Biot Number is modified to account for the liner:

$$N_T = (kW + 2k_w t_w) / (h\pi D^2)$$

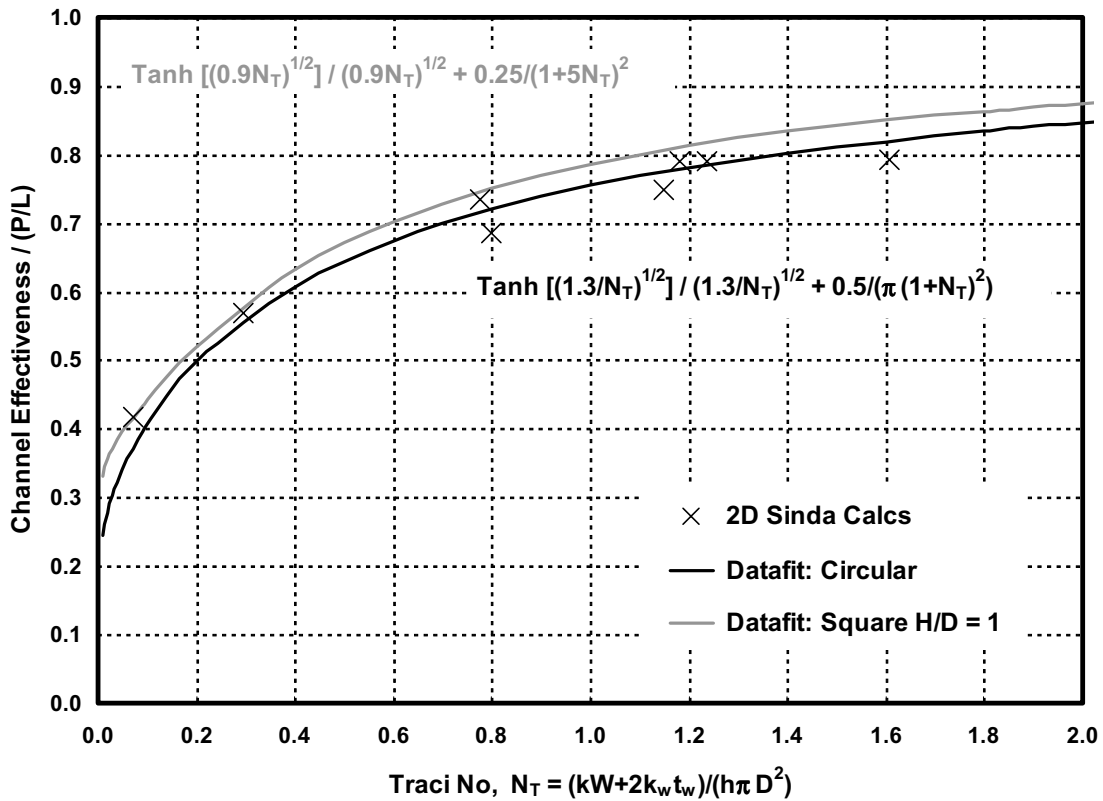


Figure 5.18 Circular Channel Effectiveness Correlation for High Biot Number

The final correlation results are shown in Figure 5.19 and the scatter plot of Figure 5.20. They are judged to be quite good, especially in the important range, $N_T < 1$. The scatter plot indicates that the correlation is within 1 % of the SINDA results even considering the relatively low number of “data points”. Also shown on Figure 5.20 are the four SINDA results for a candidate GTX configuration, a specific circular cooling channel design utilizing anisotropic Carbon Carbon material. Detailed SINDA results with comparison to 1D VITMAC results are presented below to close the circular cooling channel analysis.

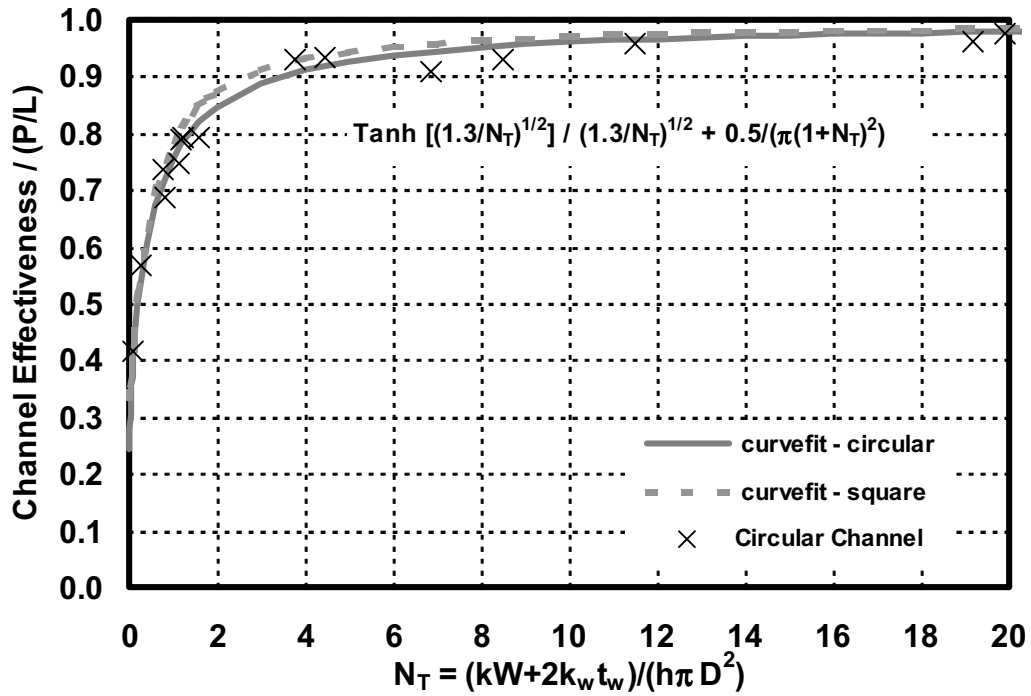


Figure 5.19 Circular Channel Effectiveness Correlation

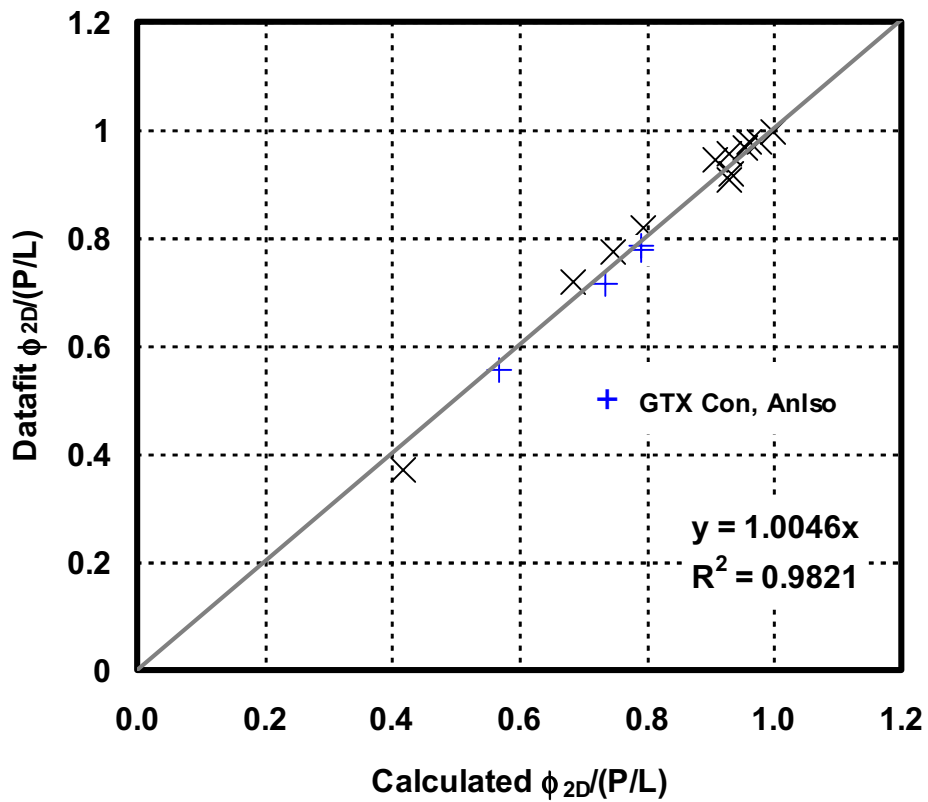


Figure 5.20 Circular Channel Effectiveness Correlation Scatter Plot

SINDA calculations were performed for two representative circular cooling channel shapes that are being investigated for use in the GTX concept. The channels, along with the SINDA temperature contour predictions are presented in Figures 5.21 through Figure 5.24 for an isotropic version of the channel and for the anisotropic Carbon-Carbon (C-C) material. Both calculations are performed with a uniform heat flux on the top surface and convective cooling on the inside channel surface, using representative operational values given by:

Heat flux =	125 watts/cm ²
Cooling fluid (hydrogen) temperature =	-120 °C
Channel Heat transfer Coefficient =	0.37watts/(cm ² °C)
Channel geometry: D, W, t	GTX Configuration

For the isotropic and anisotropic cases, the following values of vertical, k_v , (through the thickness) and horizontal, k_h , material conductivity are used:

Isotropic Conductivity:	$k_h : k_v = 35. : 35. \text{ W/m-K}$
Anisotropic Conductivity:	$k_h : k_v = 70. : 39.3 \text{ W/m-K}$

The results for the isotropic conductivities are presented first in Figures 5.21 and 5.22 which depict the predicted temperature contours through the cooling panel material and temperature distributions on the channel surfaces respectively. The results for this case show a pronounced effect of the copper liner in directing the heat load to the coolant within the channel. Of most interest to this study is that the VITMAC 1D solution (which uses the channel correlation developed here) for the “cold-side” channel temperature compares very well to the 2D SINDA results as shown in Figure 5.22. Note that the uncorrected VITMAC solution ($\phi_{2D}=1$) significantly over-predicts the channel temperature.

Corresponding results for the anisotropic C-C material are presented in Figures 5.23 and Figure 5.24. These results are similar to the isotropic case but exhibit the cooling effect of the higher horizontal conductivity which serves to magnify the channel liner cooling by directing a greater proportion of the heat towards the channel. Both “hot-side” and “cold-side” temperature distributions are shown in Figure 5.24 to provide a measure of validation of the VITMAC predictions. Using the geometry correlation (Equation 30) presented in this section, the VITMAC 1D results provide a credible prediction of both sides of the cooling channel. The VITMAC hotside results are within about 20°C of the SINDA results and the coldside prediction is reasonably close to the average of the inside channel temperature. Note again that the 1D result ($\phi_{2D}=1$), calculated without the channel geometry correlation, is significantly higher than the SINDA results for both “cold-side” and “hot-side” (not shown).

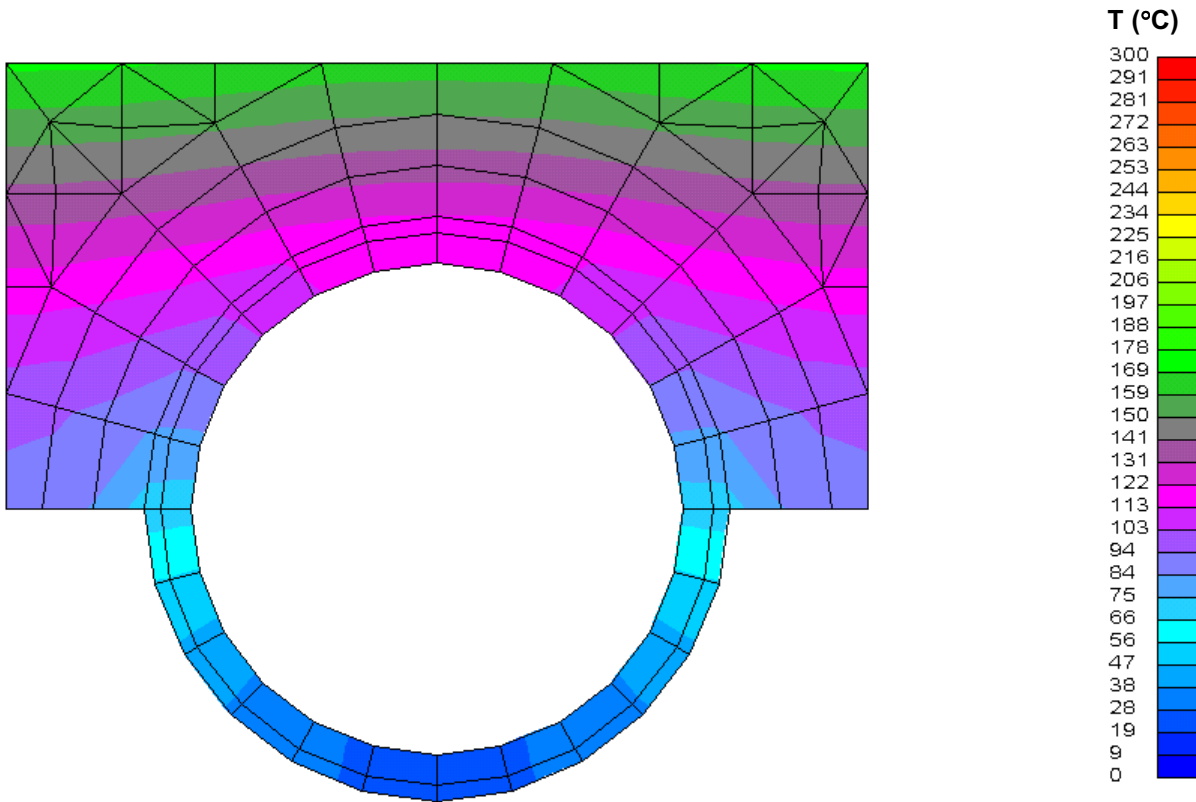


Figure 5.21 SINDA 2D Channel Temperature Profiles for Circular Channel, Isotropic Conductivity ($k_h : k_v = 35. : 35. \text{ W/m-K}$)

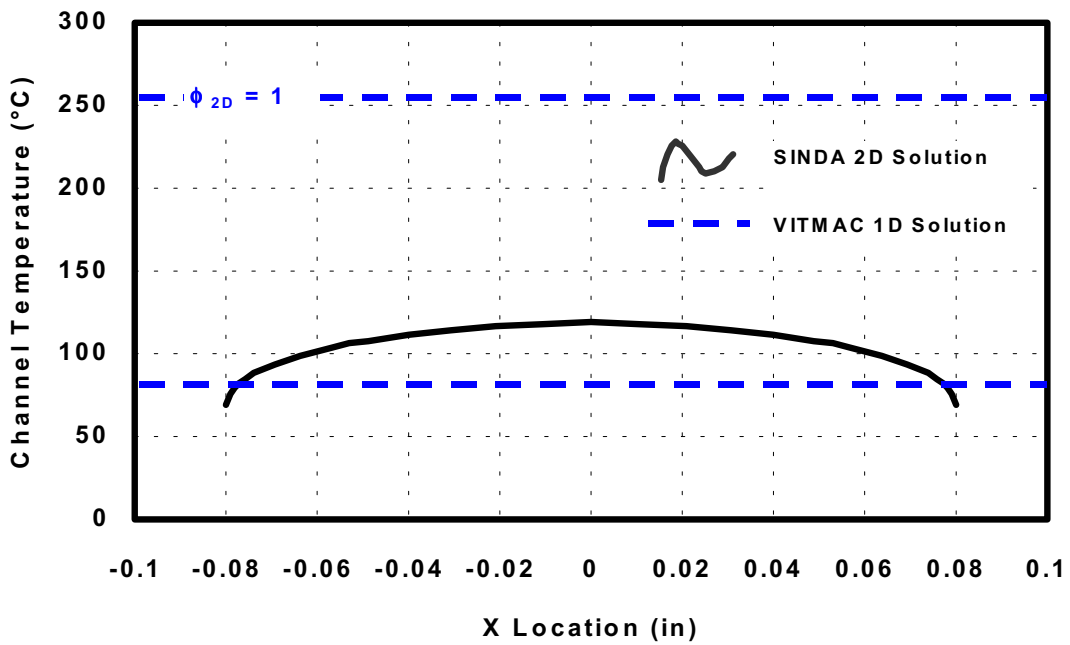


Figure 5.22 “Cold-side” Channel Surface Temperature Comparison of 2D SINDA to 1D VITMAC Calculations

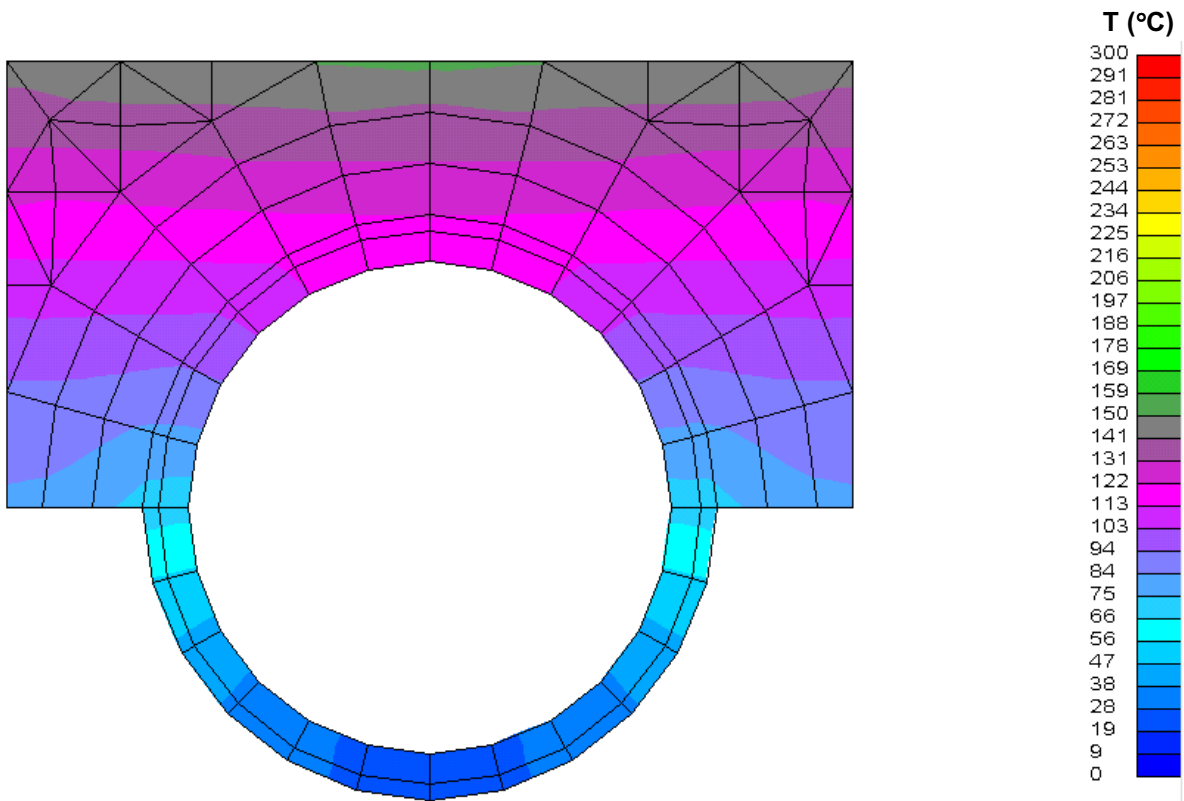


Figure 5.23 SINDA 2D Channel Temperature Contours for Circular Channel, Anisotropic Conductivity ($k_h : k_v = 70. : 39.3 \text{ W/m-K}$)

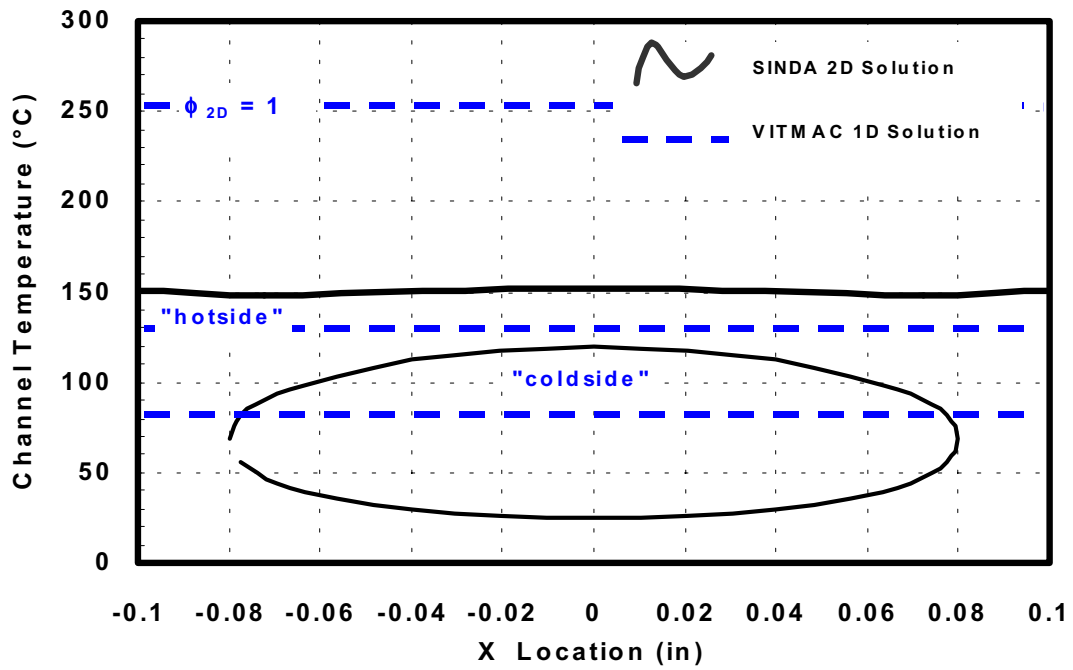


Figure 5.24 “Cold-side” Channel Surface Temperature Comparison of 2D SINDA to 1D VITMAC Calculations
Circular Channel, Anisotropic Conductivity ($k_h : k_v = 70. : 39.3 \text{ W/m-K}$)

6. Other VITMAC Model Development Studies

Additional model development studies were performed as part of this program to enhance the capability of VITMAC to model projected RBCC thermal management systems. These included the development of a gas generator model for use with the VITMAC turbine model which can be used to drive a pump component to thereby make up a detailed turbopump model. Analyses to understand the range of operation of the combined models were also performed. In addition, studies were performed to enhance the stability and convergence of the solution scheme for stressing RBCC operating conditions. The results of these investigations are described in this section.

6.1 Gas Generator Source Model

The gas generator component uses CEA to generate gas flow conditions from user input parameters. The approach follows the model already implemented as the CEA rocket engine linkage and as the “gas generator” (or RJPA fuel injection) feature which specifies fuel injection conditions for the RJPA engine model. In the present implementation, the gas generator has been added as an option to the VITMAC “source” component as shown in Figure 6.1. The source now allows for the four options shown: Tabular Input values, transient Tank Analysis, the Cryogenic Tank Model and the new Gas Generator source. Selecting each source type opens an appropriate window for model input. The first three options behave exactly as before and the Gas Generator option opens the User Input window shown in Figure 6.2 for additional model input specification.

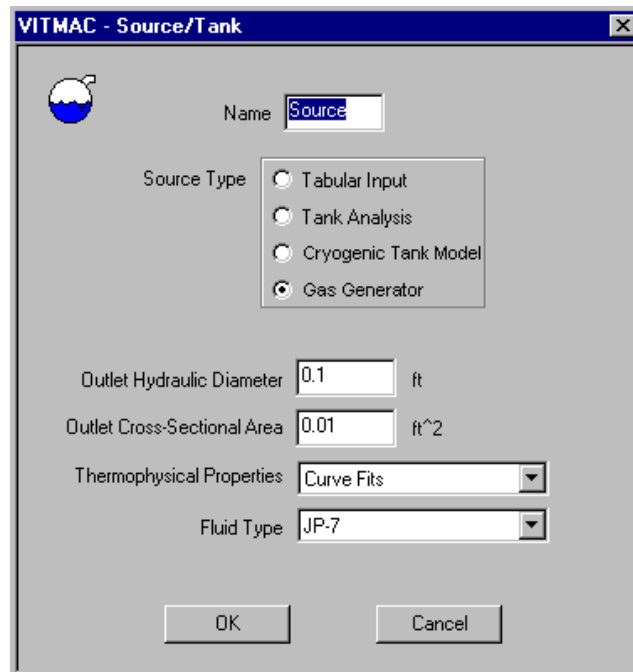


Figure 6.1 Gas Generator Source Option

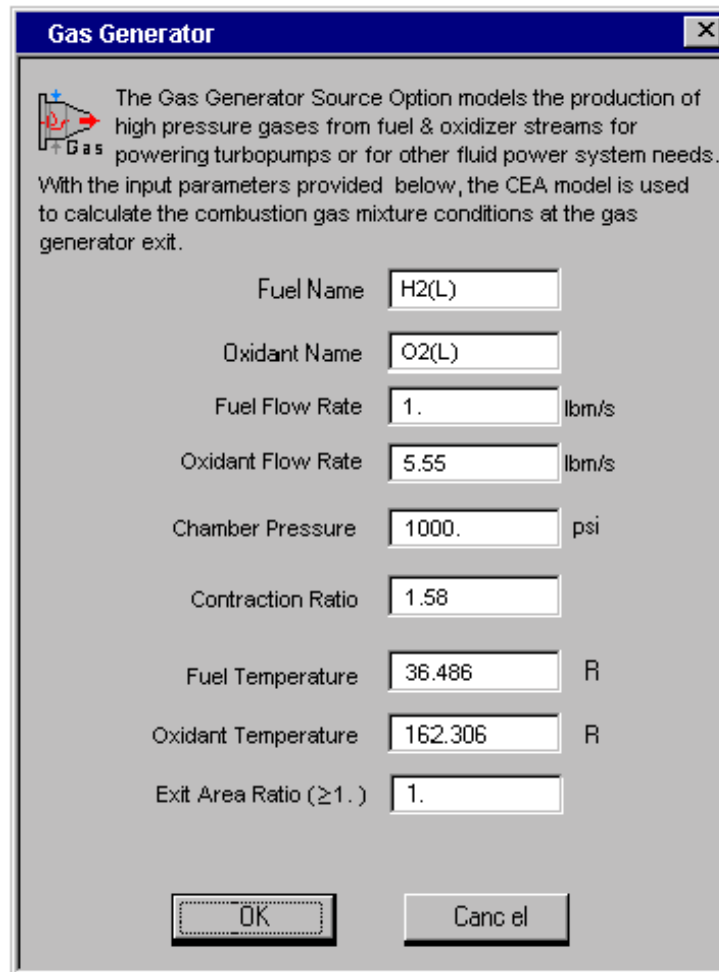


Figure 6.2 Gas Generator Input Window

Gas Generator operating parameters are input through the VITMAC GUI using the Gas Generator dialog box shown in Figure 6.2, above. The quantities displayed there are typical gas generator parameters which provide a relatively complete definition of such a device. Values are input through standard edit boxes as shown in the figure and as described here:

- *Fuel and Oxidizer Names* (Ex. H2(L) & O2(L)) are input using the reactant names given in Appendix B of NASA RP1311, and reproduced in the Appendix at the end of the VITMAC 6.0 User's Guide
- *fuel and oxidant flow rates* are input to determine the oxidizer-to-fuel mixture ratio (by weight) which determines the post-combustion conditions
- *Chamber Pressure* (Combustor pressure at the injectors) determines the combustor conditions along with the
- *Contraction Ratio*, which is the Area Ratio of the Combustor at the injectors normalized to the throat area

- *Reactant Temperatures* (pre-combustion) are input as they are a moderating influence on gas generator conditions, and the
- *Exit Area Ratio* (relative to the throat) of the gas generator is input for generality (usually = 1.).

CEA Input:		
problem rocket equilibrium		(defines an equilibrium expansion rocket problem)
fac		(finite area combustor)
p,bar =	53.	(chamber pressure in bars)
ac =	1.58	(contraction ratio, i.e. A_c/A_t)
o/f=	W_{oxid}/W_{fuel}	(oxidizer-fuel ratio)
reactant fuel="H2(L)"	wt%=100. t= $t_{fuel}/1.8$	(define fuel name from CEA reactant list, Ex. H2(L), fraction of total fuel and fuel temperature)
reactant oxid="O2(L)"	wt%=100. t= $t_{oxid}/1.8$	(define oxidizer name from CEA reactant list, Ex. O2(L), fraction of total oxid And oxidizer temperature)
Supar = Aexit		,for supersonic sections on the nozzle side of the throat, A=1
Output siunits		(CEA calculates flow results in SI units)
CEA Output for gas generator quantities: (need to convert from SI)		
temperature	=	T at EXIT
pressure	=	P "
enthalpy	=	H "
density	=	RHO "
velocity	=	MACH*SON VEL "
mixture	=	mole fractions "
Define SUPERTRAPP fluid mixture for Loop given by:		
H2O, CO, CO2, N2, H2, O2		

Figure 6.3 CEA Input and Output Definition

Using these parameters, CEA is run to determine the gas mixture conditions at the gas generator exit. A relation for source pressure as a function of flow velocity ($P_{source}(u)$) is developed from internal calls to the CEA program. This function is used in the VITMAC iterative solution to match the source pressure head relative to loop pressure losses until a solution is determined. The VITMAC "source" fluid is considered as a SUPERTRAPP fluid

consisting of: H₂, O₂, H₂O, N₂, CO₂, and CO gas components, whose relative mole fractions are determined by CEA along with the mixture temperature and pressure. The gas mixture is designed to mimic the high pressure, moderate temperature exhaust gasses from gas generators fueled by H₂ and O₂ fuels. All “minor” species calculated by CEA but not in the SUPERTRAPP exhaust fluid list are “lumped” into the H₂O component. It should be noted that as long as the exhaust temperature is below about 3500R, (i.e. undissociated) this mixture approximation is accurate. It also provides a less accurate, but perhaps acceptable, approximation to hydrocarbon/air fueled gas generators for high excess-air operation. The CEA model provides an accurate estimate of real gas flow conditions exiting the gas generator and the current implementation is limited only by the accuracy of the SUPERTRAPP fluid component types described below. For example, various radical species (H, OH, HO₂ etc.) are not included in SUPERTRAPP so accuracy at high temperature operation may be limited. However, model comparisons indicate that this is not a significant concern at typical gas-generator operating conditions.

Tests have been performed using hydrogen-oxygen fuels, which indicate that this fluid component mixture provides an excellent gas model for typical gas-generator conditions. The mixture should also be adequate for certain hydrocarbon fuels, as well, and preliminary tests with CEA indicate this to be the case but our primary interest is an accurate model for hydrogen fueled gas generator operation. Finally, the VITMAC fluid model presented in Figure 6.4 has been used in comparative tests of the fluid behavior using the new gas generator model along with the previous source model with an equivalent SUPERTRAPP fluid. As indicated, the gas generator model produces the identical loop results.

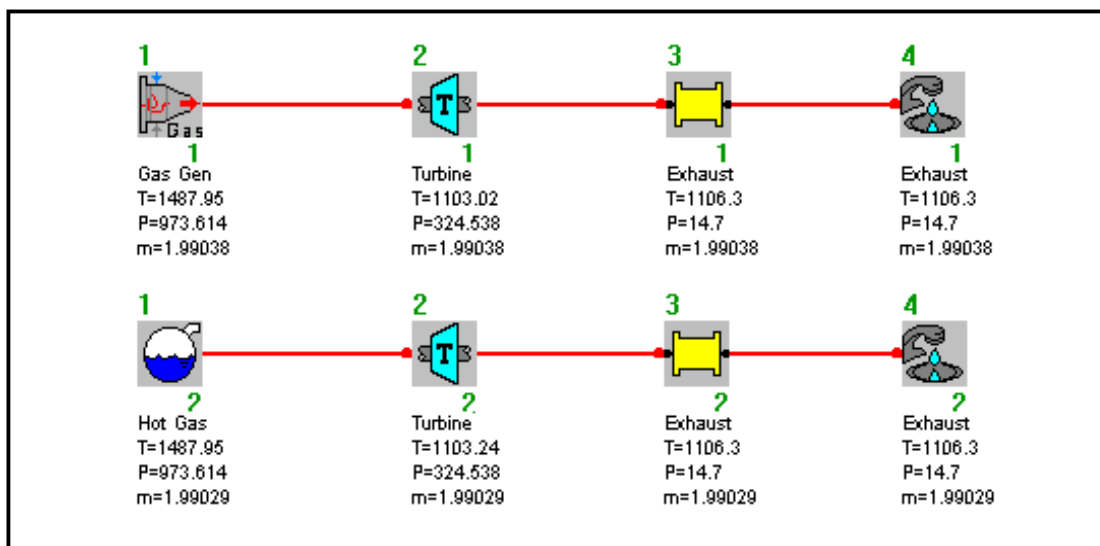


Figure 6.4 Gas Generator Test Case

Tests performed to date with the gas-generator capability have been quite robust. The capability may be used in an example gas loop which includes the gas-generator source, a turbine component with waste-gate and a valve for flow control, such as shown in Figure 6.5 below. In general application, the turbine in the gas generator loop would run a pump in a

fuel and/or oxidizer loop as well. All components can be fine-tuned for user needs by the usual VITMAC component parameter modification methods. Additionally, the Level 1 optimization methodology (see VITMAC 6,0 User's Guide) can be used to ensure that the mass flow rate in the gas-generator loop matches the desired flow rate, i.e. $W_{\text{fuel}} + W_{\text{oxid}}$.

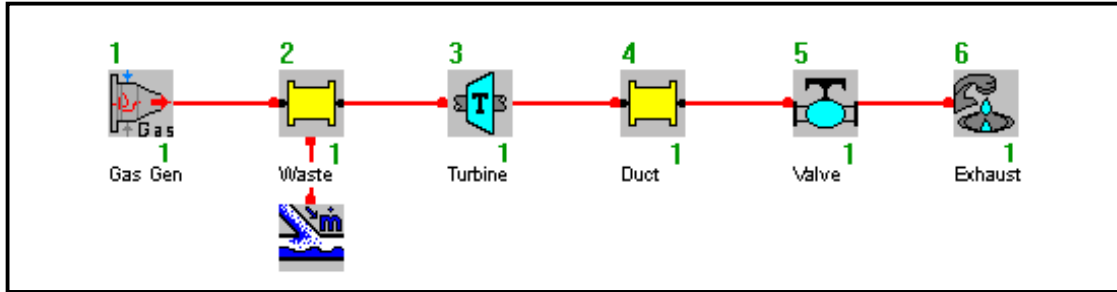


Figure 6.5 Example Gas Generator/Turbo-pump Loop

6.2 Turbo-pump Considerations

The other aspect of the gas generator/turbo-pump model is the treatment of the turbine, which extracts the energy from the high pressure gas stream and the cryo-pump which drives the fuel/oxidizer cooling/fuel loops. The existing VITMAC turbine and pump models contain the functionality needed as a first level turbo-pump model. In this regard, the “power-matching” algorithm for linking turbomachinery on a shaft was recently improved and has been verified for gamma-law gases. A more exact treatment of fluid enthalpy change across a turbine or compressor has also been formulated. In this approach, SUPERTRAPP is used to determine the turbomachinery output flow conditions.

The present turbomachinery model determines the isentropic enthalpy change across the component given its efficiency, η , and specified pressure ratio, R_t for a turbine, as follows:

$$R_t = P_{\text{in}}/P_{\text{out}} \quad (31)$$

then:

$$h_{\text{out}} = h_{\text{in}} + \eta (h_{\text{out,S}} - h_{\text{in}}) \quad (32)$$

where

$$h_{\text{out,S}} = h_{\text{in}} \times R_t^{(1-\gamma)/\gamma} \quad (\text{VITMAC fluid, assumes a constant } \gamma \text{ expansion})$$

$$\text{or } h_{\text{out,S}} = H(S_{\text{in}} , P_{\text{out}}) \quad (\text{SUPERTRAPP fluid})$$

and

$$W_{\text{out}} = \dot{m} (h_{\text{out}} - h_{\text{in}}) \quad (33)$$

When a turbine runs a compressor/pump, the turbine pressure ratio is calculated to supply the necessary compressor or pump power requirements on the specified shaft, i.e.

$$\dot{m} (h_{\text{in}} - h_{\text{out}}) \Big|_t = \dot{m} (h_{\text{out}} - h_{\text{in}}) \Big|_c \quad (34)$$

The isentropic enthalpy change for the SUPERTRAPP fluid requires an iteration procedure to determine the output flow conditions given the output pressure and input entropy. Such a procedure has been developed and is currently being implemented. However, a new version of SUPERTRAPP (version 3.0) has just been acquired which has a built-in routine for providing equation-of-state (eos) information, given entropy and pressure. The implementation of this version into VITMAC is being considered as an alternative to our iteration scheme. The new version has the attendant benefit that it also provides built-in routines for eos calls with enthalpy-pressure thereby simplifying iterations already implemented in VITMAC. This implementation of SUPERTRAPP 3.0 is clearly the direction to take and will be implemented in a future version of VITMAC.

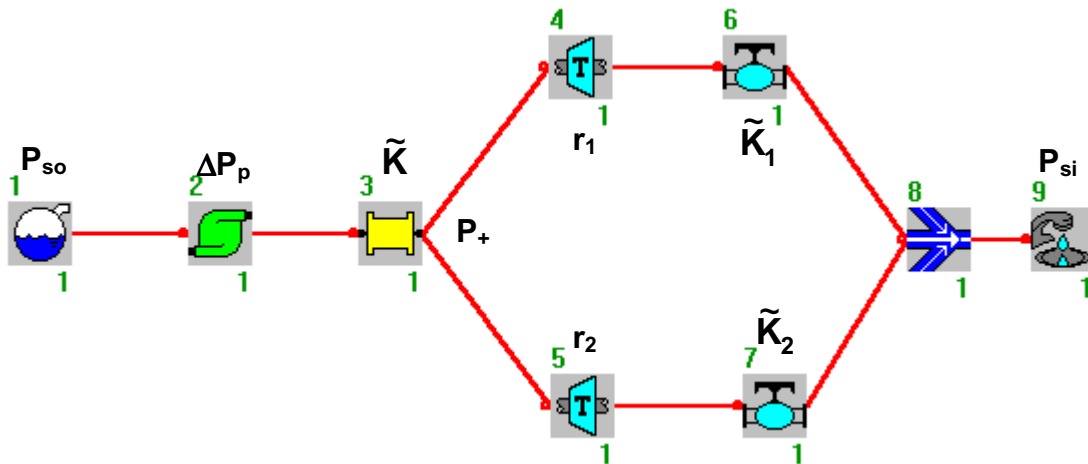


Figure 6.6 Generic Turbine Network

Although a typical gas generator driven turbo-pump would drive a pump in another loop, turbopumps may also be used in an “expander cycle” to drive the fluid in the same loop by utilizing the heated fuel in a regenerative fueled engine loop. Such implementations require special consideration, such as described here to reach an achievable solution. For example, consider a generic VITMAC fluid network including a pressure head supplied by a combination of source and pump pressure (P_{so} and ΔP_p), general flow losses (with an

effective $K_{\text{loss}} = \tilde{K}$), and parallel turbine legs (pressure ratio r_i , and $K_{\text{loss}} = K_i$), exhausting into a sink (pressure P_{si}) as indicated in the figure.

First consider the pressures in a single turbine leg:

$$P_{\text{so}} + \Delta P_p - \tilde{K} \dot{m}^2 = p_+ = r_t (P_{\text{si}} + \tilde{K}_1 \dot{m}^2) \quad (35)$$

Solving for the flowrate results in:

$$\dot{m}^2 = \frac{P_{\text{so}} + \Delta P_p - r_t P_{\text{si}}}{\tilde{K} + r_t \tilde{K}_1} \quad (36)$$

which implies that:

$$1 < r_t < \frac{P_{\text{so}} + \Delta P_p}{P_{\text{si}}} \quad (37)$$

This provides the perhaps obvious requirement that the turbine pressure ratio must be less than the available pressure head (relative to sink pressure) to ensure a positive flow through the system.

A similar examination of the parallel turbine legs begins with the requirement for equivalent pressure losses through each leg, as follows:

$$\frac{p_+ - \tilde{K}_1 \dot{m}_1^2}{r_{t1}} = P_{\text{si}} = \frac{p_+ - \tilde{K}_2 \dot{m}_2^2}{r_{t2}} \quad (38)$$

Rearranging each equation to eliminate the intermediate pressure, p_+ , provides:

$$r_{t1} (P_{\text{si}} + \tilde{K}_1 \dot{m}_1^2) = r_{t2} (P_{\text{si}} + \tilde{K}_2 \dot{m}_2^2) \quad (39)$$

which can be solved for the leg 2 flowrate:

$$\dot{m}_2^2 = \frac{1}{\tilde{K}_2} \left[P_{\text{si}} \left(\frac{r_{t1}}{r_{t2}} - 1 \right) + \frac{r_{t1}}{r_{t2}} \tilde{K}_1 \dot{m}_1^2 \right] \quad (40)$$

Which provides a positivity requirement for the leg 2 flowrate, given by:

$$\frac{r_{t1}}{r_{t2}} > \frac{1}{1 + \frac{\tilde{K}_1 \dot{m}_1^2}{P_{\text{si}}}} \quad (41)$$

which basically implies that a positive flowrate requires that the leg 1 pressure loss be greater than the leg 2 turbine pressure ratio requirement. This can be written in another way:

$$\boxed{\frac{\tilde{K}_1 \dot{m}_1^2}{P_{si}} > \frac{r_{t2}}{r_{t1}} - 1} \quad (42)$$

This relation demonstrates the need for some pressure loss mechanism in the leg with the lowest pressure ratio turbine. Again, an obvious requirement in hindsight. One final relation can be garnered from the above analysis Equation 40. can be solved for the flowrate ratio in the respective turbine legs:

$$\left(\frac{\dot{m}_2}{\dot{m}_1} \right)^2 = \frac{\tilde{K}_1}{\tilde{K}_2} \left[\frac{r_{t1}}{r_{t2}} + \frac{P_{si}}{\tilde{K}_1 \dot{m}_1^2} \left(\frac{r_{t1}}{r_{t2}} - 1 \right) \right] \quad (43)$$

For turbine pressure ratios that are equal, Equation 43. shows that the leg flowrates are proportional to the inverse of the respective K_{loss} in each leg; a useful relation for balancing the flow and turbine power for parallel turbine configurations.

6.3 Solution Convergence Studies

Considerable technical effort during the present program has focused on improving the numerical procedures used in VITMAC to improve the “robustness” of the solution for general cooling circuits typical of GTX applications. This has centered on improving:

- parameter initialization procedures
- numerical solution iteration procedures
- heat load “ramp-up” implementation
- turbo-machinery “power-matching” methodology

A number of fluid loop initialization procedures have been examined to little benefit in solution “robustness.” All aspects of the numerical solution procedure have been reexamined. It has been found that under-relaxation of the fluid iteration and implementation of a time-dependent “ramp-up” in the heat loads have the greatest benefit for handling the high impulsive levels of fluid pressure and heat load respectively. These are briefly described in the following. In addition, under-relaxation of the pump/turbine shaft power matching has also been investigated to improve the convergence (or lack of non-convergence) in that algorithm. Additional studies are in progress on this as well as other methods for improving reliable convergence for power-matched turbo-machinery.

Fluid Iteration Under-relaxation: GTX fluid loops are typically characterized by very high pressure levels powered by turbo-pumps. Convergence of the circuit fluid parameters is

made difficult by such extreme “forcing functions” since they may engender unphysical fluid properties leading to failure of the iteration scheme. As indicated above, improvements to the initial guess for the fluid parameters were examined to little avail. Rather, it was found that under-relaxation of the solution at early iteration steps leads to a smooth application of the forcing function to the system so that it is able to respond without going haywire. Figure 6.7 shows the relaxation parameters that may be input to implement this new feature.

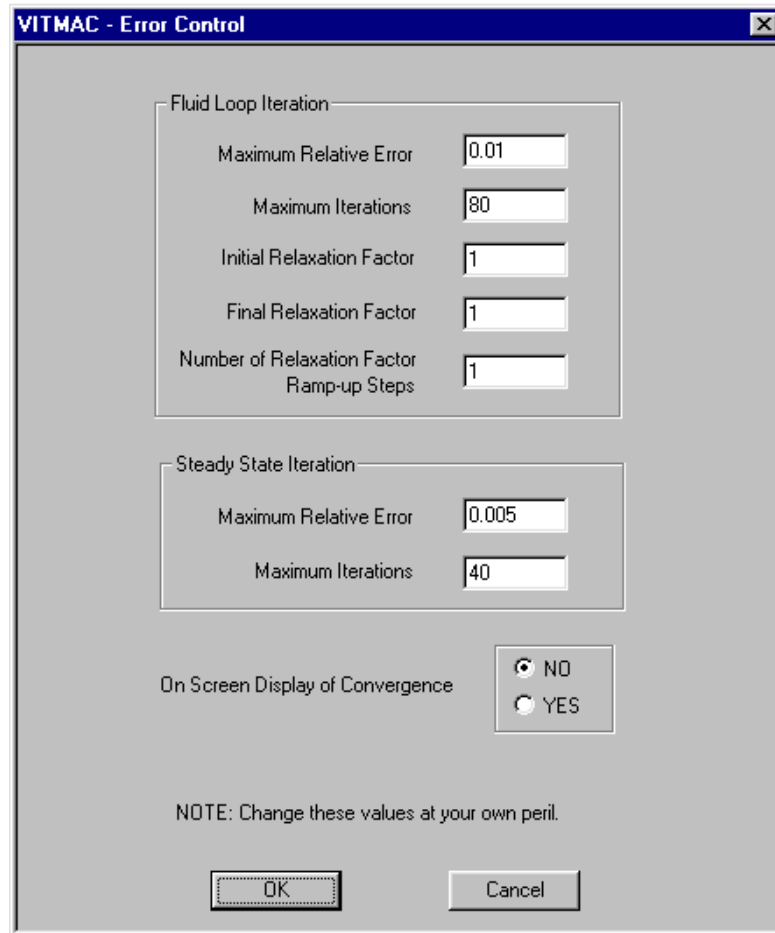


Figure 6.7 Under-Relaxation Parameter

As indicated in Figure 6.7, the relaxation factor is linearly increased from its initial value, Initial Relaxation Factor (typically 0.05), to its final value, Final Relaxation Factor (typically 1.0), over a number of fluid iteration steps, Number of Relaxation “Ramp-up” Steps (typically 20). These parameters have been found to work well for typical GTX cooling circuits.

Engine Heat Transfer “Ramp-up”: GTX fluid loops are also characterized by very high heating levels input by the rocket or scramjet engine hot-structures. Convergence of the circuit thermal parameters is made difficult by these extreme “forcing functions” since they also may engender unphysical fluid properties leading to failure of the iteration scheme. One

solution is to increase the structural heating rate gradually over a “ramp-up” time increment in a transient approach to a steadystate solution. Figure 6.8 shows the heating rate parameters that may be input to implement this new feature.

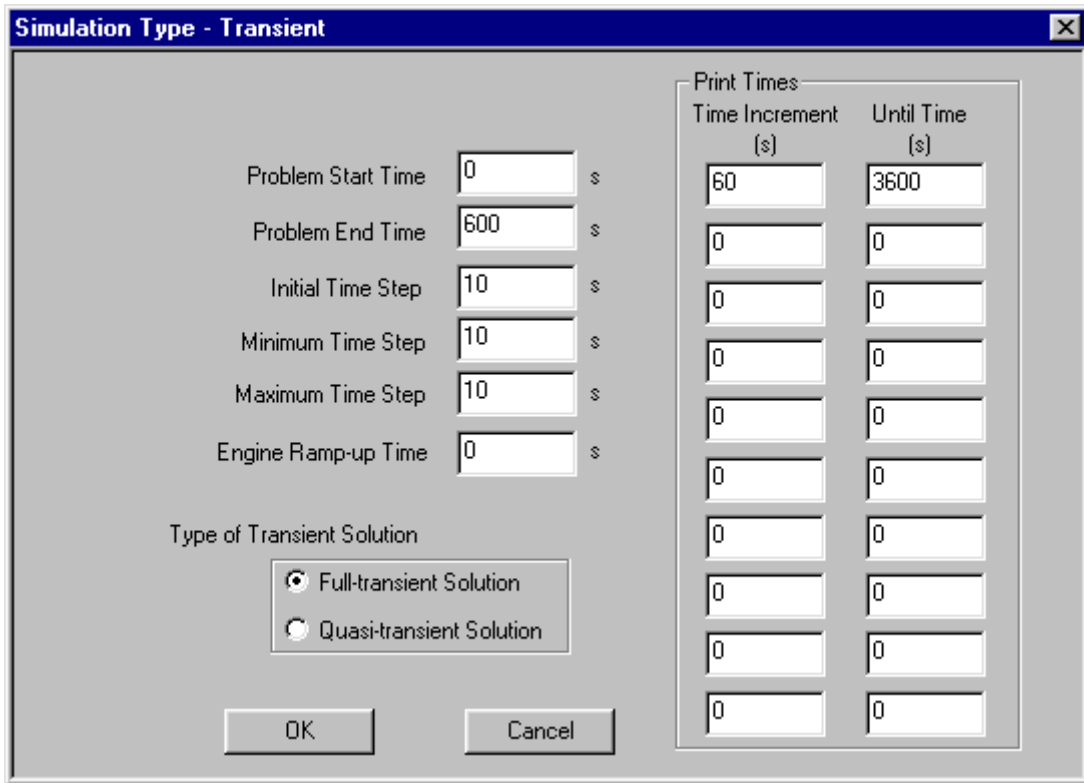


Figure 6.8 Engine Heat Transfer “Ramp-up” Parameter

As indicated in Figure 6.8, this feature is implemented as part of a transient solution. The Engine Ramp-up Time parameter is used to linearly increase the engine heat transfer over the specified time. It has also been found to significantly help the convergence of the thermal solution scheme for GTX cases with typical high heating levels.

7. New Technology

In the present program, described in this report, the VITMAC thermal management system simulation model has been developed for application to rocket-based-combined-cycle launch vehicle cooling system design. The effort extended an existing computer program to include capabilities for rocket engine and scramjet engine linkage, automatic engine flowpath heat transfer calculation, improved “coldside” coolant panel heat transfer models and an upgraded solution method. The effort resulted in a new version of VITMAC, version 6.1, which has been delivered in executable form on a computer compact disk.

8. Discussion and Recommendations

The VITMAC thermal management system simulation model has been described with special attention to recently developed capabilities for rocket engine and scramjet engine applications. The model has been linked to industry standard models: CEA for rocket engine flowpath definition and RJPA for ram/scramjet engine cycle analysis, for the purpose of automatically defining engine “hot-structures” heat transfer properties. To this end, an engineering level model for engine flowpath heat transfer has been implemented and verified. An option for including heat transfer information from experiments or CFD calculations was also included. Comparisons to detailed rocket engine thrust chamber data as well as NASP “direct connect” combustion heated and arcjet heated wind tunnel data attest to the validity and utility of the approach.

Extensive improvements to the “Cooling Panel” model were also implemented to upgrade the treatment of the coolant side heat transfer model. These included addition of engineering correlations for coolant “film” temperature gradient effects, channel entrance and curvature effects, as well as channel geometry enhancement effects. The latter involved the performance of two-dimensional conduction calculations for rectangular and circular geometries with the development of a correlation to relate the equivalent one dimensional heat transfer to the real channel geometry. All of these effects are available within the VITMAC flow channel component as options.

A detailed gas generator source model was implemented which permits the modeling of a gas generator driven turbo-pump flow circuit. The model makes use of the CEA model for accurate definition of source flow properties as a function of user input data with implicit coupling to the loop hydraulic characteristics. In related developments the VITMAC turbine model and its “pump power matching” algorithm were also improved. Analytical guidelines were also developed for turbo-pump driven coolant loops to guide the construction of physically realistic series and parallel circuits.

Finally, the numerical solution procedure was significantly improved. Some bug fixes were found but most notably, an under relaxation procedure and engine heat load “ramp-up” procedure were implemented which accommodate the intense pressures and heat loads common to the present regeneratively cooled thermal management system applications. These numerical control procedures were implemented into as user options following the usual VITMAC GUI and model development practice.

With the completion of the enhancements and preliminary validation of the analysis tool described above, advanced propulsion systems such as the GTX RBCC concept can be analyzed to determine coolant and power balance requirements for candidate propellant feed systems. The integrated characteristic of the RBCC propulsion system requires the use of both the CEA and RJPA modules of the current version of VITMAC to model each mode of operation. The rocket only mode used during the last portion of the mission to orbit can be adequately modeled using the CEA code alone. Of course, more sophisticated analysis

performed apart from the VITMAC model is required to determine the rocket plume free expansion process as it expands from the end of the rocket's physical nozzle to the larger duct. Such information can be fed into the VITMAC model to determine the surfaces subjected to the rocket plume. In a similar manner, the initial portion of the flight (Sea-Level-Static) can also be modeled using just the CEA module. An alternated approach is to use the CFD heat transfer option implemented under this effort. Finally, the ramjet and scramjet portions of the mission can be modeled using the RJPA module. With this approach, it is believed that the critical points along the mission profile can be addressed. Consequently, conceptual design assessment of cooling system approaches for RBCC single-stage-to-orbit vehicle analysis is presently underway.

Proposed additional model development studies include

- Engine Flowpath Heat Transfer Model: Improved RJPA Linkage and Usage
 - Combustor “streamwise” marching
 - CEA integration for eos
 - “Hotside” heat transfer – film & transpiration cooling
 - Expanded Model Validation Studies
- Cooling Panel Analysis
 - Channel Optimization
 - “Coldside” Heat Transfer Validation (Laminar & Cryo Fluids)
 - Panel Test Definition and Analysis
- Integrated Turbo-pump Component
- Cooling Fluids
 - SUPERTRAPP – true two-phase implementation
 - GasPlus Linkage
 - Cryogenic Fluid Curvefits
 - Simple Liquid and Gas User Input Fluid
- Control Valve and “Shutoff” Valve
- Cryo-tank Source Model Update and Checkout
- GTX Thermal Management System Support

9. References

1. Daines, R. and Segal, C., "Combined Rocket and Airbreathing Propulsion Systems for Space-Launch Applications," *J. of Prop. and Power*, vol. 14, no. 5, Sep/Oct 1998.
2. Wassel, A.T., Issacci, F., and Van Griethuysen, V., "An Integrated Modeling Approach for Hypersonic Aircraft Thermal Management," AIAA Paper No. AIAA 95-6022, 6th Inter. Aero. Plane and Hyper. Tech. Conf., April 1995.
3. Farr, J.L. Jr., et al., "VITMAC 4.0 User's Guide," December 1996.
4. Traci, R.M. and Farr Jr., J.L., "Development of an Endothermic Fuel Capability for the Vehicle Integrated Thermal Management Analysis Code (VITMAC)," AFRL-PR-WP-TR-1998-2037, Oct. 1997.
5. Farr, J.L. Jr., et al., "VITMAC 5.0 User's Guide," June 1999.
6. Farr, J.L. Jr., et al., "VITMAC 6.0 User's Guide," September 2000.
7. Gordon, S. and McBride, B.J., (1976), "Computer Programs for the Calculation of Complex Chemical Equilibrium Compositions," NASA TR-1751.
8. Gordon, S. and McBride, B.J., (1994), "Computer Programs for the Calculation of Complex Chemical Equilibrium Compositions and Applications, I. Analysis," NASA RP-1311, vol. I and II.
9. Bartz, D.R., (1957) "A Simple Equation for the Rapid Estimation of Rocket Nozzle Convective Heat Transfer Coefficients," Technical Note, pp. 49, Jet Propulsion, Jan. 1957.
10. Quentmeyer, R.J. and Roncace, E.A., "Hot-Gas-Side Heat Transfer Characteristics of Subscale, Plug-Nozzle Rocket Calorimeter Chamber," NASA Technical Paper 3380, July 1993.
11. Masters, P.A., Armstrong, E.S., Price, H.G., "High-Pressure Calorimeter Chamber Tests for Liquid Oxygen/Kerosene (LOX/RP1) Rocket Combustion," NASA Technical Paper 2862, 1988.
12. Schacht, R.L., Quentmeyer, R.J. (1973), "Coolant-side Heat Transfer Rates for a Hydrogen-Oxygen Rocket and a New Technique for Data Correlation," NASA Technical Note TN D-7207, March 1973.
13. Pandolfini, P.P., and Friedman, M.A., (1992), "Instructions for Using the Ramjet Performance Analysis (RJPA) IBM-PC Version 1.24," JHU/APL AL-92-P175, June 1992.

14. Sullins, C.A., et al., "Direct-Connect Combustor Experiments," Fifth National Aerospace Plane Tech. Sym., Oct. 1988, also other presentations from 1988 to 1990.
15. Sullins, C.A., et al., "Final Report for High Enthalpy Arc Tunnel Combustor Tests GWP 107A, vol. 1," APL-NASP-94-004, March 4, 1994.
16. Pandolfini, P., and Thompson, M.W., "High Enthalpy Direct-Connect Combustor Tests Final Report GWP#50," APL-NASP-92-005, June 12, 1992.
17. Orth, R.C., Torrillo, D., Rizkalla, O.F., and Erdos, J.I., "Summary Report of Parametric Scramjet Experiments Conducted for Pratt & Whitney in the Calspan Shock Tunnel- 4th Entry," vol. 1, GASL TM 243, March 1991.
18. Taylor, M.F., "Correlation of Local Heat Transfer Coefficients for Single Phase Turbulent Flow of Hydrogen in Tubes with Temperature Ratios to 23," NASA TN D-4332, 1968.
19. Taylor, M.F., "A Method of Predicting Heat Transfer Coefficients in the Cooling Passages of NERVA and Phoebus-2 Rocket Nozzles," NASA TM X-52437, 1968.
20. Ito, H., "Friction Factors in Turbulent Flow in Curved Pipes," J. Basic Engineering, vol. 81, no. 2, June 1959, pp. 123–134.
21. Mills, A.T., *Basic Heat and Mass Transfer*, Richard H. Irwin, Inc., 1995.

REPORT DOCUMENTATION PAGE			<i>Form Approved</i> <i>OMB No. 0704-0188</i>	
Public reporting burden for this collection of information is estimated to average 1 hour per response, including the time for reviewing instructions, searching existing data sources, gathering and maintaining the data needed, and completing and reviewing the collection of information. Send comments regarding this burden estimate or any other aspect of this collection of information, including suggestions for reducing this burden, to Washington Headquarters Services, Directorate for Information Operations and Reports, 1215 Jefferson Davis Highway, Suite 1204, Arlington, VA 22202-4302, and to the Office of Management and Budget, Paperwork Reduction Project (0704-0188), Washington, DC 20503.				
1. AGENCY USE ONLY (Leave blank)		2. REPORT DATE June 2002	3. REPORT TYPE AND DATES COVERED Final Contractor Report	
4. TITLE AND SUBTITLE A Thermal Management Systems Model for the NASA GTX RBCC Concept			5. FUNDING NUMBERS WU-708-90-63-00 NAS3-99147	
6. AUTHOR(S) Richard M. Traci, John L. Farr, Jr., and Tony Laganelli				
7. PERFORMING ORGANIZATION NAME(S) AND ADDRESS(ES) Science Applications International Corporation 21151 Western Avenue Torrance, California 90501-1724			8. PERFORMING ORGANIZATION REPORT NUMBER E-13372	
9. SPONSORING/MONITORING AGENCY NAME(S) AND ADDRESS(ES) National Aeronautics and Space Administration Washington, DC 20546-0001			10. SPONSORING/MONITORING AGENCY REPORT NUMBER NASA CR-2002-211587 SAIC-284-002-017	
11. SUPPLEMENTARY NOTES Project Manager, James F. Walker, Turbomachinery and Propulsion Systems Division, NASA Glenn Research Center, organization code 5880, 216-977-7465				
12a. DISTRIBUTION/AVAILABILITY STATEMENT Unclassified - Unlimited Subject Categories: 07, 20, and 61 Available electronically at http://gltrs.grc.nasa.gov/GLTRS This publication is available from the NASA Center for AeroSpace Information, 301-621-0390.			12b. DISTRIBUTION CODE	
13. ABSTRACT (Maximum 200 words) The Vehicle Integrated Thermal Management Analysis Code (VITMAC) was further developed to aid the analysis, design, and optimization of propellant and thermal management concepts for advanced propulsion systems. The computational tool is based on engineering level principles and models. A graphical user interface (GUI) provides a simple and straightforward method to assess and evaluate multiple concepts before undertaking more rigorous analysis of candidate systems. The tool incorporates the Chemical Equilibrium and Applications (CEA) program and the RJP code to permit heat transfer analysis of both rocket and airbreathing propulsion systems. Key parts of the code have been validated with experimental data. The tool was specifically tailored to analyze rocket-based combined-cycle (RBCC) propulsion systems being considered for space transportation applications. This report describes the computational tool and its development and verification for NASA GTX RBCC propulsion system applications.				
14. SUBJECT TERMS Thermal management; Heat transfer; Rocket; Scramjet; RBCC			15. NUMBER OF PAGES 95	
			16. PRICE CODE	
17. SECURITY CLASSIFICATION OF REPORT Unclassified	18. SECURITY CLASSIFICATION OF THIS PAGE Unclassified	19. SECURITY CLASSIFICATION OF ABSTRACT Unclassified	20. LIMITATION OF ABSTRACT	